Volcanic Eruptions and their Impacts on Tropical Climate: A comparison of Model Simulations with Observational Datasets

Master's Thesis

Faculty of Science

University of Bern

presented by

Lucien Chabbey

2015

Supervisor:

University Prof. Dr. Stefan Brönnimann
Oeschger Centre for Climate Change Research

Advisor:

Abdul Malik
Oeschger Centre for Climate Change Research

Declaration

under Art. 28 Para. 2 RSL 05

Last, first name: Lucien Chabbey
Matriculation number: 10-419-745

Programme: Climate Science

Bachelor ☐ Master ⊘ Dissertation ☐

Thesis title: Volcanic Eruptions and their Impacts on Tropical Climate: A comparison of Model Simulation with Observational Datasets

Thesis supervisor: Stefan Brönnimann

I hereby declare that this submission is my own work and that, to the best of my knowledge and belief, it contains no material previously published or written by another person, except where due acknowledgement has been made in the text. In accordance with academic rules and ethical conduct, I have fully cited and referenced all material and results that are not original to this work. I am well aware of the fact that, on the basis of Article 36 Paragraph 1 Letter o of the University Law of 5 September 1996, the Senate is entitled to deny the title awarded on the basis of this work if proven otherwise. I grant inspection of my thesis.

Bern, 16.11.2015
Place, date

Lucien Chabbey
Signature

Contents

List of Figures

List of Tables

Chapter 1: Introduction

Since the beginning of mankind, explosive volcanic eruptions have exerted a great influence on the men and their way of living by causing climatic variations on different timescales. The tracks of those events can be found all along the last millennia. Sometimes the volcanic eruptions have direct and sharp effects on the population living nearby. One of the most famous examples is of course the city of Pompeii, which was mostly destroyed and buried under the ashes of the Mount Vesuvius in 79 AD. But often, and particularly in the case of explosive tropical volcanic eruptions, the consequences are not only undergone by the local populations but can be worldwide spread. The eruption of Mount Tambora in 1815, one of the most powerful eruptions in recorded story with a Volcanic Explosivity Index (VEI) of 7 (Newhall and Self. 1982), is an interesting and clear example.

On one hand, the local effects were enormous and the whole island of Sunbawa was buried under tons of smoking ashes causing the death of most of the animals and plants present there. Even in 1831, 16 years after the eruption, a Dutch official sailing along the cost of Sunbawa describes the landscape he was seeing: “a horrendous scene of devastation . . . in its fury the eruption has spared, of the inhabitants, not a single person, of the fauna, not a worm, of the flora, not a blade of grass” (D’Arcy Wood 2014). But on the other hand, the effects were not confined to Indonesia’s islands, and many others regions of the world were impacted by the Tambora’s eruption. Indeed those explosive tropical eruptions inject a consequent amount of sulfur species in the stratosphere which were then converted into sulfuric acid. The H_2SO_4 molecules formed have the potential to absorb and scatter-back the solar radiation once they reach the stratosphere. According to Gao et al. (2007), 55 Mt of SO_2 gas have been injected into the stratosphere during the Tambora eruption and then converted into 107 Mt of H_2SO_4 causing high impact on the Earth radiative balance.

The impacts observed are multiple and complex. During the summer following the Tambora eruption, a global cooling has been observed over most parts of the globe since the amount of solar radiation reaching the ground decreased. On the contrary, Robock (2000) discovered that the winters following major tropical eruptions were often showing positive temperature anomalies in Europe. The reason behind this observation is not completely clear nowadays. The most common theory explains that, due to the inhomogeneous stratospheric warming, the meridional stratospheric temperature gradient between the tropics and the poles is enhanced and the stratospheric winds are also intensified. This leads to a wind perturbation in the troposphere. Indeed most of the volcanic eruptions are followed by a positive Northern Atlantic Oscillation (NAO) phase which brings moist and warm air over northern Europe. This could contribute to the observed winter warming (Robock 2000).

The injection of sulfur species into the stratosphere also has an effect on precipitation. In the tropics, due to the reduced amount of solar radiation reaching the ground, the evaporation is sharply reduced. Thus a negative precipitation anomaly is regularly observed in the tropics after major explosive eruptions. Outside the tropics, the pattern is less clear and not really understood nowadays. Indeed it is well known that the year 1816, following Tambora’s eruption, was really rainy over all Europe. But actually, the reasons behind these observations are not completely clear. This year 1816, which was called “The year without a summer”, demonstrates well the indirect consequences following a major volcanic event. According to D’Arcy Wood (2014), the Tambora eruption directly triggered the extremely wet and cold summer 1816 over Ireland. The mean temperature recorded in Dublin between February and October 1816 was 2 K lower than the average and the precipitation in July 1816 were four times higher than the one registered in July 1815 (Harington 1992). This extremely wet weather in the hearth

of the growing season contributed to the Irish famine of 1816-1818. India was also affected by alteration in the hydrological cycle of the monsoon and large reductions in summer rainfall were observed over South Asia (Schneider et al. 2009). According to D'Arcy Wood (2014), this could have been the driver of the unprecedented cholera epidemic outbreak in Bengal in 1817. Indeed, because of the monsoon failure, the water tanks were not replenished and the water stored there grew fetid, facilitating the development and the proliferation of the cholera bacteria. The extreme climatic condition of 1816 could therefore have triggered the first Asiatic cholera pandemic (1817-1824). More surprisingly, the Tambora eruption has also affected the literature indirectly. Indeed, Mary Shelley spent the whole summer 1816 in Geneva where the meteorological conditions were really rainy. The amount of precipitation during this summer was 80% higher compared to the reference period 1799-1821 (Auchmann et al. 2012). Hence, she was confined in her house and it is there that she got the idea and the inspiration to write her first novel which is famous now: Frankenstein, or the modern Prometheus.

Thus the present study, which is published for the bicentenary of the eruption of the Mount Tambora, tries to shed light on the influence of volcanic forcing on climate. To reach that goal, we investigated the effects of 13 tropical and 4 extra-tropical volcanic eruptions on tropical and Asian climate by employing the Atmosphere Ocean Chemistry Climate Model (AOCCM) SOCOL-MPIOM as well as different observational and reconstructed datasets. One of the advantages of the study is the use of a global climate model without prescribed SSTs. It is then interesting to compare the outputs of the AOCCM SOCOL-MPIOM model with other global climate models. Indeed, models with a simplified ocean circulation could have missed some parameters and it would then be interesting to compare our work with other similar studies (Joseph and Zeng 2011; Wegmann et al. 2014).

The spatial scope of this study is restricted to the Tropics and the Asian monsoon regions. Indeed, the influence of tropical explosive volcanic eruptions on Asian monsoon was not really carefully analyzed in the previous studies investigating the links existing between volcanic eruptions and climate perturbations. An outbreak of the monsoon over these densely populated areas could have a sharp effect on local populations and it is therefore important to understand the link between climate perturbation and volcanic forcing.

Thus and to sum up, this study tries to understand and model the effects on tropical climate and Asian monsoon due to volcanic eruptions using the newly developed AOCCM SOCOL-MPIOM model. As a consequence, the following research questions emerged and this thesis should provide some possible answers.

1. How do the tropical climate and the Asian monsoon region respond in the model to major tropical volcanic eruptions in term of precipitation and temperature?

2. With which time lag (0, +1, +2 … years) do the previous climate variable respond to volcanic eruption and how long does the anomaly last?

3. Do the responses depend on the location and on the magnitude of the eruption? Is there a difference between the effects generated by extra and tropical volcanic eruptions?

4. Is the global atmospheric circulation significantly affected in AOCCM SOCOL-MPIOM by volcanic forcing? Do we see significant zonal and vertical wind anomaly at any pressure levels?

5. Are different monsoon indices as well as dynamical variables (Southern Annular Mode, Tropical easterly jet, ITCZ) affected by major volcanic eruptions?

6. Is there a significant difference between the SOCOL-MPIOM and other models using fixed SSTs (CCC400)? Are the SSTs significantly affected after major tropical volcanic eruptions?

7. Do we see significant differences between the different AOCCM SOCOL-MPIOM simulations (EnsembleL1L2 and EnsembleM1M2) computed with different solar forcing and different initial ocean conditions?

In order to answer the research questions, we will first describe exhaustively the global climate model as well as different observational and reconstructed dataset (Chapter 2). Later on in Chapter 3, the methods used in this thesis are investigated. In Chapter 4, the results obtained thanks to the data and methods described previously are presented. Finally in Chapter 5 and 6 we will discuss the results which have been obtained and answer the research questions.

Chapter 2: Data

This chapter describes the different datasets used in this study in order to answer the research questions. The thesis uses model simulations from the Atmosphere Ocean Chemistry Climate Model (AOCCM) SOCOL-MPIOM as well as different observational and reconstructed datasets. First the Global Climate Model AOCCM SOCOL-MPIOM is described in chapter 2.1. Then some evaluation datasets such as the 20CR reconstructed dataset are carefully described in section 2.2.

2.1: AOCCM SOCOL-MPIOM data

In this study we used simulations of the AOCCM SOCOL-MPIOM, which was developed jointly by the University of Bern, ETH Zürich, and PMOD/WRC Davos (Muthers et al. 2014). The simulations are used to determine the effects of major tropical volcanic eruptions on different climatic variables. This AOCCM SOCOL-MPIOM has been obtained by coupling the Chemistry Climate Model (CCM) SOCOL to the ocean model MPIOM.

The CCM Solar Climate Ozone Links (SOCOL) (Stenke et al. 2013) used in this GCM is based on the middle atmosphere model MA-ECHAM5 version 5.4.01 (Roeckner et al. 2003) and a slightly modified version of the chemistry model MEZON (Model for Evaluation of Ozone trends) developed by Egorova et al. (2003). The newly obtained CCM SOCOL has then been coupled to the ocean-sea-ice model MPIOM (Jungclaus et al. 2006) using the OASIS3 coupler. The Short Wave (SW) radiation scheme in SOCOL originates from the European Center of Medium-Range Weather Forecasts (ECMRWF) model IFS (Fouquart and Bonnel 1980). The solar spectrum considered by this model is split into 6 wavelength intervals: 3 bands in the UV and in the visible range (185-250 nm; 250-440 nm; 440-690 nm), as well as 3 bands in the near-infrared range (690-1190 nm; 1190-2380 nm; 2380-4000 nm). In the computation, scattering and absorption of SW radiations by aerosol and clouds as well as water vapor, CO_2 and ozone is taken into account. The SOCOL model considers 31 chemical species that can generate about 200 chemical reactions (gas phases, photolysis and heterogeneous). The climatic effects of stratospheric sulfate aerosol are also considered in the chemistry model of SOCOL and allow to study the effects of volcanic eruptions which inject sulfur species into the stratosphere. The scheme for the Long Wave (LW) radiation follows the Rapid Radiative Transfer Model (RRTM) (Mlawer et al. 1997) and contains 16 spectral bands covering 10-3000 cm^{-1}. In the computation, the absorption of LW radiation by aerosol, water vapor and cloud is also considered. The SOCOL simulations used in this study have a horizontal resolution of T31 (3, 75° x 3, 75°) and contain 39 vertical different level starting from 1000 hPa (ground surface) and reaching 0.01hPa (approximately 80km).

As mentioned before, the CCM SOCOL is then coupled to the MPIOM ocean model which also includes a sea ice component. This oceanic model has a horizontal resolution of 3°x3° and a vertical resolution containing 40 levels with a decreased resolution at the bottom of the ocean. The MPIOM is coupled every 24 hours with the CCM SOCOL by using the OASIS3 coupler (Budich et al. 2010; Valcke 2013). Every day we have thus an exchange of momentum, heat, freshwater fluxes, information on sea ice extent, sea surface temperatures (SSTs), or snow cover on sea ice for example.

It is also interesting to look at the dataset obtained after running the AOCCM SOCOL-MPIOM because in contrast to many others GCM, the SSTs are not prescribed. Furthermore, some GCMs use simplified mixed-layer ocean models which is not the case of the MPIOM. For these reasons, it is interesting to look at the output of the AOCCM SOCOL-MPIOM which can differ from those obtained after running models with a simplified ocean circulation (For example CCC400). The respective performances of those two global climate models are interesting and comparisons are done in further sections.

Figure 2.1 taken from Muthers et al. (2014) shows the different sub-components which have been used and combined to develop the AOCCM SOCOL-MPIOM.

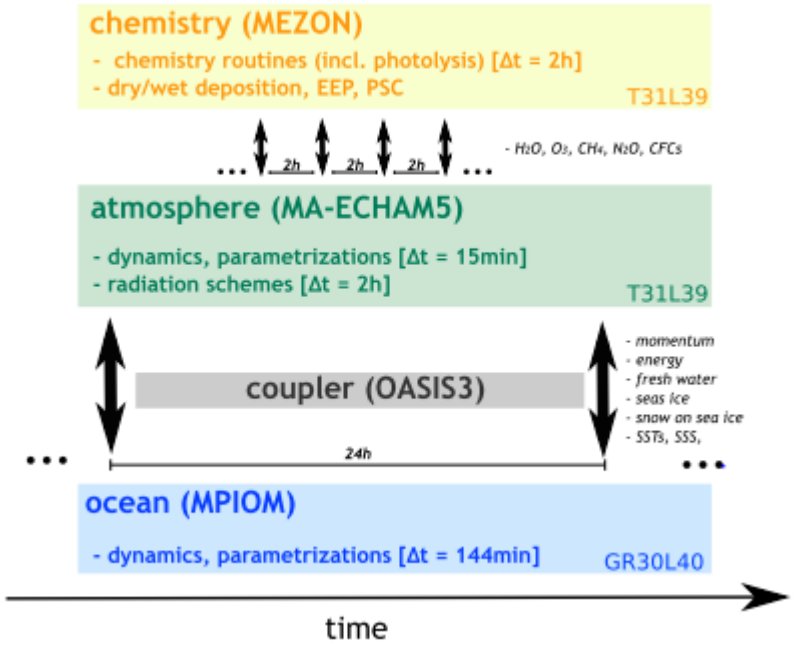

***Fig 2.1**: Summary of the different AOCCM SOCOL-MPIOM sub-components (figure created by Muthers et al. 2014).*

As this GCM contains a chemistry model, information about the total aerosol mass is not sufficient and information about optical properties and Surface Area Density (SAD) need to be prescribed for every latitude and altitude. Therefore, in the case of a volcanic eruption, it is necessary to have information about the development and the extent of the aerosol cloud. In the AOCCM SOCOL-MPIOM, Muthers et al. (2014) used the volcanic forcing data set developed by Arfeuille et al. (2014). Based on the aerosol mass estimation done by Gao et al. (2008), this newly developed model can determine and simulate for some eruption which occurred during the last millennia the transport, the nucleation, the condensation and the sedimentation of the aerosols. Finally, different optical properties can be derived with the help of this model.

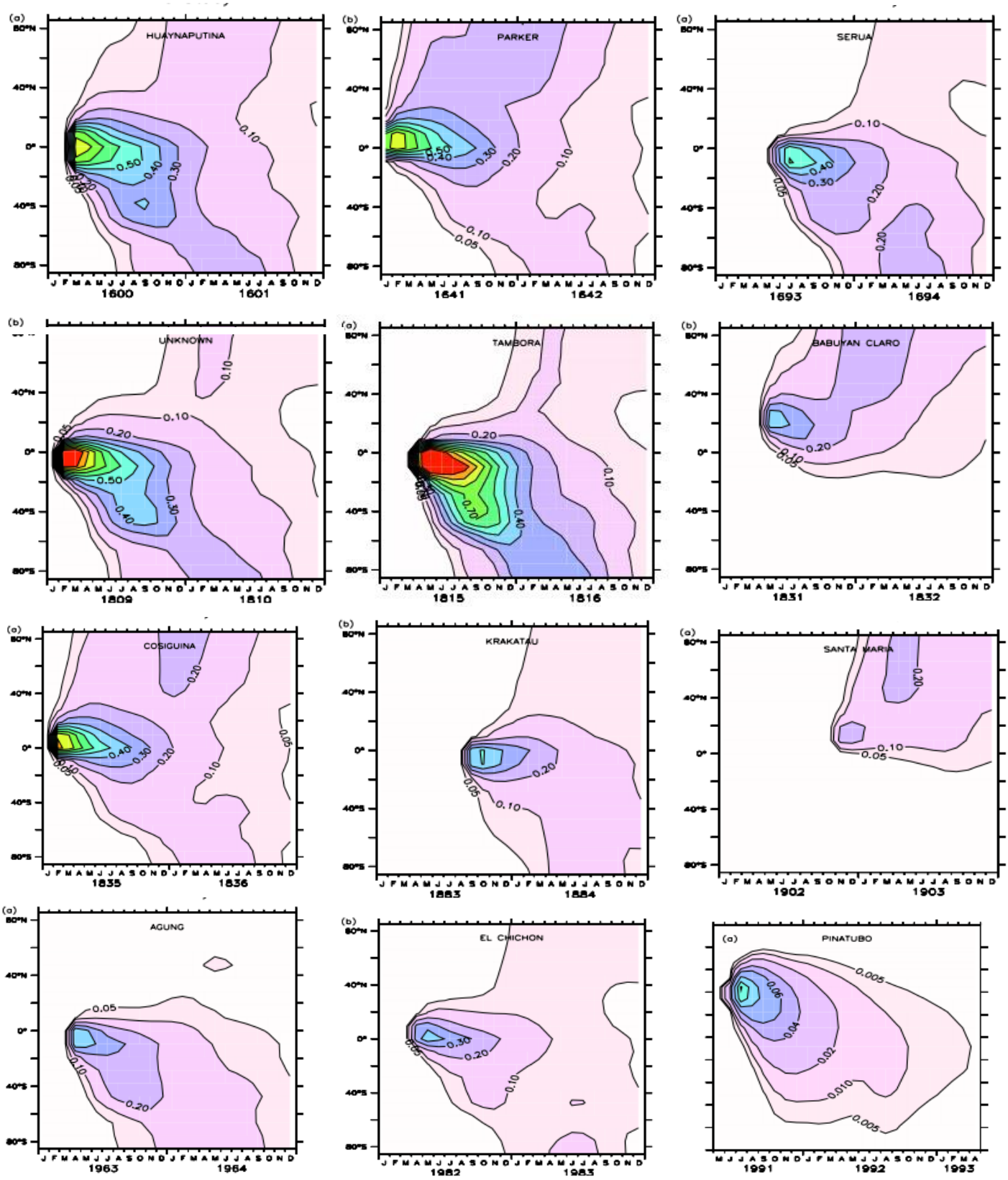

***Fig 2.2**: Aerosol optical depth after some volcanic eruptions (Huaynaputina, Parker, Serua, Unknown 1809, Tambora, B.Claro, Cosiguina, Krakatau, S. Maria, Agung, El Chichon and Pinatubo respectively.) as implemented in the AOCCM SOCOL-MPIOM simulations. Figure taken from Arfeuille et al. (2014).*

In the 4 transient simulations of the AOCCM SOCOL-MPIOM used in this study, the model-based datasets developed by Arfeuille et al. (2014) has been implemented and allows us to detect the influence of major volcanic eruptions on tropical climate. Figure 2.2 shows the development and the shape of the aerosol cloud after some major volcanic eruptions as implemented in the model of Muthers (2014).

For this thesis, the monthly dataset obtained after running the AOCCM SOCOL-MPIOM simulation with interactive chemistry is investigated. This interactive chemistry module can be switched off and, after comparison, Muthers et al. (2014) noticed a warmer stratosphere in the simulation including chemical reactions. This can be due, among other factors, to the ozone chemistry and the nucleation of aerosol which absorb and scatter solar radiation and heat the stratosphere. This is not observed in the control simulation without chemical reactions. At the surface level, the discrepancy between the two simulations is reduced. As volcanic eruptions emit sulfur species, which turn later on into aerosol after a series of chemical reactions, it makes sense to use the simulation including a chemistry module.

The simulation including the chemistry module was carried out from 1600-2000 AD and all major forcing were kept transient. It also contains 4 transient simulations with differences in the solar forcing and in the initial state of the oceans namely called L1, L2, M1 and M2. The L1 and L2 simulation have been carried out with a strong solar forcing (Shapiro et al. 2011) (6 W/m^2 mean TSI amplitude) but each run with different initial ocean conditions. For the M1 and M2 simulation, the Shapiro forcing has been reduced to 3 W/m^2 with the initial ocean condition previously used in L1 and L2 respectively. To simplify the analysis, we averaged the two simulations with a strong solar forcing and obtained the so called L1L2 simulation. The same process was repeated for the transient simulations with a medium solar forcing and the M1M2 simulation was obtained. According to Muthers et al. (2014), we might have a difference in the representation of the winter warming between those simulations. It is thus interesting to compare the evolution of other variables in those two model simulations and determine if they are affected by the different solar forcing. In this study we therefore analyze the L1L2 and M1M2 transient simulations and with the data obtained we try to assess the effects of major tropical volcanic eruption on different climatic variables.

2.2: Reanalysis and observational datasets

Once the model AOCCM SOCOL-MPIOM has been run and the 2 averaged Ensemble simulations with strong and medium solar forcing have been obtained, it was important to evaluate the output of the model. In order to see if the model is able to properly reconstruct the climate in different places and for different periods, the outputs of the GCM used in this study are compared with some reanalysis and observational datasets. This allows us to test and to monitor the validity and the capability of the AOCCM SOCOL-MPIOM to reconstruct the climate of the last 400 years. As every dataset has some strengths and weaknesses, several datasets are employed to assess the quality of the AOCCM SOCOL-MPIOM depending on the place and the period we are interested in.

Thus this section concisely describes the different dataset we selected to lead this study. The evaluation of the AOCCM SOCOL-MPIOM output and the comparison with reconstructed and observed datasets is presented in Chapter 4.3.

2.2.1: Twentieth Century Reanalysis (20CR)

In order to evaluate and assess the accuracy of any global climate model, the scientific community needs a reliable reconstructed or observed dataset covering a large period of time. This was the main motivation which leads after an international effort to the creation of the 20th century reanalysis (20CR). This project has been mostly led by the Physical Science Division (PSD) and the Cooperative Institute for Research in Environmental Science (CIRES) at the University of Colorado and provides a comprehensive global atmospheric circulation dataset covering the 20th century. This dataset is thus a powerful tool which can be used for the validation of climate model simulations (Compo et al. 2011). This dataset has been obtained by assimilating surface and sea-level pressure information into a forced GCM with monthly sea surface temperature and sea ice concentration. The assimilation is performed with a variant of the Ensemble Kalman filter, and an ensemble of 56 members is used. With these provided variables, it is then possible to obtain a global reanalyzed dataset spanning the last century.

The 20CR dataset covers the period 1871-2012 AD with a high spatial and temporal resolution.
The two dimensional spatial grid has a resolution of 2° by 2°. The temporal resolution is also high and for each climatic variables contained in this dataset a new value is obtained every 6 hours. It is also possible to work with monthly averaged dataset and this facilitates the comparison with the AOCCM SOCOL-MPIOM monthly simulations used in this study. The 20CR reanalysis dataset contains also 24 pressure levels starting from the surface (1000 hPa) and reaching 10 hPa.

This dataset is then optimal to assess the validity of the AOCCM SOCOL-MPIOM model on large scale and especially for the lower troposphere. Typically, as the aim of this study is to detect the effects of major tropical volcanic eruptions on tropical climate, one can compare the effects of a specific eruption in the 20CR dataset and in the GCM. The only problem with this dataset is that it covers only the period 1871-2012 AD and contains only 5 out of the 13 tropical eruptions picked for this study: Krakatau (1883), Santa Maria (1902), Agung (1963), Chichon (1982) and Pinatubo (1991). The extratropical eruption of the Mount Katmai (1912) also occurred during this time period. Thus the direct comparison is only possible for these 6 eruptions, as there is no other global dataset going such far in time.

2.2.2: Monsoon Asia Drought Atlas (MADA)

As the aim of this study is also to determine what are the effects of the tropical volcanic eruptions on Asian and Indian climate, it is necessary to compare the outputs of the AOCCM SOCOL-MPIOM simulations with local paleo dataset. The Monsoon Asia Drought System (MADA) which aimed at reconstructing the climate monsoon dynamic of the last millennia with the help of tree rings is a project supported by the U.S National Science Foundation. The project started in 2004 after the success of a similar atlas for North America: the North American Drought Atlas (Cook and Krusic 2004). Based on a network of 327 chronology tree rings covering the period 1000-1989 AD and by using an Ensemble Point by Point Regression (EPPR), it was possible for the authors to reconstruct the hydroclimatic evolution and response of the Asian monsoon. Figure 2.3 (Cook et al. 2010) shows the 534 grid cells of each 2.5° covered by the MADA.

We still have to note that these paleo data have been obtained by sampling several kinds of trees (teaks, tropical pines, conifers…) in a number of different countries: Vietnam, Philippines, Pakistan, Kyrgistan, India, Sri Lanka, Nepal, Bhutan, Thailand, Laos, Cambodia, Malaysia, Indonesia, China, Taiwan, Mongolia, Russia, Korea and Japan.

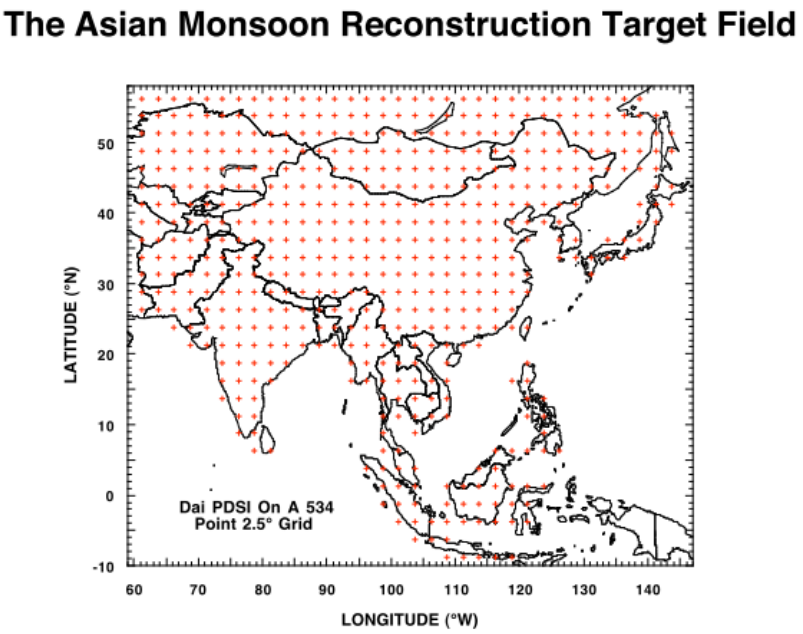

***Fig 2.3**: The 534 grid points covered by the MADA (Cook et al. 2010).*

With this dataset, one can evaluate the validity of the AOCCM SOCOL-MPIOM model to reconstruct volcanic effect on the Asian monsoon. Indeed, in contrary to the 20th century reanalysis, the MADA contains 12 (out of 13) of the tropical volcanic eruptions which interest us. Only the eruption of the Mount Pinatubo (1991) is missing in this dataset. Therefore we can reconstruct the PDSI response of the model and compare it to the MADA. The PDSI in the model is calculated by using the precipitation, the temperature, the soil wetness, as well as a Matlab tool developed by Jacobi et al. (2013). Thus with all those elements, it was possible to compare the PDSI response to volcanic forcing in the MADA paleo dataset and in the AOCCM SOCOL-MPIOM simulations.

Chapter 3: Methodology

In this chapter, an overview of the different methods used to obtain the results presented in the chapter 4 is given. First the choice of the volcanic eruptions analyzed in this study is presented and justified in chapter 3.1. Second, in chapter 3.2 the anomaly and the reference period used to assess the effects of volcanic eruption on tropical and Asian climate are defined. Third, to control if the monsoon over Asia is significantly affected by powerful tropical volcanic eruptions, various dynamical monsoon indices have been employed. These indices are fully described and explained in chapter 3.3. Finally, an overview of the different statistical methods employed in this thesis is given. Thus the methods employed to perform linear regression (Chapter 3.4), Superposed Epoch Analysis (SEA) (Chapter 3.5) as well as the test of significance (Chapter 3.6) are fully described.

3.1: List of volcanic eruption

The main aim of this study is to investigate the effects of major tropical volcanic eruptions on tropical climate by using the AOCCM SOCOL-MPIOM. As the model employed covers the period 1600-2000 AD, we were interested in eruptions which occurred during the last 400 years. The choice of volcanic eruptions is mainly based on the list of volcanic events picked by Wegmann et al. (2014), list which was already derived from the work of Shindell et al. (2004) and Fischer et al. (2007).

This list is of course not exhaustive and does not contain all the volcanic events which occurred during the 1600-2000 AD period. Only the most powerful and major events have been selected by Wegmann et al. (2014). But as the AOCCM SOCOL-MPIOM is forced with the new volcanic forcing microphysics-based dataset developed by Arfeuille et al. (2014), we had to adapt slightly the list used in Wegmann's study and remove two eruptions. Indeed, in the dataset of Arfeuille, we do not find any event corresponding to the eruption of Mount Colima (Mexico, 1622), as well as the eruption of Tolbachik (Russia, 1740). Thus these events had to be removed and the final list contains 13 tropical and 4 extra-tropical volcanic eruptions.

Table 3.1 (based on the work of Arfeuille et al. (2014)) shows the 17 volcanic eruptions picked for this study and gives information about the magnitude, the location as well as the period of eruption as implemented in the model. In this table, the data concerning the total mass of aerosol emitted in each hemisphere is derived from the work of Gao et al. (2008).

As the dataset is not complete and some information are missing, the timing as well as the exact location of the eruption had to be artificially determined in order to be implemented in the global climate model. Therefore, firstly when the timing of the eruption is unknown, it was artificially set to April by Arfeuille et al. (2014). This method was used for the eruption of Krafla, Laki, Babuyan Claro and the Unknown eruption of 1861. Thus Babuyan Claro is the only tropical eruption whose timing was unknown and had to be artificially set. Second the location of an eruption is set to the Tropics if unknown but recorded in both hemispheres (Unknown eruption of 1809). If the eruption is only recorded in the Northern hemisphere, the artificial location is set to 55°N-65°N (for example the Unknown eruption of 1729). Conversely, when the eruption is only perceived in the southern hemisphere (Unknown eruption of 1861), it is implemented in the model at 40°S (Arfeuille et al. 2014).

Date	Aerosol Mass Tg (H_2SO_4) NH	Aerosol Mass Tg (H_2SO_4) SH	Location	Eruption
02.1600	46.0	10.5	Peru (16.6° S)	Huaynaputina
01.1641	33.8	17.8	Philippines (6°N)	Parker
05.1673	6.3	9.8	Indonesia (1.4°N)	Gamkonora
06.1693	0.0	27.0	Indonesia (6.3° S)	Serua
?? 1729 *	12.0	0.0	????? NH	Unknown (no large eruption recorded)
?? 1783 *	93.0	0.0	Iceland (64°N)	Laki
02.1809	27.6	26.2	Unknown	Unknown eruption 1809
04.1815	58.7	51.0	Indonesia (8°S)	Tambora
?? 1831	17.0	0.0	Philippines (19.5°N)	Babuyan Claro
01.1835	26.4	13.8	Nicaragua (13°N)	Cosiguina
?? 1861 *	0.0	4.2	???? SH	Unknown (no large eruption recorded)
08.1883	11.2	10.7	Indonesia (6°N)	Krakatau
10.1902	0.0	3.8	Guatemala (14°N)	Santa Maria
06.1912 *	11.0	0.0	Alaska (68°N)	Katmai
03.1963	7.6	13.3	Indonesia (8°S)	Agung
03.1982	7.0	7.0	Mexico (17.2°N)	El Chichón
06.1991	15.0	15.0	Philippines (15°N)	Pinatubo

***Table 3.1**: Date, location and magnitude of the volcanic eruption as implemented in the AOCCM SOCOL-MPIOM. Table derived from the work of Arfeuille et al. (2014). Note that the Aerosol mass data are issued for the study of Gao et al. (2008). The four stars (*) indicate the extra-tropical volcanic eruptions.*

3.2: Definition of reference periods and anomaly

The creation and definition of reference period after each volcanic eruption is a powerful tool and has already been used in several studies (Wegmann et al. 2014, Fisher et al. 2007). This allows us to calculate an anomaly during the year following such an event and thus to investigate the effects of volcanic eruptions on climate.

Then the first aim is to define a reference period without any major volcanic forcing. Then it is possible to compare and subtract the year following an eruption with the reference period. In this thesis we are mainly interested in boreal summer anomalies and we thus investigate summer anomalies at lag +1, +2 and +3 years. The same operation can be reproduced for any of the climate variables modelled by the AOCCM SOCOL-MPIOM (temperature, precipitation, evaporation, cloud cover, zonal winds…).

As the period investigated is long, it is not possible to build a unique reference period on which the 17 volcanic eruptions can be reported. Indeed, by looking at the surface temperature for example, we observe a clear warming between 1600 and 2000. By building a reference period for each of those eruptions, it is possible to cancel out this trend and to have a robust analysis.

Based on a literature review, we created two sorts of reference periods and anomalies. The first reference period has been developed by Wegmann et al. (2014) and is defined as a 20-year period wrapped around the eruption. Basically, they chose and averaged two periods of 10 years directly preceding and following each volcanic eruption. The years of smaller volcanic eruptions occurring during the reference period (with a forcing bigger than -0.5W/m^2 in Crowley 2000) were deleted. For the eruption of Huaynaputina (1600), the 10 years preceding the event are not covered by the model. For this reason, they took a 20-years reference period starting 5 years after the volcanic eruption.

In order to compare, we also took the reference period developed by Fischer et al. (2007), defined as the 5-year pre-eruption period. By comparing the outputs obtained between these two methods, we did not notice any significant differences. Therefore, we decided to present here only the results obtained by applying Wegmann's reference period and thus to avoid an overloading of repeating plots.

The reference period developed by Wegmann et al. (2014) and corresponding to the 17 volcanic eruptions analyzed in this thesis are shown in Table 3.2. As aerosol needs time to be transported in the stratosphere and at higher latitude, a lag of two months between the eruption and the season considered is required. Therefore, the first boreal summer do not always occur during the year of the eruption. For example, the first considered boreal summer following eruption of Mount Tambora occurs in 1816 because this volcano erupted in April and the lag of two month is not respected (Table 3.2).

Volcanic eruption	Reference periods	First boreal winter (DJF) after eruption	First boreal summer (JJA) after eruption
Huaynaputina	1604-1612, 1615-1621, 1624-1627	1601	1600
Parker	1631-1640, 1644-1653	1642	1641
Gamkonora	1661-1666, 1669-1672, 1676-1680, 1683-1687	1674	1674
Serua	1683-1688, 1690-1693, 1697-1706	1694	1694
Unknown eruption 1729	1719, 1721-1728, 1732-1740, 1745-1746	1730	1730
Laki	1773-1782, 1785-1788, 1790-1795	1784	1784
Unknown eruption 1809	1799-1808, 1812-1814, 1818-1824	1810	1809
Tambora	1802-1808, 1812-1814, 1818-1824	1816	1816
Babuyan Claro	1820-1829, 1833-1834, 1837-1839, 1841-1842, 1845-1847	1832	1832
Cosiguina	1822-1829, 1833-1834, 1837-1839, 1841-1842, 1845-1849	1836	1835
Unknown eruption 1861	1851-1860, 1864-1873	1862	1862
Krakatau	1873-1882, 1885-1894	1884	1884
Santa Maria	1892-1901, 1904-1911, 1915-1916	1904	1903
Katmai	1900-1901, 1904-1911, 1915-1923, 1926	1913	1913
Agung	1953-1962, 1967, 1971-1974, 1976-1980	1964	1963
El Chichon	1971-1974, 1976-1981, 1985-1990, 1995-1998	1983	1982
Pinatubo	1978-1981, 1985-1990, 1995-2004	1992	1992

***Table 3.2**: List of the 17 volcanic eruptions with their respective reference periods. Table derived from Wegmann et al. (2014).*

3.3: Definition of indices

As one aim of this thesis is to determine whether or not major tropical volcanic eruptions have a significant effect on the dynamics of the atmosphere with a focus on the Asian monsoon region, we use several dynamical indices found in the literature. This section will describe 4 different dynamical monsoon indices used and presented in the result sections 4.1 and 4.2.4. Furthermore other indices to define El Niño Southern oscillation, the tropical jet or the Southern Mode oscillation (SAM) are described in this section.

The first index investigated is the Indian Summer Monsoon index (ISM) developed by Lau et al. (2000). This index is calculated by subtracting the meridional wind at 850 hPa (V850 m/s) from the meridional wind at 200 hPa (V200 hPa m/s) over the following region: 10°N-30°N, 70°E-110°E. The strength of the monsoon over India is closely linked to this meridional wind shear. Indeed the correlation between the precipitation over the Indian continent and the ISM index is positive and equal to 0.75 in both Ensemble simulations.

The second index employed is the Webster and Yang Monsoon Index (MYMI) developed by Webster et al. (1992). This time, the zonal wind shear between 850 hPa (U850hPa m/s) and 200 hPa (U200 hPa m/s) is investigated. To build this index, we simply subtract the zonal averaged wind at 850 hPa from the zonal averaged wind at 200 hPa. This has been done over the following region: 0°N-20°N, 40°E-110°E. This index allows us also to see the evolution in the strength of the Indian monsoon and precipitation over Asia. In both Ensemble simulations, the precipitation over Asia and the MYMI are significantly positively correlated (0.95)

The third index employed describes the North Pacific monsoon and is well correlated with precipitation over the eastern and south-eastern part of Asia. The Western North Pacific Monsoon index (WNPM) was developed by Wang et al. (2001) and will allow us to sharpen our analysis. This index, as the precedent, is based on zonal wind. To calculate it, one needs to subtract the averaged zonal wind at 850 hPa (U850 hPa m/s) over these two regions 5°N-15°N, 100°E-130°E and 20°N-30°N, 110°E-140°E. As for the MYMI, the WNPM is well correlated with the precipitation over Asia (0.85) in both Ensemble simulations.

Finally it is also interesting to look at the Australian monsoon to see if any significant changes are observed after major volcanic eruptions. Therefore, we chose the Australian Monsoon index (AUSM) built up by Kajikawa et al. (2010). To calculate this index, one needs to average the zonal winds at 850 hPa (U850 hPa m/s) over the following region: 5°S-15°S, 110°E-130°E. In both Ensemble simulation, rainfall over Australia are well correlated with the AUSM (0.91)

The four dynamical monsoon indices used in this thesis are shown in Figure 3.1.

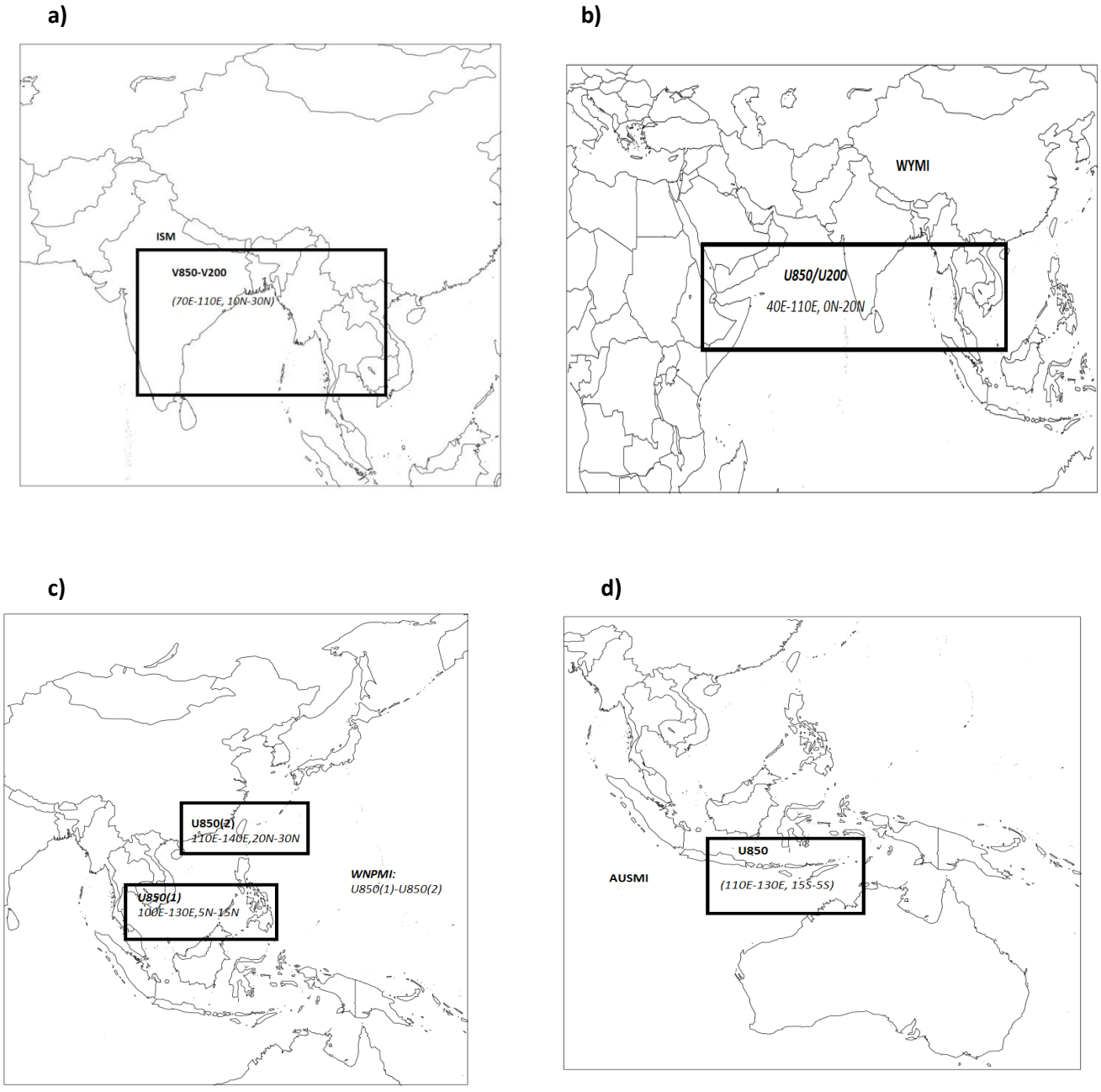

***Figure 3.1**: Representation of 4 dynamical monsoon indices: **(a)** ISM, **(b)** WYMI, **(c)** WNPM and **(d)** AUSM. Figure inspired by the Asia-Pacific Data-Research Center (APDRC).*

We also wanted to see if the position of the Intertropical Convergence Zone (ITCZ) and the strength of the easterly tropical jet were affected by volcanic eruptions (Chapter 4.2.4.2). To reach that goal, we had to define an index permitting us to locate the ITCZ and we picked the index defined by Schneider et al. (2014). According to this study, the ITCZ can be defined as the maximum zonal mean precipitation or vertical wind in the tropical region.

Later in section 4.2.4.2 we try to evaluate the strength of the tropical easterly jet. To define it, we looked at the zonal winds at 200 hPa over the following region: 13°N-17°N; 50°E-80°E. In section 4.2.1 we try to evaluate the influence of volcanic eruptions on El Niño Southern Oscillation (ENSO). To reach that goal we used the averaged sea surface temperature over the El Niño 3.4 regions (5°S-5°N; 120°W-170°W)

Finally, it was also interesting to test the response of Southern Annular Mode (SAM) to volcanic forcing. To define the strength of the SAM we used the index described by Ho et al. (2012) and looked at the normalized zonal sea level pressure between 40 ° South and 65° South. According to the aforementioned study, the SAM index can be calculated by applying the following equation:

$$SAMI = P40°S - P65°S$$

3.4: Linear regression

To answer some of the research questions, simple linear regression models have been used in this thesis. It was indeed important to test the significance of the link existing between an anomaly and the magnitude of the eruption in term of Aerosol Optical Depth (AOD). In those simple models, the AOD peak at 500 nm following each eruption is the explanatory variable while the anomaly of any component of the GCM (temperature, precipitation, zonal winds…) is the dependent variable. This AOD peak (500nm) was calculated by taking the total aerosol masses emitted after each eruption (M) and presented in Table 3.1 (Gao et al. 2008) and by applying the following formula (Arfeuille et al. 2014):

$$AOD_{peak} = 0.02 . M^{0.658}$$

The AOD peak is then linked to a spatially and time-averaged anomaly of any climate variable. To calculate this anomaly, we took and averaged the 24 months following each eruption (see Table 3.2). To calculate the boreal winter or summer anomaly, we selected and averaged the months January, February and Mars (JFM) and June, July, August and September (JJAS) respectively.

3.5: Superposed Epoch Analysis

The superposed Epoch Analysis (SEA) is a powerful statistical tool which can detect and isolate the response of particular events from noise (Haurwitz and Brier 1981). This tool is thus ideal for this study because we have a list of key events supposed to significantly influence the climate. The SEA performed in Chapter 4 clarifies and statistically tests the result obtained.

In order to perform this SEA, we used the freely available R package "*dplR*". After entering a list of key events (1641,1674,1694,1809,1816,1832,1835,1884,1903,1963,1982,1992) we took the yearly (spatially averaged over Tropics or India) mean for 1600-2000 AD and obtained a new dataset. Then this time series had to be detrended before the SEA is performed. In the list of the key events, we removed the eruption of Huaynaputina because the model is not covering the years preceding the events. All the other tropical eruptions picked for this study are present in this "key event" list.

We have to keep in mind that the list of key data corresponds to the first boreal summer following each tropical volcanic eruption. But sometimes the first boreal summer considered occurred only 14 month after the eruption (see Table 3.2). This is the case for the eruption of the Mount Tambora which occurred in April 1815, while the first boreal summer considered begins in June 1816. This could explain some of the significant anomaly observed at lag -1 in some of the plots presented in Chapter 4 (see Figure 4.22 for example). Furthermore, as the list of key events is relatively small (12 events), the uncertainty is relatively large and could also partially explain the significant pics at lag -1.

3.6: Confidence test

To test the statistical significance of the composite pictures (13 volcanoes) anomaly presented in chapter 4, we used the method applied by Fischer et al. (2007). For each grid point, we conducted a two-sided Mann-Whitney test with the following null hypothesis: The mean anomaly during the reference period does not differ from the anomaly modelled 1, 2 and 3 years after the eruption. By applying this statistical test, we obtained for each grid point a p-value which allowed us to evaluate the significance of the anomaly. If the p-value is smaller than 0.05 it means that we can reject the null hypothesis with a confidence level of 95%, meaning that volcanic eruption do have a significant impact on climate. All the grid points with a p-value smaller or equal to 0.05 were shaded in the composite pictures of anomaly after volcanic eruptions (Chapter 4).

Chapter 4: Results

Atmosphere Ocean Chemistry Climate Model (AOCCM) simulations with SOCOL-MPIOM along with observational datasets are used in this section to investigate the influence of volcanic eruptions on tropical climate and on Indian monsoon. The results of these investigations and some of the model output are presented in the following section and should answer the research questions.

4.1: Global time-series

In order to get a first impression of the influence of major tropical volcanic eruptions on global climate, different time series were plotted. The time series presented in this section contain important climate variables averaged over the whole globe, which could be significantly affected by major tropical volcanic eruptions. The thin grey vertical lines on the graphics represent the years where one of the 13 tropical eruptions picked for this study occurred. As the difference between the time series obtained after running the EnsembleL1L2 and EnsembleM1M2 simulations were negligible, we subjectively decided to present in this section only the outputs of the first simulation.

Figure 4.1 shows the evolution of the ground temperature in Kelvin for the period AD 1600-2000. The warming due to the increased emission of greenhouse gases is clearly captured in the model and we observe a clear trend in the temperature evolution since the second half of the 19th century. The temperature increase during this period is slightly higher than 2 K. The AOCCM SOCOL-MPIOM also captures the Dalton minimum and a drop in the temperature is observed between 1790 and 1830 in the time series. It is also interesting to note that after the majority of the volcanic eruptions one can distinguish a cooling. This cooling is especially pronounced after the Unknown eruption of 1809 and the eruption of Mount Tambora (1815). Indeed, there is a drop of about 1 K between the yearly temperature mean in 1815 and in 1817. In the case of the Unknown eruption, the temperature drop reaches about 0.5K two years after the eruption. This cooling tendency can be observed after the majority of the 13 events selected for this study.

It is also interesting to look at the stratospheric temperature evolution. Indeed, as described in section 4.2.2, volcanic eruptions significantly influence this variable. This phenomenon is clearly seen in Figure 4.2. After each of the 13 eruptions, one can observe a rapid and sharp increase in temperature at 100 hPa. This phenomenon is clearly visible after the Tambora eruption where a warming of about 3 K can be observed. The eruption of Mount Parker (1641, Philippines) also had a large effect on temperature at this height with a warming of approximately 2 K.

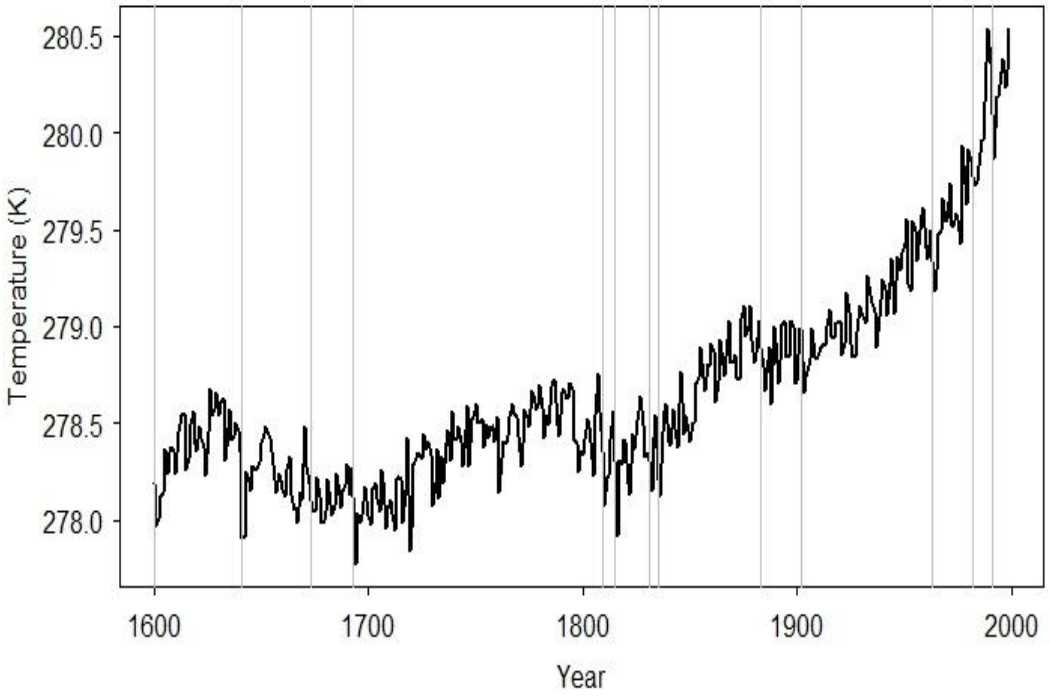

***Fig 4.1**: Annual global mean 2m temperature from the EnsembleL1L2 simulation. The 13 grey vertical lines indicate years where large tropical volcanic eruption occurred.*

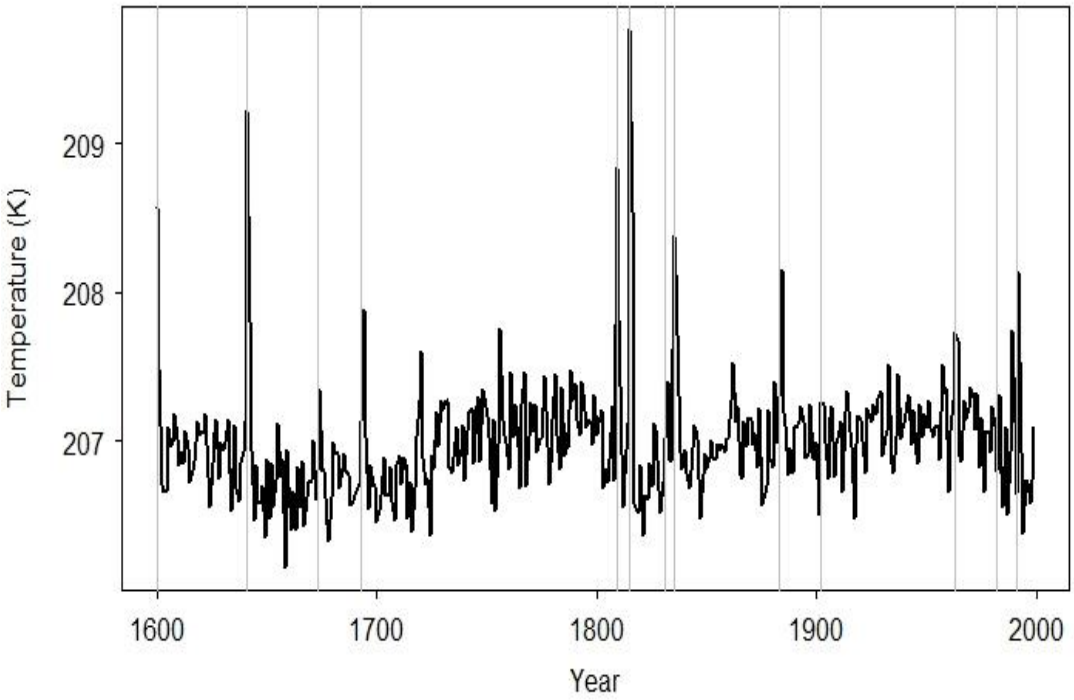

***Fig 4.2:** Annual global mean temperature at 100 hectopascal for the EnsembleL1L2 simulation. The 13 grey vertical lines indicate the years where large tropical volcanic eruptions occurred.*

The water cycle also seems to be perturbed after major tropical volcanic eruptions and one can observe a drying following the majority of these events (Figure 4.3). Indeed, volcanic eruptions release aerosol in the stratosphere, which increases the absorption and scattering of a significant part of the incoming solar radiation. This, in turn, reduces evaporation. By and large, after a major volcanic eruption, the amount of energy available to evaporate water decreases and therefore the amount of precipitation is reduced. This phenomenon is especially observed in the tropical regions. Indeed the formation of tropical precipitation is mainly driven by the incoming solar radiation whereas in the higher latitude other dynamical phenomena can play a major role.

Figure 4.3 and 4.4 show the yearly averaged precipitation evolution for the period AD 1600-2000 for the whole globe and the tropical regions respectively. At a global level, the model reconstructs a drying of about 0.07 mm/day 2 years after the eruption of Mount Tambora. One can also well distinguish the eruption of Huyanaputina (1600), Parker (1641), Serua (1693), the Unknown eruption of 1809, Cosiguina (1835), Agung (1963) and Pinatubo (1991) in this figure.

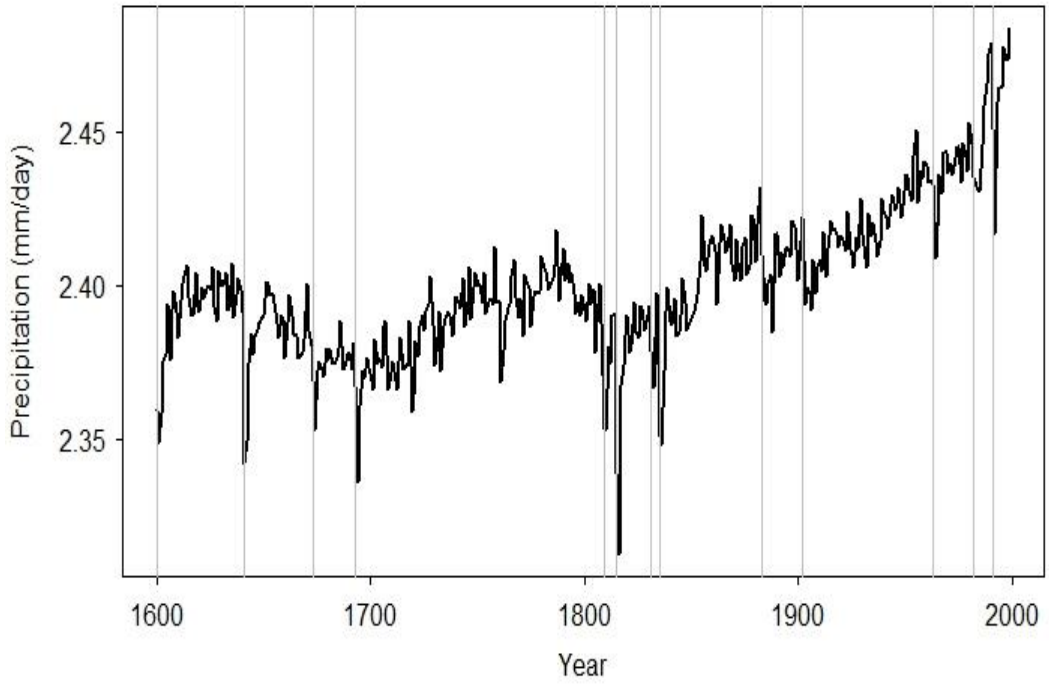

***Fig 4.3**: Annual global mean precipitation evolution for the EnsembleL1L2 simulation. The 13 grey vertical lines indicate the years where large tropical volcanic eruptions occurred.*

If we consider tropical regions only, the effects of volcanic eruptions on precipitation are generally higher. Indeed, for the reasons mentioned above, the tropical precipitation is directly linked to the amount of solar radiation reaching the surface of the Earth. For example, the averaged drying in tropical regions following the eruption of Mount Tambora exceeds 0.1 mm/day. We also observe that since the beginning of the 19th century, the amount of precipitation has increased. Indeed, due to the emission of greenhouse gases and the warming of the atmosphere, the global water cycle is accelerated and this leads to a general increase of the rainfall.

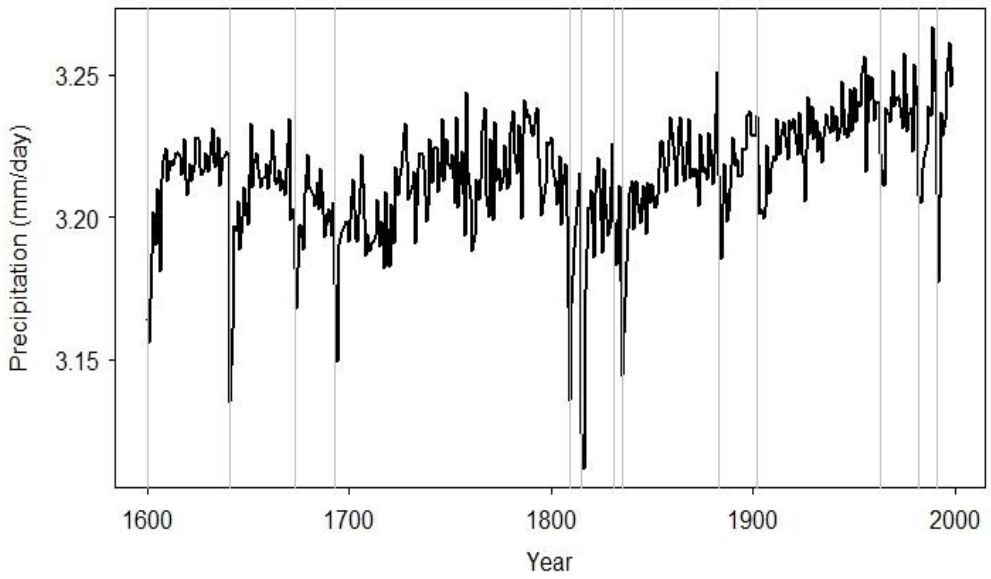

***Fig 4.4**: Annual tropical mean precipitation for the EnsembleL1L2 simulation. The 13 vertical grey lines indicate years of large tropical volcanic eruptions.*

The evolution of evaporation is illustrated in Fig 4.5. As expected, evaporation follows the precipitation and temperature pattern, and decreases after a major tropical volcanic eruptions. We have to keep in mind that in the AOCCM SOCOL-MPIOM, evaporation is a negative flux. Thus after the eruption of the Mount Tambora we observed a reduction of the averaged global evaporation of 0.06 mm/day. We can note that evaporation has increased since the industrial period mainly because of the industrialization and the rising temperatures.

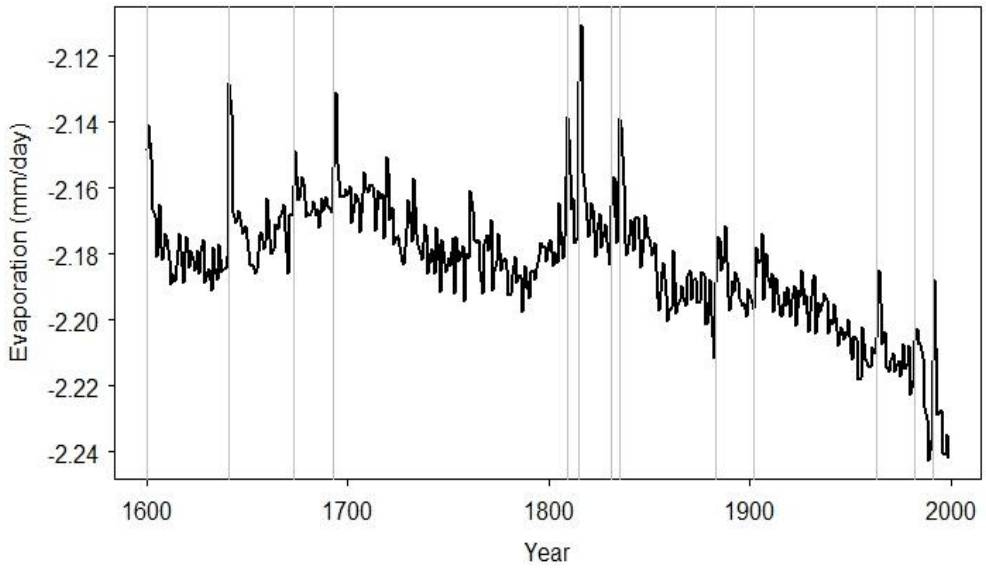

***Fig 4.5**: Annual global mean evaporation for the EnsembleL1L2 simulation. The 13 vertical grey lines indicate year of large tropical volcanic eruptions.*

Unlike most of the chemistry-climate model simulations, the sea surface temperatures (SSTs) are not prescribed in the AOCCM SOCOL-MPIOM but react according to the total solar irradiance (TSI) and all others forcings. Figure 4.6 illustrates the SSTs evolution for the period AD 1600-2000 and shows that this variable is also sensitive to volcanic forcing. Two years after the Tambora eruption the global SSTs decrease, according to the model, by about 0.4 K. It is interesting to note that the SSTs react rather quickly after the eruptions and by and large, a drop in temperature can already be observed only one year after major tropical volcanic eruptions. But the response as expected also seem to last longer after most of the eruptions.

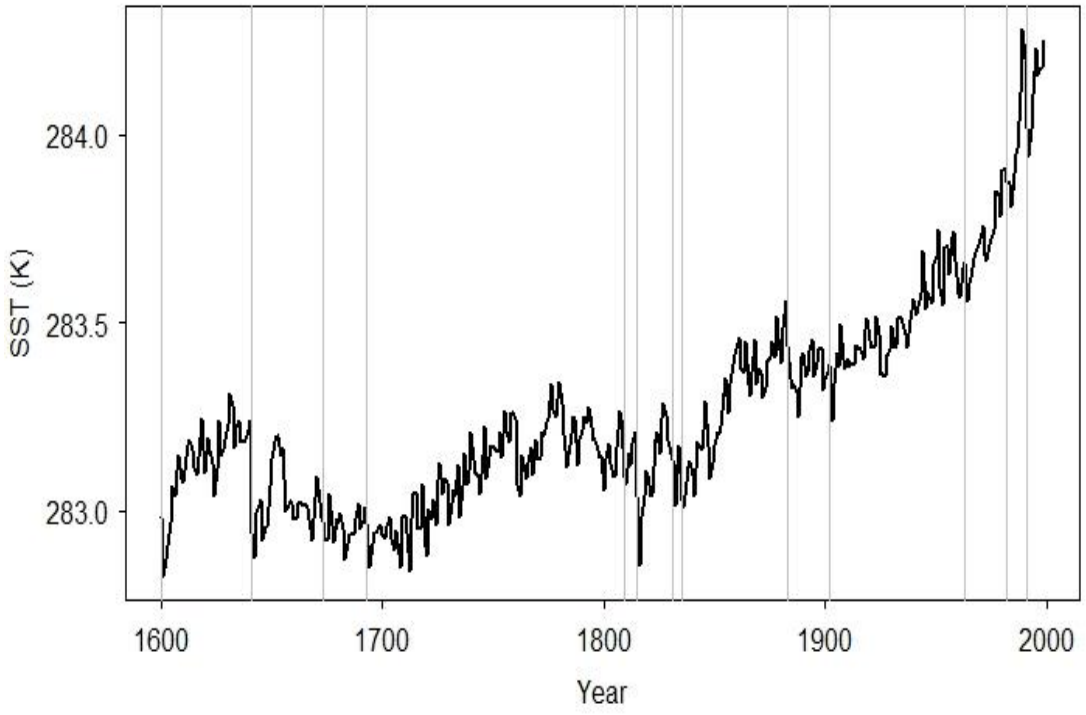

***Fig 4.6**: Annual global mean SSTs for the EnsembleL1L2 simulation. The 13 vertical grey lines indicate years of large tropical volcanic eruptions*

Figure 4.7 illustrates the response of cloud cover to volcanic forcing at 850 hPa. At this altitude, the pattern is not very clear and we do not see any clear signal after volcanic eruptions. Even after the Unknown eruption of 1809 and the Tambora eruption the cloud cover response do not seem to be significant.

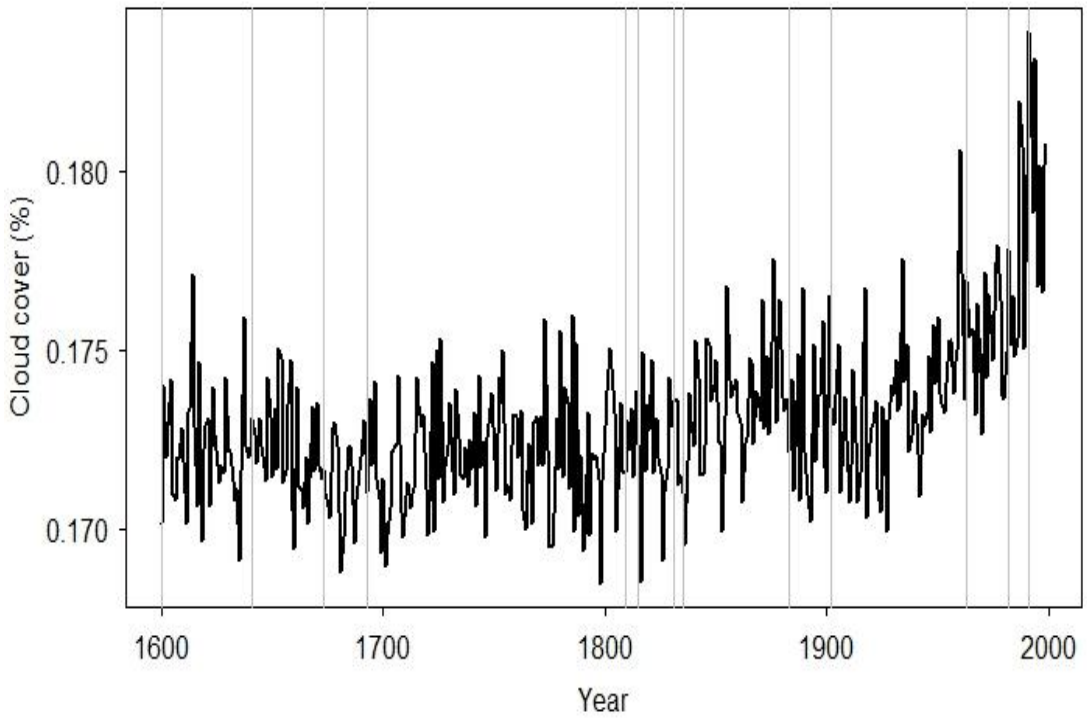

***Fig 4.7**: Annual global mean cloud cover for the EnsembleL1L2 simulation at 850 hPa. The 13 grey lines indicate years of large tropical volcanic eruptions.*

The dynamics of the atmosphere can also be affected by volcanic eruption and Figure 4.8 shows the evolution of 4 different monsoon indices during the last 400 years: the Australian Summer Monsoon Index (AUSMI) as defined by Kajikawa et al. (2010), the Webster and Yang Monsoon Index (WYI) as defined by Webster et al. (1992), the Western North Pacific Monsoon (WNPM) as defined by Wang et al. (1999) and finally the Indian Summer Monsoon index (ISM) developed by Lau et al. (2000). The 4 indices mentioned above are completely described in Chapter 3.4.

At this stage, and after having analyzed these four time series, it is hard to distinguish any clear response of the different monsoon system. We will investigate later more carefully and try to find out if these dynamical indices are indeed significantly affected by major tropical volcanic eruption (Chapter 4.2.4).

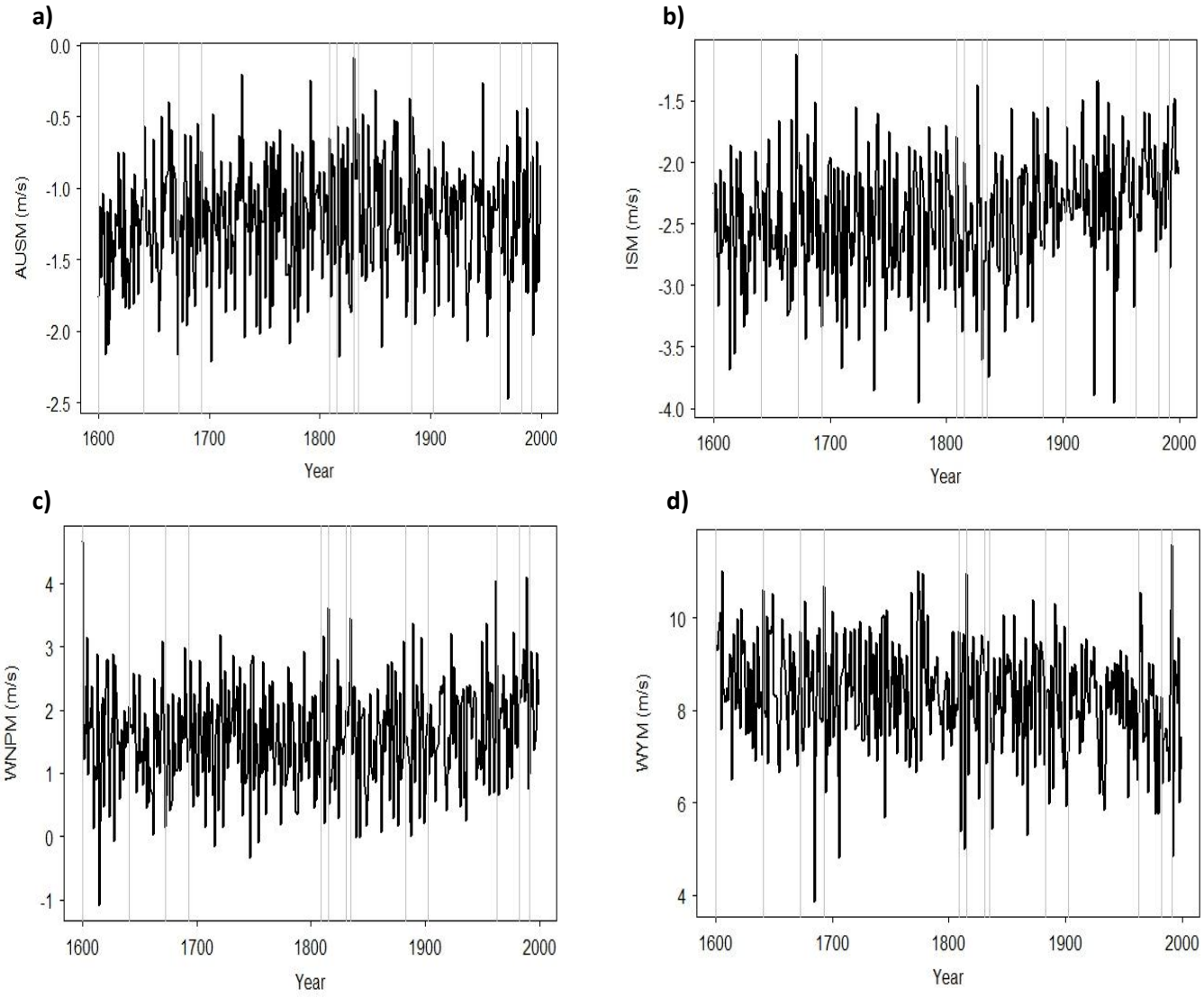

***Fig 4.8**: Yearly evolution of 4 different monsoon indices for the EnsembleL1L2 simulation: **(a)** AUSMI, **(b)** ISM, **(c)** WNPM and **(d)** WYM. The 13 vertical grey lines indicate years of large tropical volcanic eruptions.*

4.2: Analysis of different climate variables

In this section, we will describe carefully the evolution of several climatic variables after major volcanic eruption in the AOCCM SOCOL-MPIOM. We will also try to determine if there is a link between the power of the eruption and the magnitude of the anomaly. Firstly, the surface as well as the stratospheric temperature evolution are investigated. Secondly, the response of precipitation pattern is analyzed and finally we will have a look at wind anomaly as well as the response of some dynamical indices. The geographical focus in this section is set on tropical and Asian regions.

4.2.1: Temperature anomaly

Temperatures are directly influenced by volcanic forcing and a number of studies already demonstrated that a significant cooling was observed after major tropical eruptions. This phenomenon is due to the massive emission of sulfur species which are then converted into H_2SO_4. This aerosol has the capability to scatter-back and absorb the incoming solar radiation, and thus perturbs the radiative balance of the Earth. As mentioned by D'Arrigo et al. (2008), major volcanic eruptions taking place in the tropical regions have much higher cooling potential and the effects are worldwide spread. In the case of extra tropical eruptions, the effects seem to be more local and constrained to one hemisphere. This is due to the global atmospheric circulation which restrains the interhemispheric exchanges of atmospheric air masses. Therefore, despite the relative long residence time of the aerosols formed after an eruption, the effects are mainly felt in one hemisphere. In the AOCCM-SOCOL-MPIOM model it also seems to be the case. Figure 4.9 shows the evolution of the average tropical temperature for 13 tropical and 4 extra tropical eruptions in the EnsembleL1L2 and EnsembleM1M2 simulations of the AOCCM-SOCOL-MPIOM.

On one hand, the 4 extra-tropical eruptions chosen (the Unknown eruption of 1729, Laki, the Unknown eruption of 1861 and Katmai) do not seem to have a significant influence on tropical temperature. The mean anomaly in both cases is around 0 K. On the other hand, the response of tropical temperature after major tropical eruptions is clear and a cooling is observed, reaching a minimum of about -0.4 K after 10 month in the two Ensemble simulations. It is also interesting to note the discrepancy between the two Ensemble simulations. In the EnsembleL1L2, the Tambora eruption has the highest impact with a mean cooling of 0.9 K after 13 month, whereas for the EnsembleM1M2 a maximum cooling of 0.75 K is reached after 9 month. It is worth to note that in the second Ensemble simulation, the Unknown eruption of 1809 (-1 K after 13 month) has the highest effect on tropical temperature. The temperature drop after the eruption of the Huaynaputina in this simulation has approximately the same magnitude as the one observed after the Tambora eruption.

It is also interesting to note that in the AOCCM-SOCOL-MPIOM model there is a significant link between the magnitude of the eruption in term of Aerosol Optical Depth (AOD) and the temperature anomaly during the two years following the event (Figure 4.10). This can be shown with a simple linear regression model (Chapter 3.4). With this model, where the temperature anomaly is the dependent variable whereas the AOD is the explanatory variable, we tried to see if the magnitude of the temperature anomaly could be explained by the strength of the eruption.

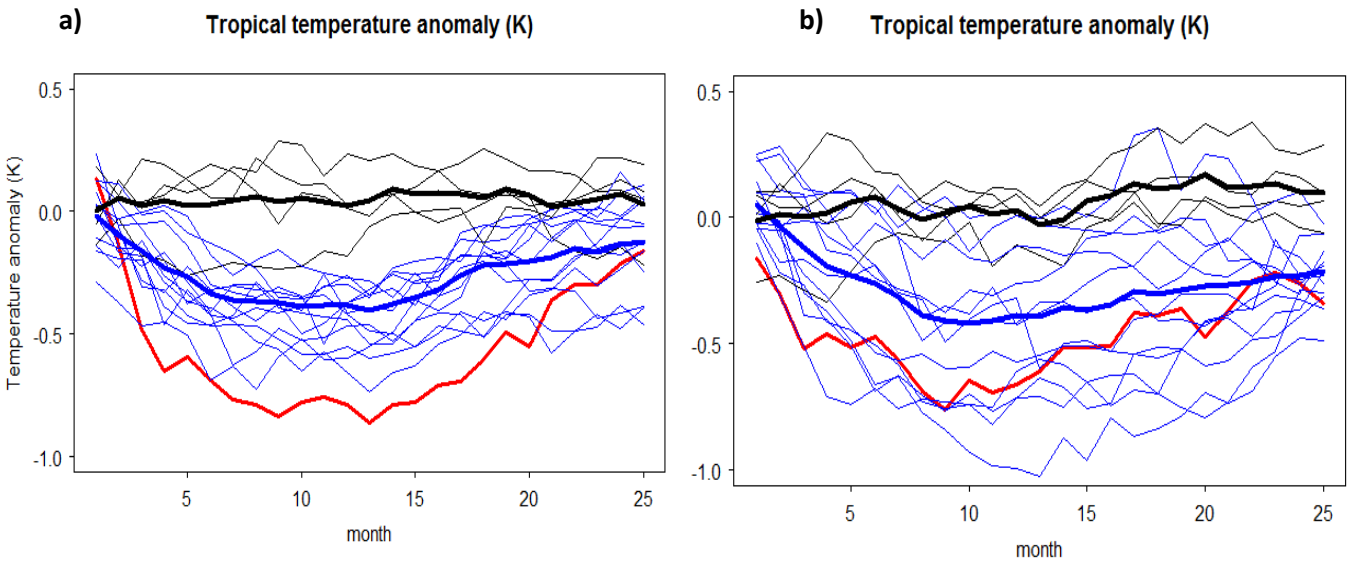

***Fig 4.9**: Monthly averaged temperature evolution after the 13 tropical and 4 extra-tropical eruptions over the Tropics (40N-40S; 180W-180E) for the **(a)** model EnsembleL1L2 and **(b)** model EnsembleM1M2 simulations. The thick red line shows the evolution of the temperature after the eruption of the Tambora. The blue lines represent the tropical eruptions while the black lines represent the extra-tropical eruptions. The two thick lines (black and blue) are the mean for extra and tropical eruptions respectively.*

Fig 4.10 shows the relation between the AOD and tropical temperatures for the EnsembleL1L2 simulation. The R-squared obtained is equal to 0.54, meaning that when considering only the global AOD following one eruption, about 54% of the surface temperature anomaly can be explained. The same analysis was done selecting only the boreal summer (JJAS) and winter (DJF). The R-squared obtained are equal to 0.54 and 0.40 respectively and both values are significant at the 0.01 level. The results for the EnsembleM1M2 simulation are really close and therefore not shown here. We obtained a R-squared equal to 0.58 for the whole year, 0.57 for the summer and 0.49 for the winter

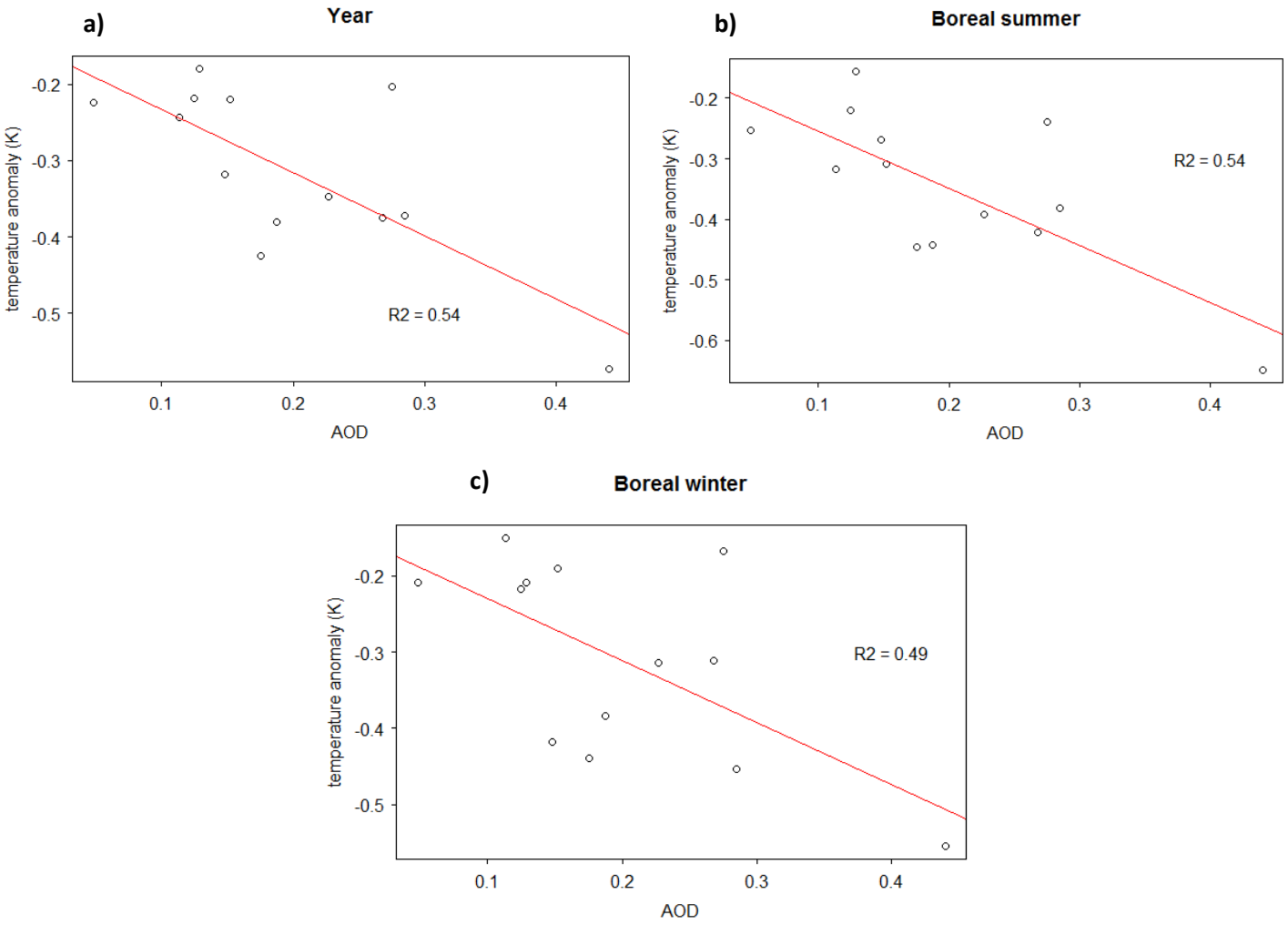

Fig 4.10*: Simple linear regression model explaining tropical surface temperature anomaly through AOD (EnsembleL1L2 simulation). The dots represent 13 different tropical volcanic eruptions and the red line is the regression line. In* ***(a)*** *the 24 months following the eruptions have been chosen whereas in* ***(b)*** *and* ***(c)*** *the boreal summer (JJAS) and the boreal winter (DJF) months have been selected*

By considering the Indian continent only (5N-40N; 65E-95E), a clear cooling can still be observed even if the pattern is more chaotic (Fig. 4.11). As for the tropical surface temperatures, the extra-tropical volcanic eruptions do not really influence the surface temperature of the Indian continent and the anomalies in both Ensembles stay around 0 K. Fig 4.11 also shows that in both model simulations, the tropical eruptions are followed by a cooling. Anomalies of about -0.6 K after 13 months in the EnsembleL1L2 simulation and -0.4 K after 12 months in the EnsembleM1M2 simulation are observed.

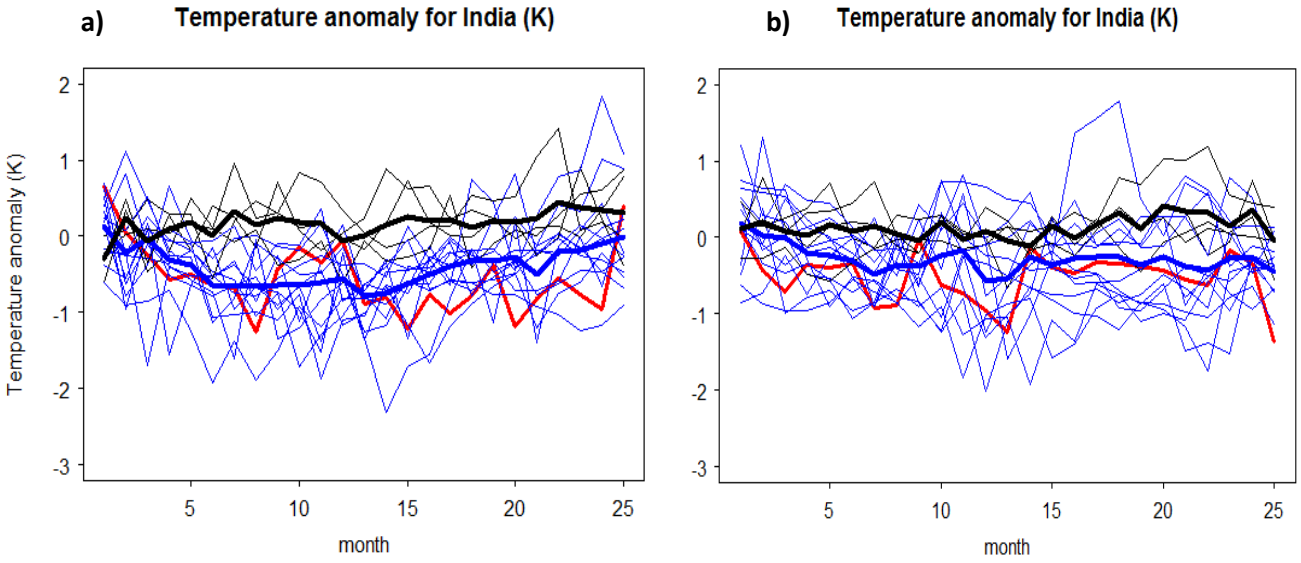

***Fig 4.11**: Monthly averaged evolution of temperature after the 13 tropical and 4 extra-tropical eruptions over the Indian continent (40N-5N; 65E-95E) for the **(a)** model EnsembleL1L2 and **(b)** model EnsembleM1M2. The thick red line shows the evolution of the temperature after the eruption of the Tambora. The blue lines represent the tropical eruptions whereas the black lines represent the extra-tropical eruptions. The two thick lines (black and blue) are the mean for extra and tropical eruptions respectively.*

It is also interesting to note that in both cases the Tambora eruption, which created the highest AOD perturbation, is not followed by the highest cooling. In the first Ensemble simulation the Cosiguina (1835) and the Pinatubo (1991) eruptions seem to have a greater influence. In the second case, the eruptions of Parker (1641), Huyanaputina (1600) and the 1809 eruption exert a greater influence on the temperature over this region.

The results of the linear model for the Indian continent differ notably between the two Ensemble simulations. On one hand, for the EnsembleL1L2 simulation the R-squared obtained are very low and none are significant at the 0.05 level (0.04 for the whole year as well as for the boreal winter and 0.26 for the boreal summer). On the other hand, for the EnsembleM1M2 simulation, the relation between the AOD and the Indian temperature anomaly is much higher (0.44 for the whole year, 0.45 for the boreal summer and 0.47 for the boreal winter). The R-squared obtained are all significant at the 0.05 level and tend to prove that the Indian surface temperature react negatively to volcanic forcing.

It is also interesting to note that in the linear models for the two Ensemble simulations there is an outlier which reduces the R-squared obtained. This outlier is the Tambora eruption and, according to the linear models, the anomaly observed after the Tambora eruption should be much higher over India. It was already the case when we looked at the tropical temperature but the divergence was much smaller. The magnitude of the anomaly seems thus to be proportional to the strength of the eruption even if we do not see a perfect linear dependence between these two variables.

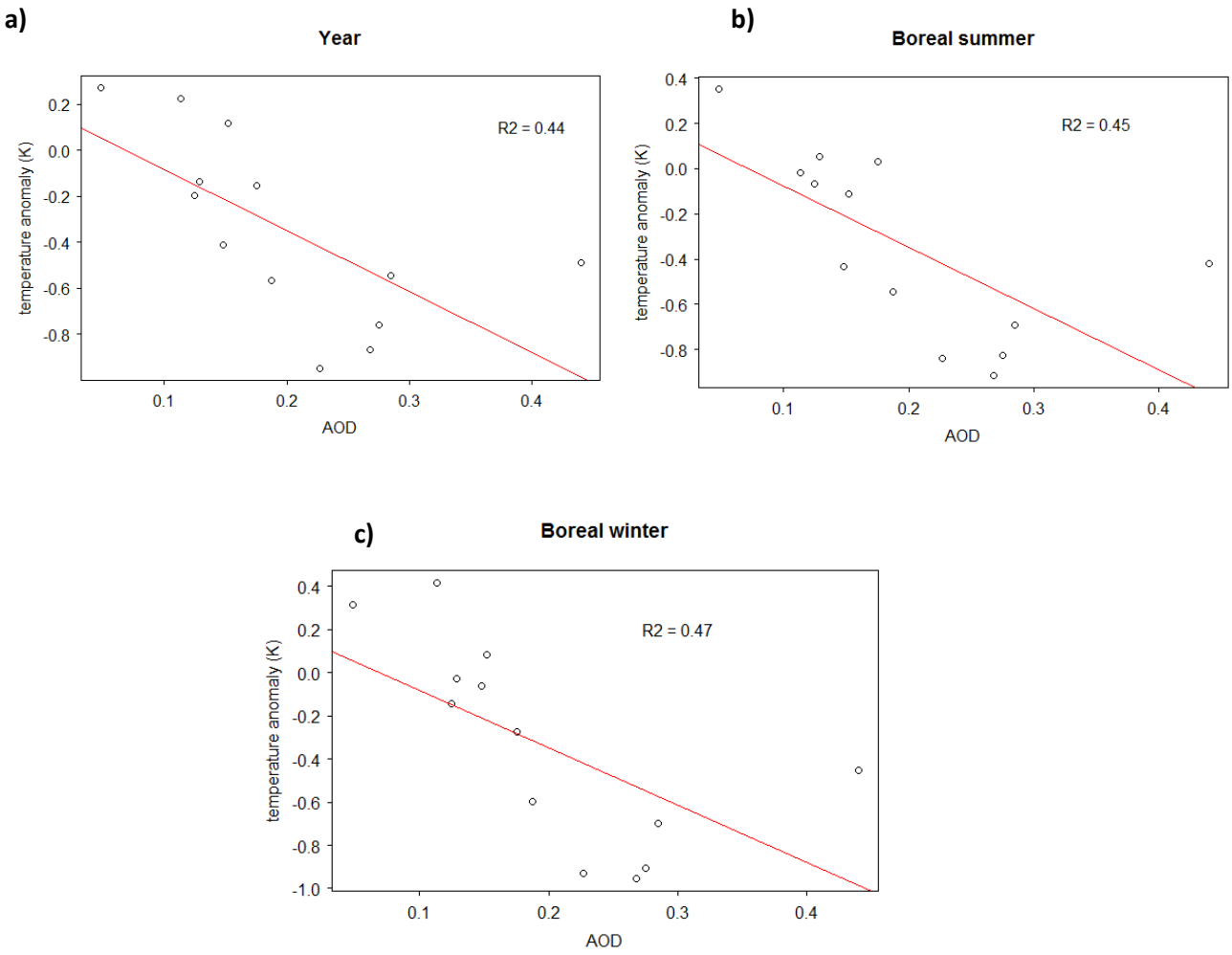

***Fig 4.12**: Simple linear regression model explaining Indian surface temperature anomaly through AOD (EnsembleM1M2 simulation). The dots represent 13 different tropical volcanic eruptions, and the red line is the regression line. In **(a)** 24 month following the eruptions have been chosen whereas in **(b)** and **(c)** the summer (JJAS) and the winter (DJF) months have been selected.*

If we look at the geographical surface temperature anomaly repartition, we discern interesting patterns. In Fig 4.13 we can see in average a clear cooling of the landmasses after tropical volcanic eruptions and none of the warming signals indicated are significant. In the summer season (Figure 4.13 a), the strongest cooling is found over South America, with values exceeding -1 K. Significant cooling is also found over large parts of Africa, India and South Asia.

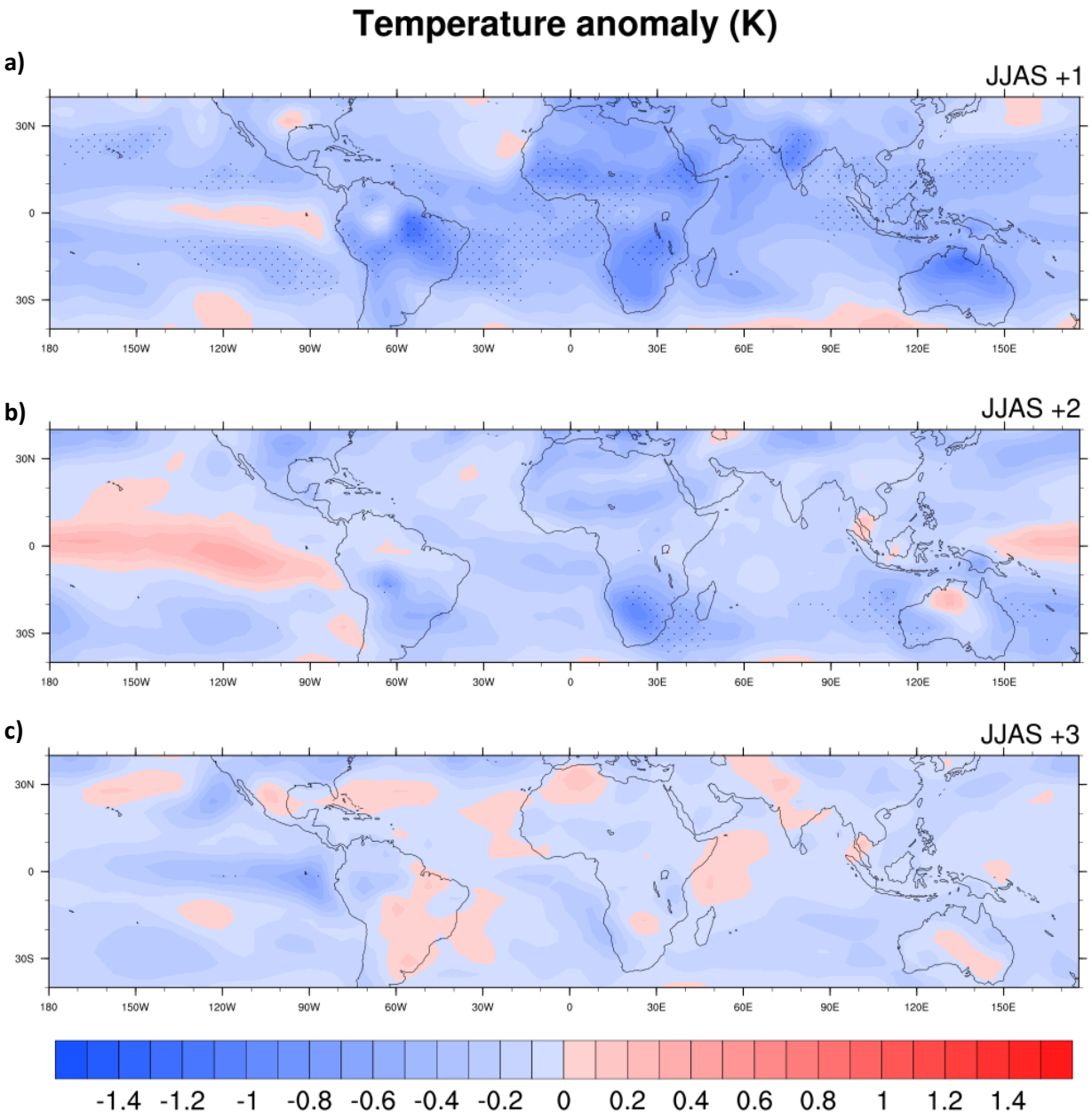

***Fig 4.13**: Averaged surface temperature anomalies (K) for the **(a)** first, **(b)** second and **(c)** third boreal summer (JJAS) following the 13 major tropical volcanic eruptions (EnsembleL1L2 simulation). Dotted areas represent 95% inter-eruption confidence level.*

It is also interesting to note that, unlike many other models and temperature reconstruction, the AOCCM SOCOL-MPIOM model does not capture any warming over Africa at summer 1. This warming, found in other studies (Robock 2000 ; Wegmann et al. 2014) could be due to the slowdown of the water cycle and the reduction of the cloud cover in the Intertropical Convergence Zone (ITCZ) but is not modelled by the GCM used in this study. If we look at the boreal summer evolution in the EnsembleM1M2 simulation, the situation is similar and no major changes can be perceived. It is although interesting to note that the cooling over India and South Asia is less prominent.

During the second boreal summer (Figure 4.13 b), the negative anomaly is significantly reduced. The only significant cooling patches are found over the south of Africa and on the west coast of Australia. But in general, the tropical regions still undergo a cooling even though it is not always significant at the 95% confidence level. In addition, almost no warming patterns are observed over land. Finally during the third summer (Figure 4.13 c), the negative anomalies are sharply reduced and the effects of the volcanic eruptions seem to disappear. Major volcanic eruptions seem thus to influence the summer surface temperature until two summer after the eruption. By and large, the cooling is also well observed over the ocean even if the signal is less homogeneous due to the thermal inertia. Some patches even undergo a warming. For example, a warming signal can be seen on the west coast of South America, especially during the second summer following an eruption. An El Niño like response with a lag of two years seems then to be computed by the model in the equatorial Pacific Ocean. This warm anomaly can also be found in the EnsembleM1M2 simulation after three years (Appendix A1).

It is interesting to note that the cold anomaly is not only observed over tropical regions but seems to be worldwide spread. Fig 4.14 shows the zonally averaged surface temperature anomaly and it is clear that the cooling does not only take place in the Tropics.

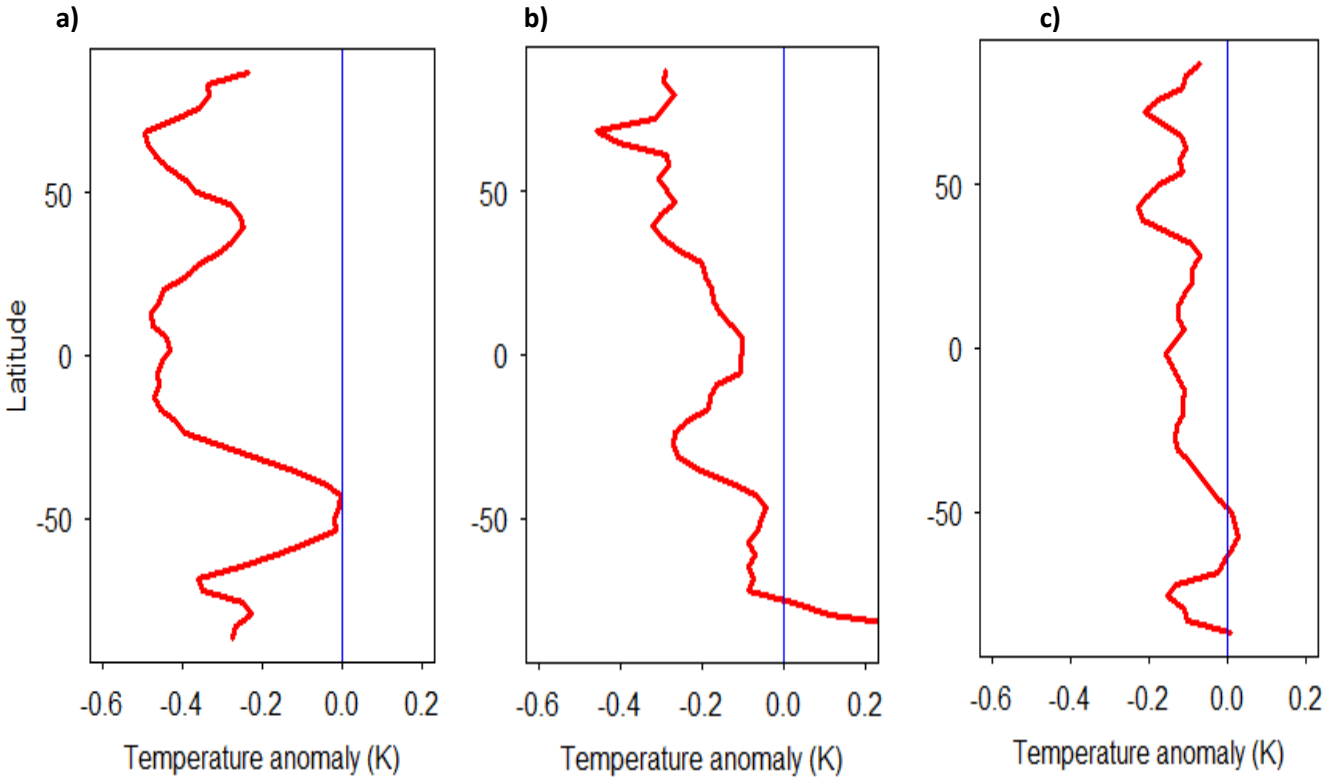

Fig 4.14*: Zonally averaged surface temperature anomaly for the* ***(a)*** *first,* ***(b)*** *second, and* ***(c)*** *third summer following the 13 major volcanic eruptions in the EnsembleL1L2 simulation.*

By and large, the average temperature anomaly reconstructed by the model is negative at all latitudes. It is also interesting to note that the temperature anomaly is much weaker in the southern hemisphere at high latitudes (around 50 °South). The absence of land masses and the higher heat capacity of the ocean seem to damp the atmospheric response.

In the previous figure, the magnitude of the anomaly gradually decreases between the first and the third summer. To be certain and because of this gradual decrease, we conducted a Superposed Epoch Analysis (SEA; see Chapter 3.5) which allows us to determine exactly during how long and with which time lag an eruption significantly affects tropical climate. The results of this SEA for the tropical regions are shown in Figure 4.15.

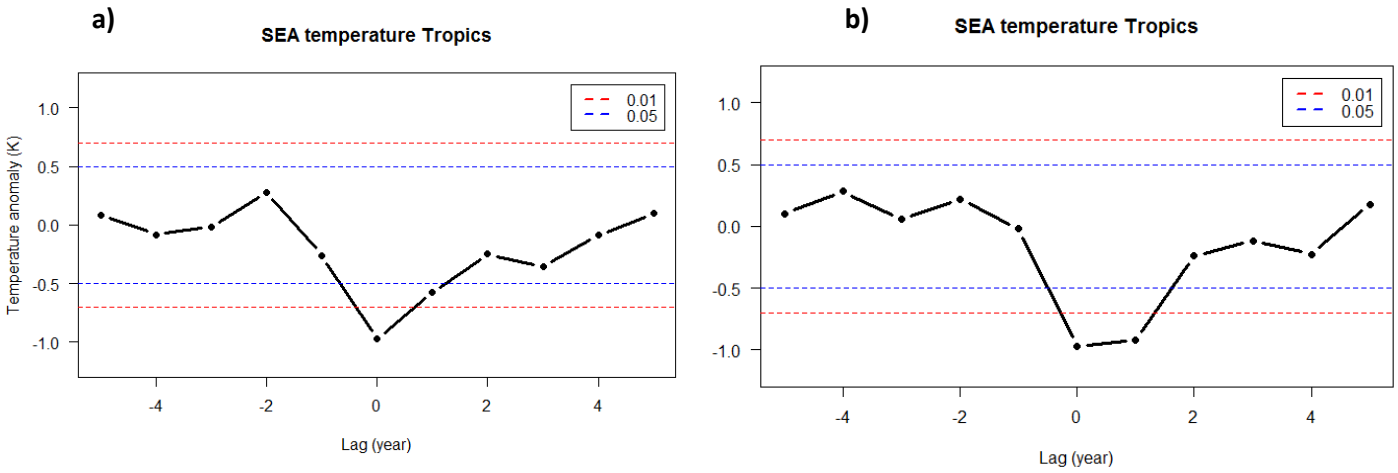

***Fig 4.15**: SEA results of boreal summer temperature over the Tropics for the 13 major volcanic eruptions for **(a)** EnsembleL1L2 and **(b)** EnsembleM1M2. The lag 0 correspond to the first summer following the eruption. The dashed lines represent the p-values at 1% and 5%.*

Our first impression is confirmed and major tropical volcanic eruptions seem indeed to have a significant effect on boreal summer temperature during the two summers directly following such an event. Note that in the case of the first Ensemble simulation, the temperature anomaly at lag +1 is slightly not significant at the 0.01 level (P-value of 0.03). If we look at the whole year and not only at the summer season, the SEA shows similar results.

If we look at the SSTs, we already observe a cooling during the first year following an eruption and surprisingly this cooling do not last longer as the surface temperature anomaly and already disappears at summer +2 (Figure 4.16 a). It is also interesting to note that in the AOCCM SOCOL-MPIOM model there is no significant link between major tropical volcanic eruptions and El Niño-Southern oscillation (ENSO) as suggested in Figure 4.13 a) and b). In contrary to the study of Adam et al. (2003), where they observed a strengthening of the El Nino phase after volcanic eruption, this index does not seem to respond significantly to volcanic forcing (Figure 4.16 b). Similar results are also found in the EnsembleM1M2 simulation (not shown).

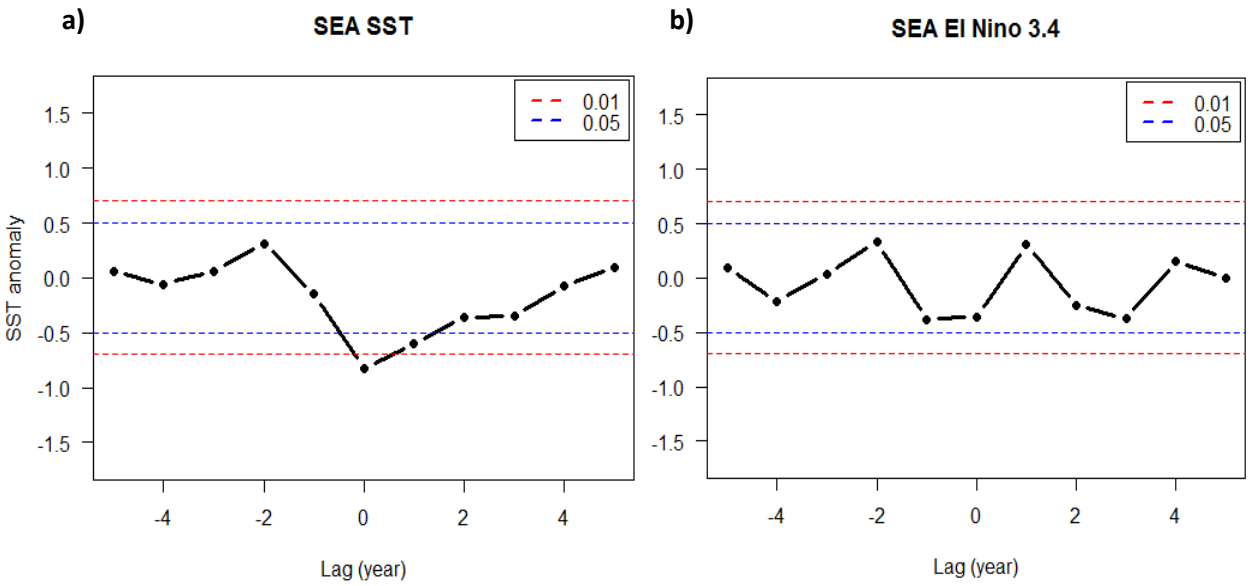

Fig 4.16: **(a)** SEA results of tropical sea surface temperature for the 13 major volcanic eruptions and **(b)** SEA results of El Niño 3.4 in EnsembleL1L2. The lag 0 corresponds to the first summer following the eruption. The dashed lines represent the p-values at 1% and 5%.

When considering only the Asian monsoon region, the pattern is relatively similar (Fig. 4.17).

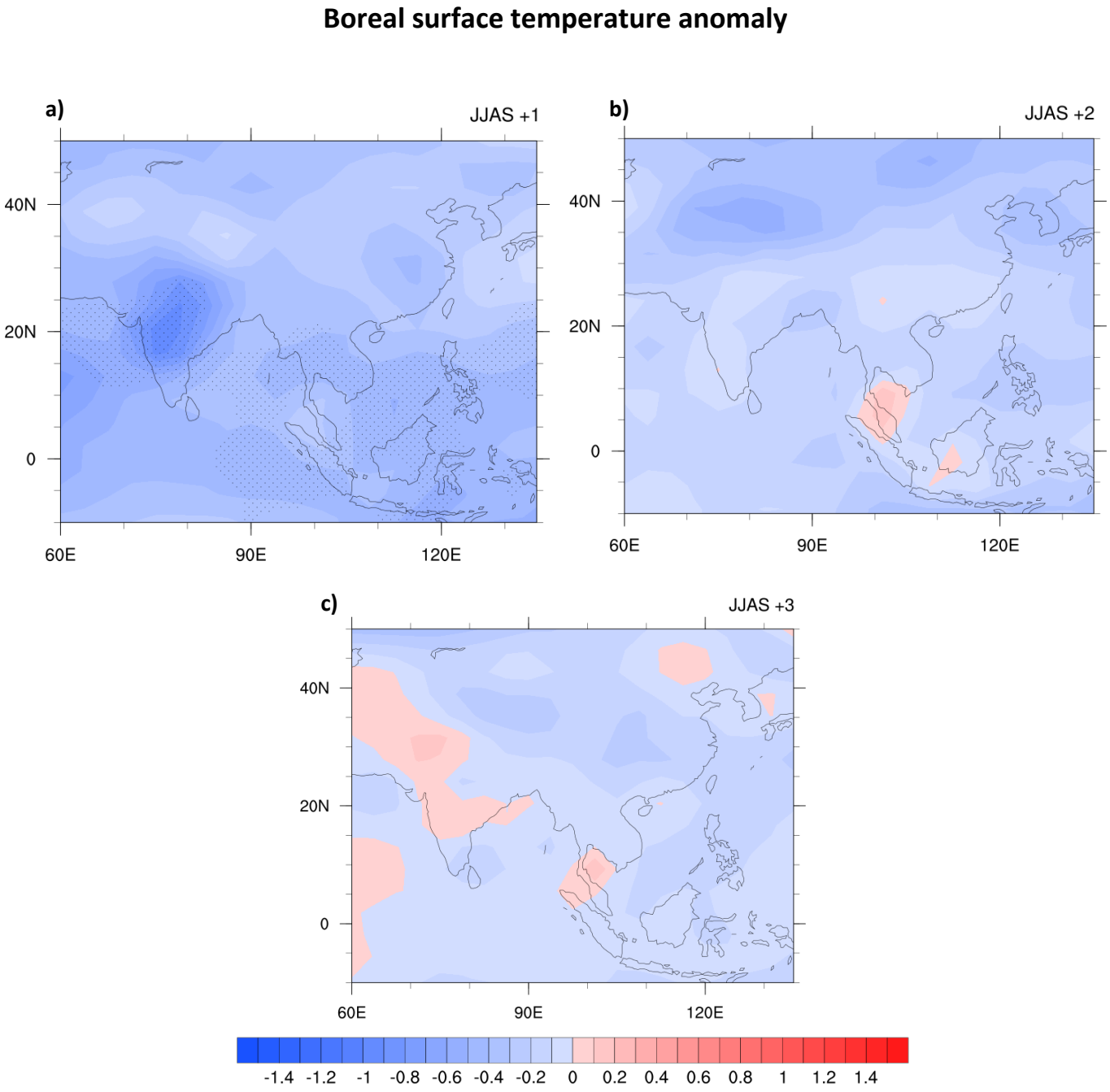

***Fig 4.17**: Averaged surface temperature anomalies (K) for the **(a)** first, **(b)** second and **(c)** third boreal summer (JJAS) following the 13 major tropical volcanic eruptions (EnsembleL1L2). Dotted areas represent 95% inter-eruption confidence level.*

A clear cooling can be observed over the whole Asian continent during the first summer directly following the eruption (Figure 4.17 a). In both Ensemble simulations, India and Southeast Asia undergo a significant cooling at the 0.05 level. Then the negative anomaly decreases gradually and almost vanishes after the second summer (Figure 4.17 b). The SEA results contained in Figure 4.18, confirms this impression. Indeed, after two years, the negative summer temperature anomaly is not significant anymore in both Ensemble simulations. Once more, if we perform the same analysis but for an anomaly averaged on the whole year similar results are obtained.

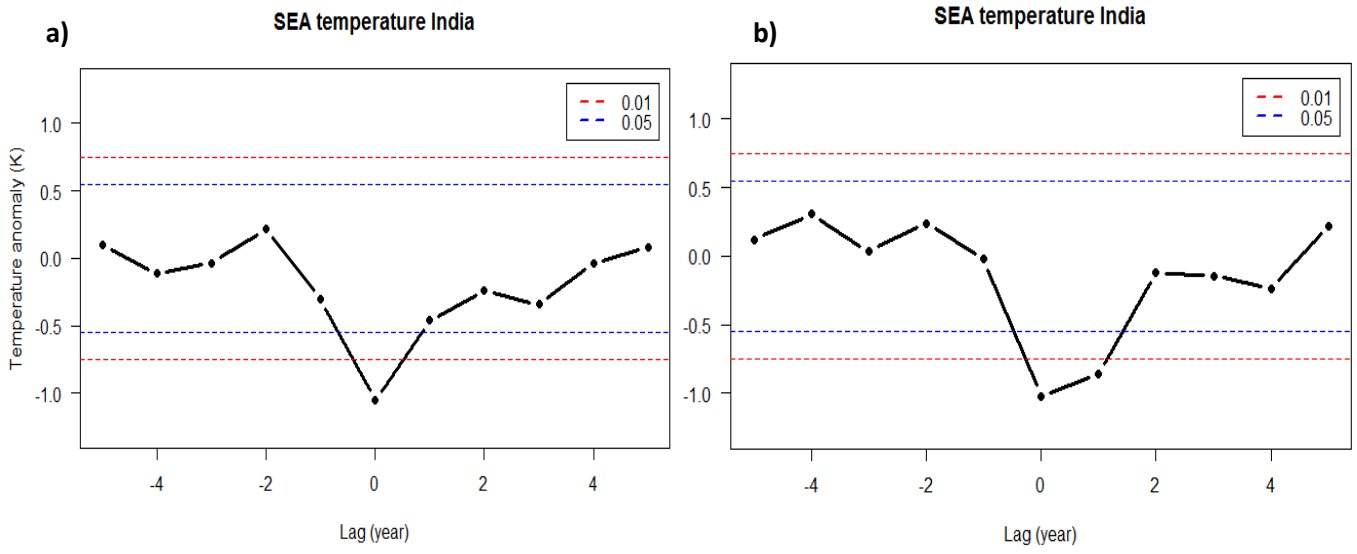

***Fig 4.18**: SEA results of boreal summer temperature over the Indian continent for the 13 major volcanic eruptions chosen for **(a)** EnsembleL1L2 and **(b)** EnsembleM1M2. The lag 0 corresponds to the first summer following the eruption. The two dashed lines represent the p-values at 1% and 5%.*

4.2.2: Stratospheric temperature

Contrary to the surface temperature (chapter 4.2.1), higher in the atmosphere, the temperature response is completely different. Due to the aerosol concentration, part of the Infrared and Near-Infrared radiations emitted by the Earth is absorbed in the stratosphere. Due to this absorption and a series of chemical reaction, this atmospheric layer is significantly heated. Therefore, the stratospheric temperature response to major tropical volcanic eruption is clear and a significant positive anomaly can be observed (Fig. 4.19) in the model.

Figure 4.19 gives an overview on the temperature evolution at 100 hPa. In both Ensemble simulations the eruption of the Mount Tambora creates the highest temperature anomaly which reaches about 6 K after 6 months. As for ground temperature, the mean influence of tropical volcanic eruptions is much higher in comparison with extra-tropical eruptions. A mean anomaly of about 1.5 K is observed 7 months after a tropical eruption, whereas none of the extra-tropical eruptions used in this study seem to have a global significant influence on the temperature at 100 hPa.

In comparison with others models (CCC400 model for example), it is interesting to note that the stratospheric temperature anomalies obtained with AOCCM SOCOL-MPIOM are much weaker and more in agreement with the stratospheric anomaly measured after the Pinatubo eruption (Robock et al. 2010).

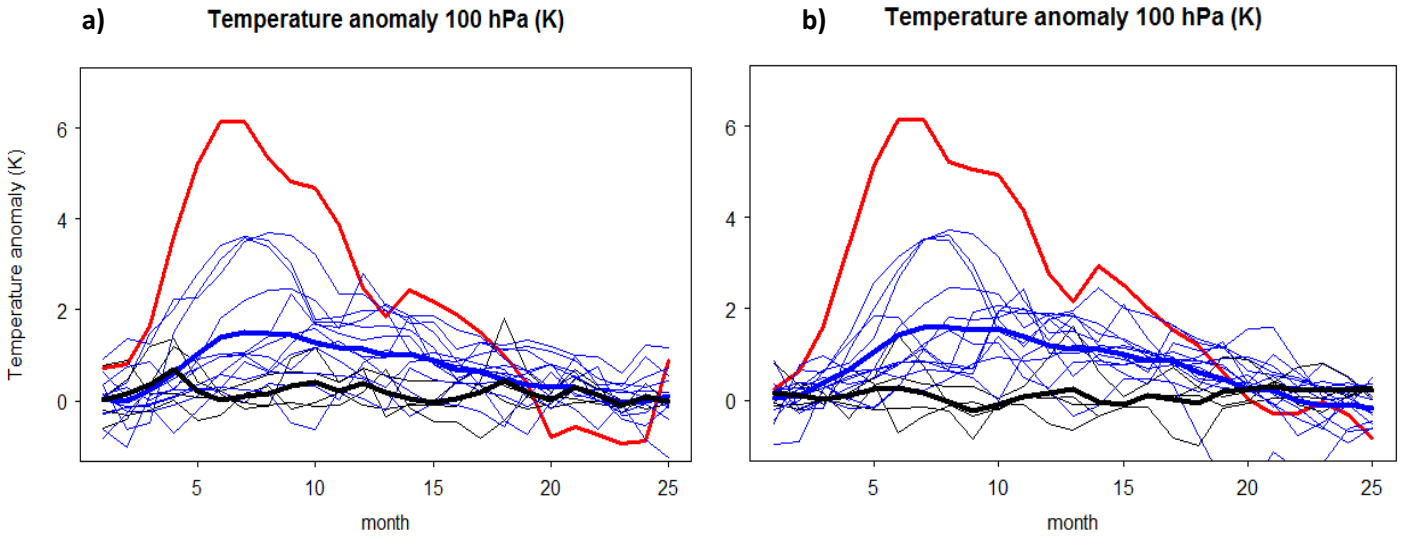

***Fig 4.19**: Monthly averaged evolution of the temperature over the Tropics (40N-40S; 180W-180E) after 13 tropical and 4 extra-tropical eruptions for the **(a)** model EnsembleL1L2 and **(b)** model EnsembleM1M2 simulations. The thick red line shows the evolution of the temperature after the eruption of the Tambora. The blue lines represent tropical eruptions, while the black lines represent extra-tropical eruptions. The two thick lines (black and blue) are the mean for extra and tropical eruptions respectively.*

Once more, the tropical and extra-tropical eruptions do not trigger the same atmospheric response. Indeed, according to Gao et al. (2008) and in term of H_2SO_4 emitted, the eruptions of the Mount Laki and Tambora were not so different. On one hand the Mount Tambora emitted about 110 Tg of H_2SO_4 equally distributed in both hemisphere (58.7 Tg for the northern hemisphere and 51 Tg for the southern hemisphere). Note that Sigl et al. (2013) disagrees: for them about 75% of the Tambora aerosol ended up in the Southern hemisphere. On the other hand the estimated mass of sulfuric acid formed after the

eruption of the Mount Laki (Iceland) is equal to 93 Tg but exclusively distributed in the northern hemisphere. The stratospheric temperature response observed in the model after these two events is drastically different due to the global atmospheric circulation and the difficulty of interhemispheric exchanges of air masses. Whereas the eruption of the Mount Tambora is followed by a strong and significant warming, the maximum anomaly reconstructed by both simulations after Laki is only equal to about 0.7K. If we look only among the 13 tropical eruptions, the linear relationship between the magnitude of the eruption and the stratospheric temperature response is really high. Both Ensemble simulations show a strong correlation between these two variables with R-squared equal to 0.87 in both cases (Fig. 4.20).

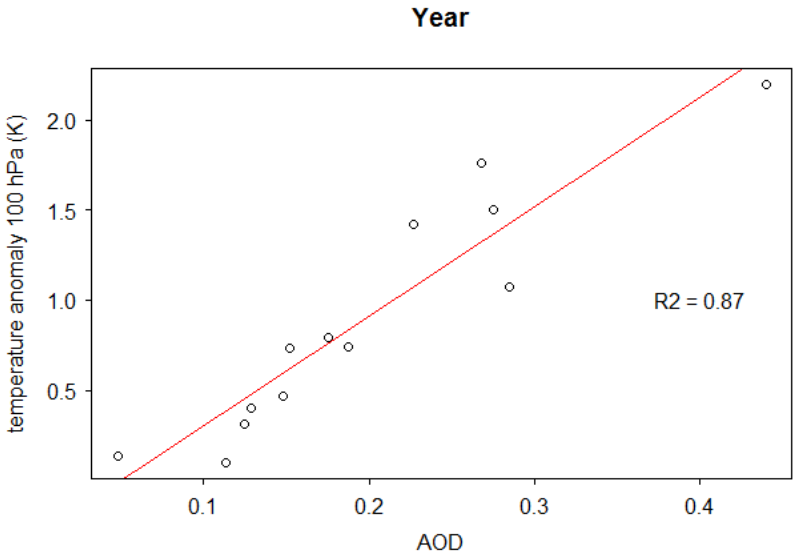

***Fig 4.20**: Simple linear regression model explaining the temperature anomaly at 100 hPa through AOD (EnsembleL1L2 simulation). The dots represent the 13 different tropical volcanic eruptions, and the red line is the regression line. The 24 months following the eruptions have been chosen to define the anomaly.*

Fig 4.21 shows the geographical repartition of the temperature anomaly at 100 hPa and some interesting results. First of all, one year after a tropical eruption, a significant warming of the stratosphere is observed over the main part of the globe. A lower warming could have been expected in the southern hemisphere because, out of the 13 tropical volcanic eruption, only 5 (Huaynaputina, Serua, Tambora, Krakatau and Agung) occurred south of the equator. Furthermore, a significant cooling is found at high latitude in the southern hemisphere and could have been generated by a strengthening of the Southern Annular Mode (SAM). Indeed, the stronger westerlies above the Southern Ocean generated by a positive SAM index isolate Antarctica and limit then the heat exchange with the higher latitude. According to Kalnay et al. (1996) a positive SAM index is indeed generally followed by a significant surface cooling over Antarctica. We investigate in a further section the link which exists between the SAM and volcanic forcing (Figure 4.43). It is also interesting to note that we can distinguish a temperature gradient between the tropical regions and the high latitude. Due to the higher incoming solar radiation and the warmer ground surface temperature in the Tropics (increased emission of Infrared radiations), the stratospheric warming recorded is bigger around the equator as at higher latitudes. In the high latitude regions, the heating is reduced because of the lower incoming solar radiation and outgoing long wave radiations.

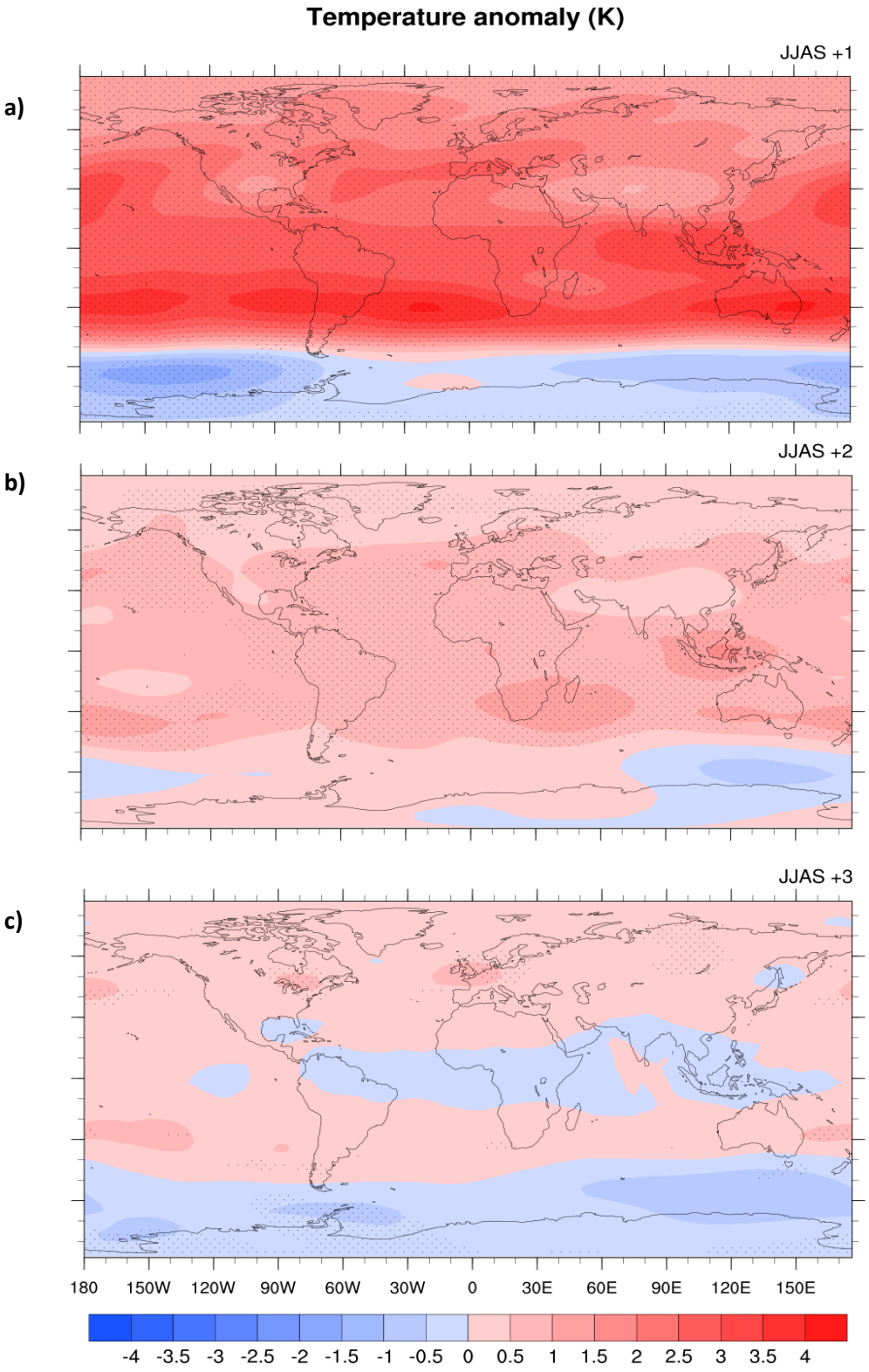

***Fig 4.21**: Averaged temperature anomalies (K) at 100 hPa for the **(a)** first, **(b)** second and **(c)** third boreal summer (JJAS) following the 13 major tropical volcanic eruptions (EnsembleL1L2 simulation). Dotted areas represent 95% inter-eruption confidence level.*

A meridional stratospheric temperature gradient is thus formed between these regions. This gradient generates then thermal winds and for example a strengthening of the polar vortex is observed after most of the eruptions. These dynamical anomalies can then be propagated downwards and perturb the global dynamic of the atmosphere (Section 4.2.4). This meridional stratospheric temperature gradient is well captured in Figure 4.21 and 4.22.

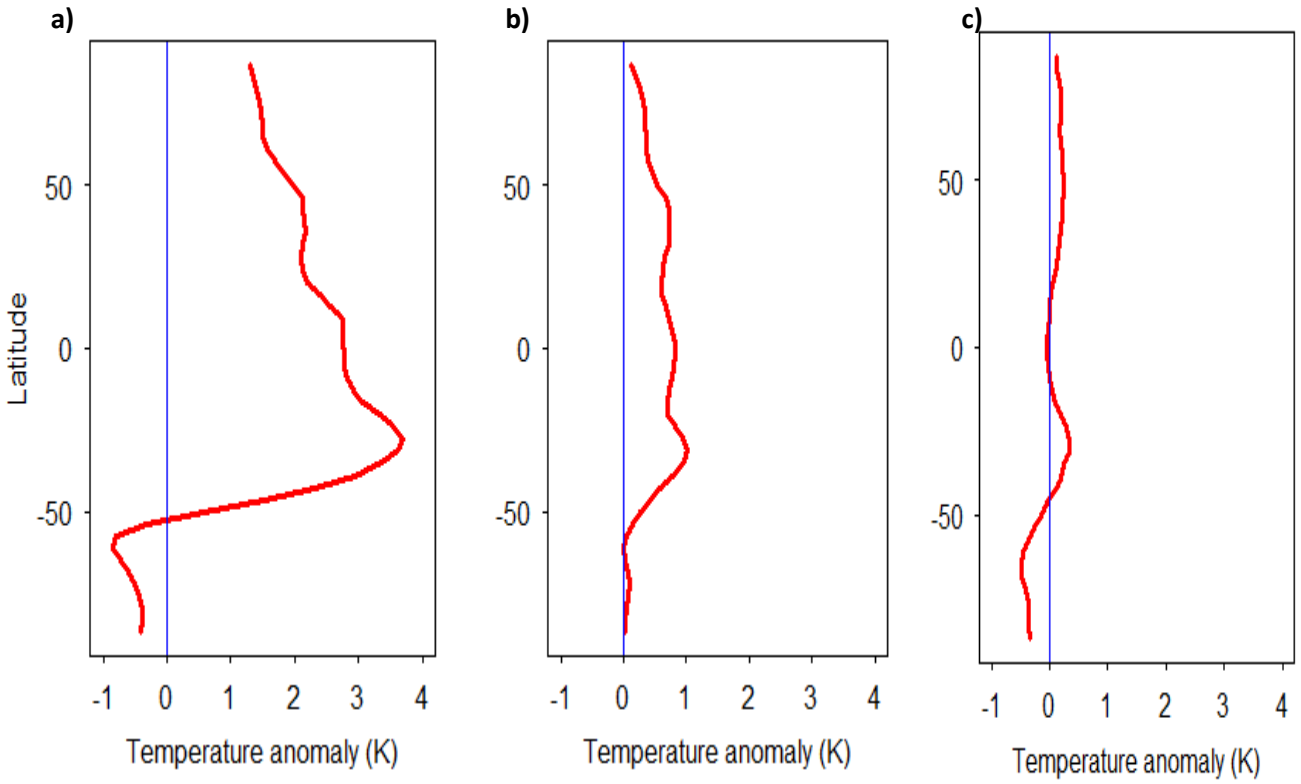

***Fig 4.22**: Zonally averaged temperature anomaly at 100 hPa for the **(a)** first, **(b)** second, and **(c)** third summer following 13 major volcanic eruptions in the EnsembleL1L2 simulation.*

The positive anomaly seems to vanish quickly and because of the relative short residence time of the sulfuric acid in the stratosphere, no significant anomaly can be found 3 years after a major tropical volcanic eruption. In both Ensemble simulations, the results are similar and the significance of the anomaly begins already to decrease at year +2 and disappears afterwards.

The SEA presented in Figure 4.23 confirms this impression. In both Ensemble simulations, the anomaly is highly significant at lag 0 but then decreases quickly. At lag +1 the anomaly is still slightly significant in the EnsembleL1L2 simulation but not anymore in the EnsembleM1M2 simulation. At lag +2 none of the anomaly registered are significant and the effects of the eruption have fully vanished.

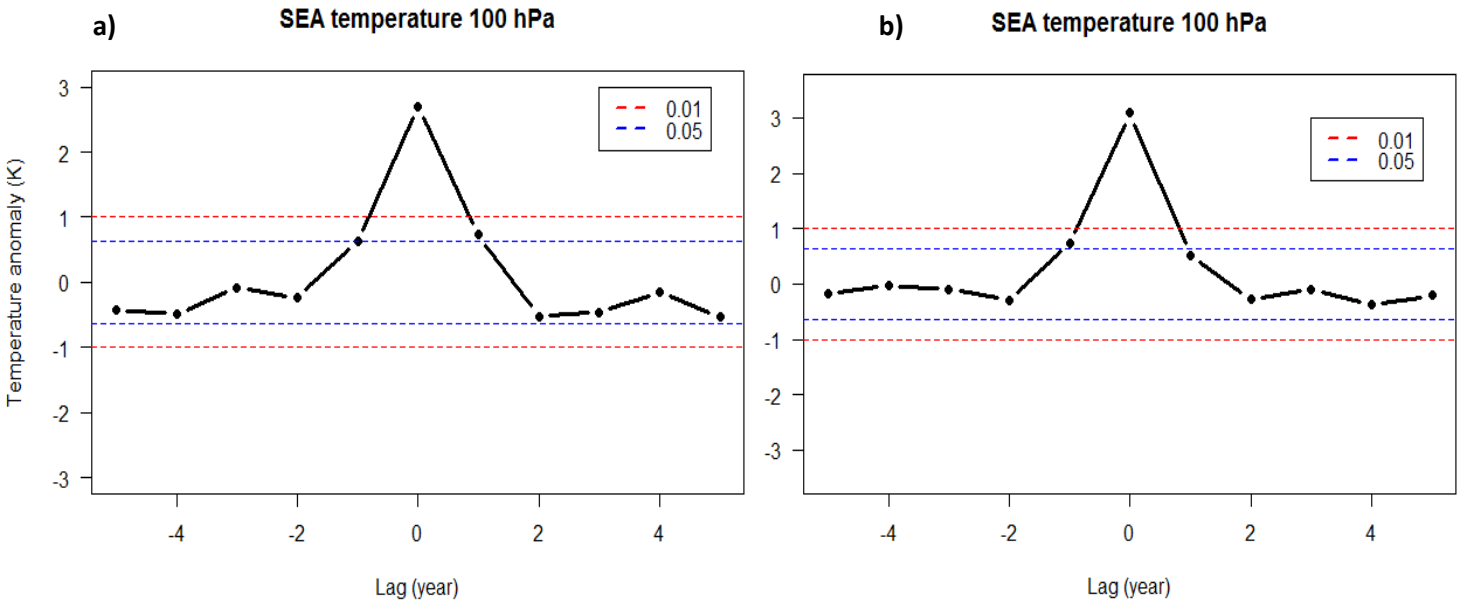

***Fig 4.23**: The SEA results of temperature at 10 hPa for the 13 major volcanic eruptions chosen for **(a)** EnsembleL1L2 and **(b)** EnsembleM1M2. The lag 0 corresponds to the first summer following the eruption. The two dashed lines represent the p-values at 1% and 5%.*

4.2.3: Precipitation

Unlike temperature, the evolution of the water cycle after major tropical volcanic eruptions is less understood. For the tropics as a whole, a drying is expected. Indeed, in those regions the formation of precipitation is closely linked to the Total Solar Irradiance (TSI). The temperature decreases observed in Chapter 4.2.1 should then lead to a decrease of the evaporation and of the precipitation. At a regional level, where dynamical processes sometimes lead to precipitation formation, the situation could be different. The Indian continent is a good example since a significant part of the summer precipitation is due to the Indian Monsoon and should not be directly impacted by TSI.

Figure 4.24 shows the evolution of precipitation over the tropics for two Ensemble simulations of the AOCCM SOCOL-MPIOM. The two Ensemble simulations show a clear decrease in precipitation. During the first 24 months the anomaly is in both models always negative and reach a minimum of about -0.07 mm/day after 9 months (Ensemble L1L2) and -0.06 mm/day after 8 months (EnsembleM1M2). Then the negative anomaly slightly decreases and, after 2 years, the effects seem to have vanished. It is interesting to note that in both case, the Tambora eruption creates the biggest perturbation which reaches about 0.2 mm/day after 9 months. Once more in this model, the 4 extra tropical eruptions do not have any significant impact on tropical perturbation and it is hard to detect any trend in the precipitation evolution.

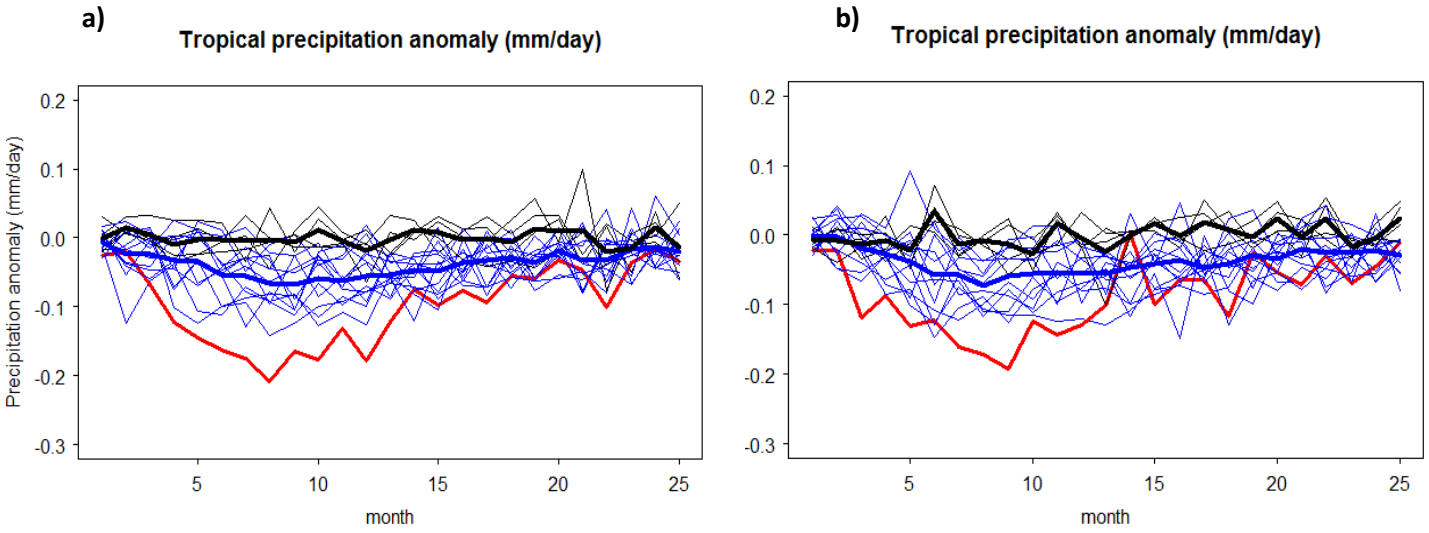

***Fig 4.24**: Monthly averaged evolution of precipitation after the 13 tropical and 4 extra-tropical eruption over the Tropics (40N-40S; 180W-180E) for the **(a)** model EnsembleL1L2 and **(b)** model EnsembleM1M2 . The thick red line shows the evolution of precipitation after the eruption of the Tambora. The blue lines represent the tropical eruptions, while the black lines represent the extra-tropical eruptions. The two thick lines (black and blue) represent the mean for extra and tropical eruptions*

As shown in Figure 4.25, the linear relationship between the strength of an eruption (expressed as AOD) and the precipitation anomaly is highly significant at the tropical scale. The two Ensemble simulations give similar result with highly significant R-squared values. It is also interesting to note that all the 13 tropical eruptions are followed by a negative precipitation anomaly. It was already the case for the temperature and this tends to prove that at the tropical level, the evolution of those 2 variables is closely

linked. The eruption of Mount Tambora creates an averaged summer anomaly of -0.1mm/day. The second biggest anomaly followed the eruption of Mount Parker with -0.08 mm/day (Figure 4.24 b).

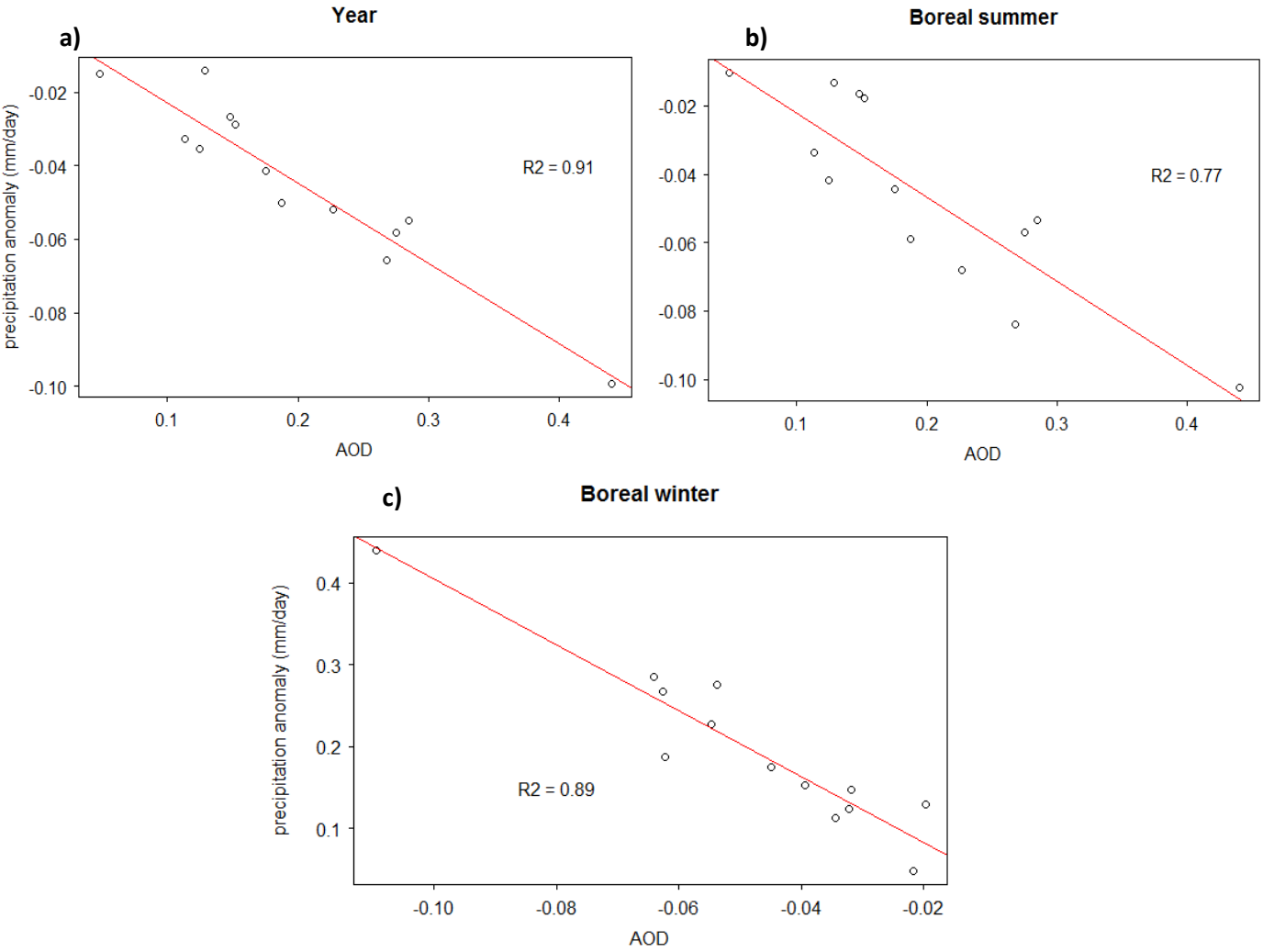

Fig 4.25*: Simple linear regression model explaining the tropical precipitation anomaly through AOD (EnsembleL1L2 simulation). The dots represent the 13 different tropical volcanic eruptions and the red line shows the regression line. In* ***(a)*** *the 24 month following the eruptions have been chosen whereas in* ***(b)*** *and* ***(c)*** *the summer (JJAS) and the winter (DJF) month have been selected*

As for temperature, the variability is higher when considering the Indian continent only and it is hard to distinguish any clear pattern. In Figure 4.26, the precipitation does not seem to be significantly affected by volcanic eruptions. Unlike what has been observed so far for the tropical regions, no drying can be seen over India. The same observation can be made after the eruption of Mount Tambora where the magnitude of the anomaly is not higher as for the 12 others tropical eruptions. The two Ensemble simulations even model a slight positive anomaly of about 1 mm/day after 13 months. But this anomaly does not persist and vanishes quickly. It is also interesting to note that the effects generated by extra and tropical eruptions are not significantly different and both mean stay around 0 mm/day during the first two years.

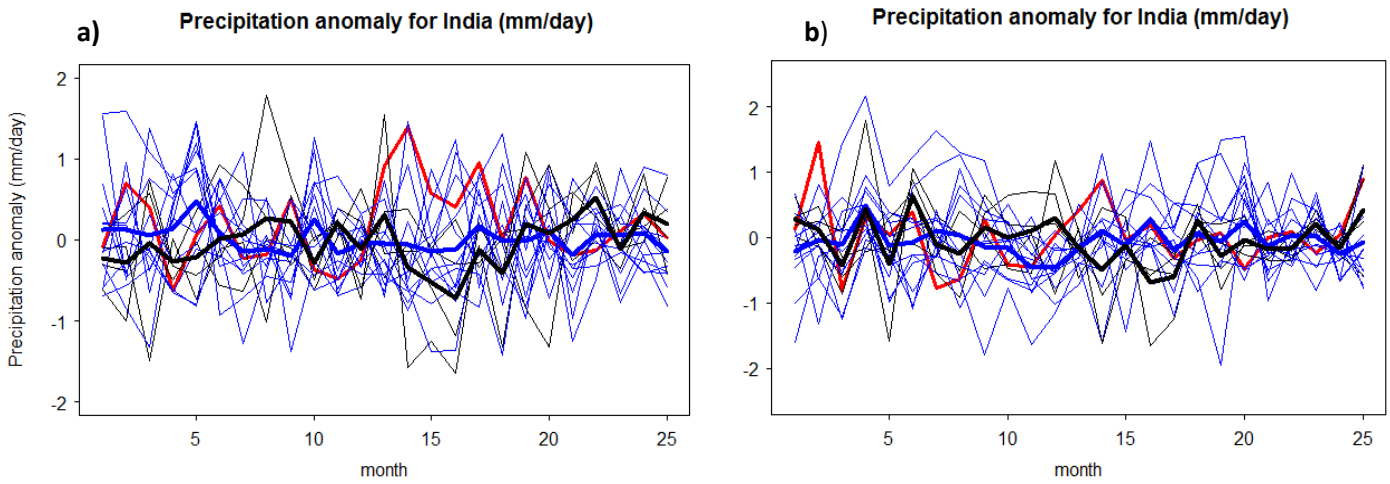

***Fig 4.26**: Monthly averaged evolution of precipitation after the 13 tropical and 4 extra-tropical eruption over the Indian continent (40N-5N; 65E-95E) for the **(a)** model EnsembleL1L2 and **(b)** model EnsembleM1M2. The thick red line shows the evolution of precipitation after the eruption of the Tambora. The blue lines represent the tropical eruptions, while the black lines represent the extra-tropical eruptions. The two thick lines (black and blue) represent the mean for extra and tropical eruptions*

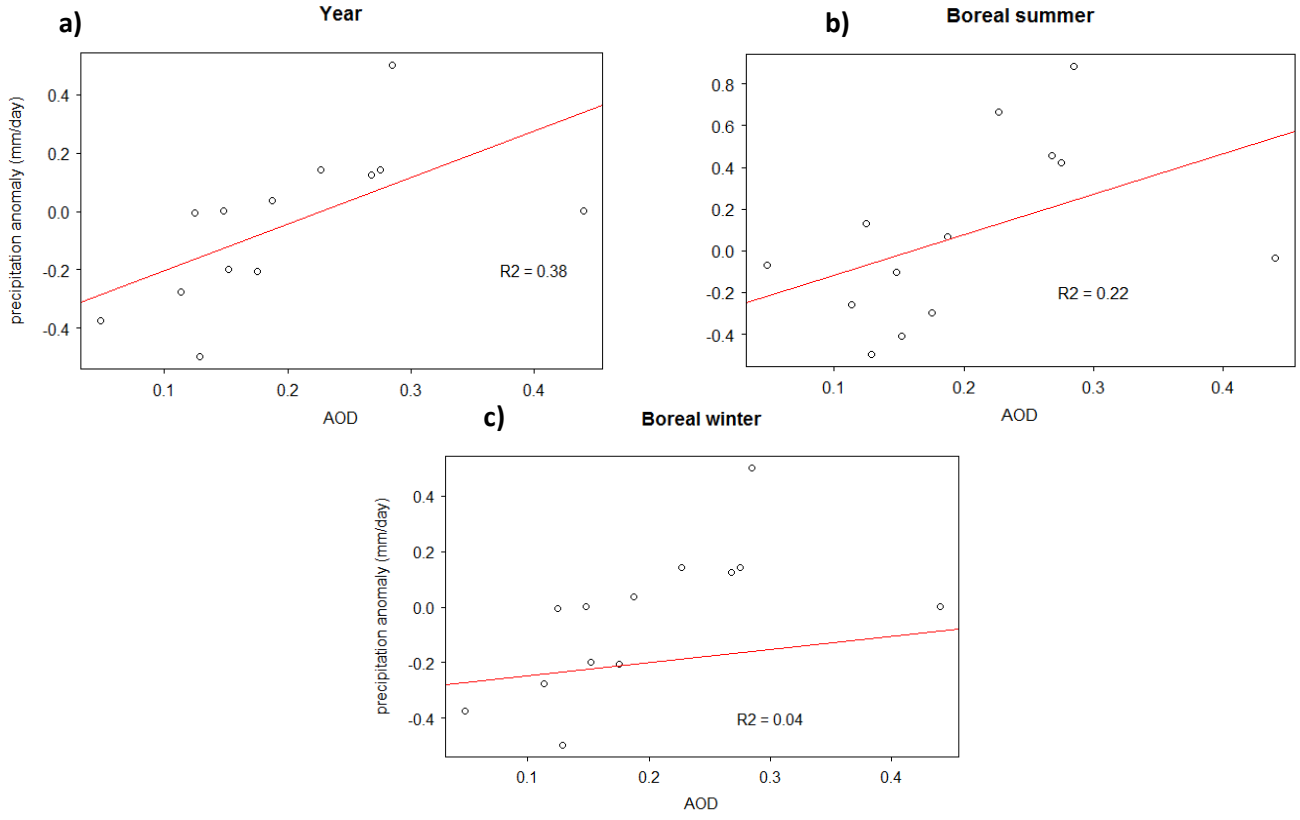

***Fig 4.27:** Simple linear regression model explaining the Indian precipitation anomaly through AOD (EnsembleM1M2 simulation). The dots represent the 13 different tropical volcanic eruptions and the red line shows the regression line. In **(a)** the 24 month following the eruptions have been chosen whereas in **(b)** and **(c)** the summer (JJAS) and the winter (DJF) month have been selected.*

Figure 4.27 confirms these impressions and the linear model constructed shows that there exists only a weak linear relationship between the precipitation anomaly observed over India and the strength of a volcanic eruption. While for the first Ensemble simulation none of the R-squared obtained are significant, the situation is different for the Ensemble M1M2 simulation. Indeed, the summer and annual precipitation seem to increase after the biggest eruptions of our dataset. A positive correlation is found between these two variables, with R-squared significant at the 0.05 (whole year) and 0.1 level (boreal summer). There is nevertheless an eruption which doesn't follow this pattern at all. Indeed the anomaly following the Tambora eruption is much weaker as expected and stays around 0 mm/day (-0.03 mm/day). This sharply reduces the values of the R-squared obtained. In this model simulation, approximately 7 out of 13 tropical eruptions are followed by a positive anomaly (Figure 4.27 b). The largest mean summer anomaly registered during the two first years reached 0.88 mm/day after the eruption of Huaynaputina and 0.66 mm/day after the eruption of Cosiguina.

Figure 4.28 shows the geographical repartition of the precipitation anomaly. By and large, a drying can be observed all over the tropical regions. Reduced precipitation is observed in the EnsembleL1L2 simulation over South America and Southeast Asia and the negative anomaly is in some places, larger than -1 mm/day. We can also observe a belt with reduced precipitation around the equator, which corresponds more or less to the Intertropical Convergence Zone (ITCZ) during boreal summer. If we look at the precipitation anomaly during the boreal winter, a dry belt can also be distinguished. But this belt seems to have moved southwards following the ITCZ position during boreal winter (Appendix A2). The precipitation in this convergence zone seems thus to react to incoming solar radiation.

Unlike the temperature anomaly, the precipitation anomaly does not seem to vanish after the second summer. Indeed, even though the magnitude of the anomaly decreases, one can still find a lot of significant dry patches during the third boreal summer. In most of the cases, the wet anomalies computed by the model are not significant. Nevertheless, it is interesting to note the significant wetting over Western Ghats (India) and the Arabian basin during the first summer. During the second summer a wet anomaly appears over the Pacific Ocean. This could be due to the temperature increase noticed in Figure 4.13 b. Once more, the two Ensemble simulations showed more or less similar results. A dry belt is also seen around the equator and none of the wet patches displayed are significant. With one notable exception: a significant positive anomaly over the Indian continent can be found during the second summer in the EnsembleM1M2 simulation (Appendix A2). As for the first Ensemble simulation, the anomaly seems to persist during at least three years. In contrary to the tropics where a clear drying is observed, the response is less clear for the rest of the globe. Nevertheless, a slight zonally averaged drying can be observed at almost all latitude in Figure 4.29.

The magnitude of the zonally averaged anomaly is not as pronounced as the one recorded in the tropical region (-0.3 mm/day), but still reaches -0.1 mm/day at higher latitudes. Then this dry anomaly decreases sharply after the first summer but is still visible until the third summer. At summer +3, the negative anomaly reaches about 0.1 mm/day and none of the positive anomaly recorded seem to be significant (Figure 4.29 c).

This impression is confirmed in Figure 4.30. The results of the SEA show that the negative precipitation anomaly is highly significant during the year of the eruption (lag 0) and then decreases slowly. The anomaly observed three years after the eruption is in both case still significant. This was not the case for the temperature where the negative anomaly already began to vanish at lag +1. The precipitation anomaly seems thus to persist and last longer as the temperature anomaly. This can be explained by the thermal inertia of the oceans which stay cold a bit longer in comparison with the landmasses.

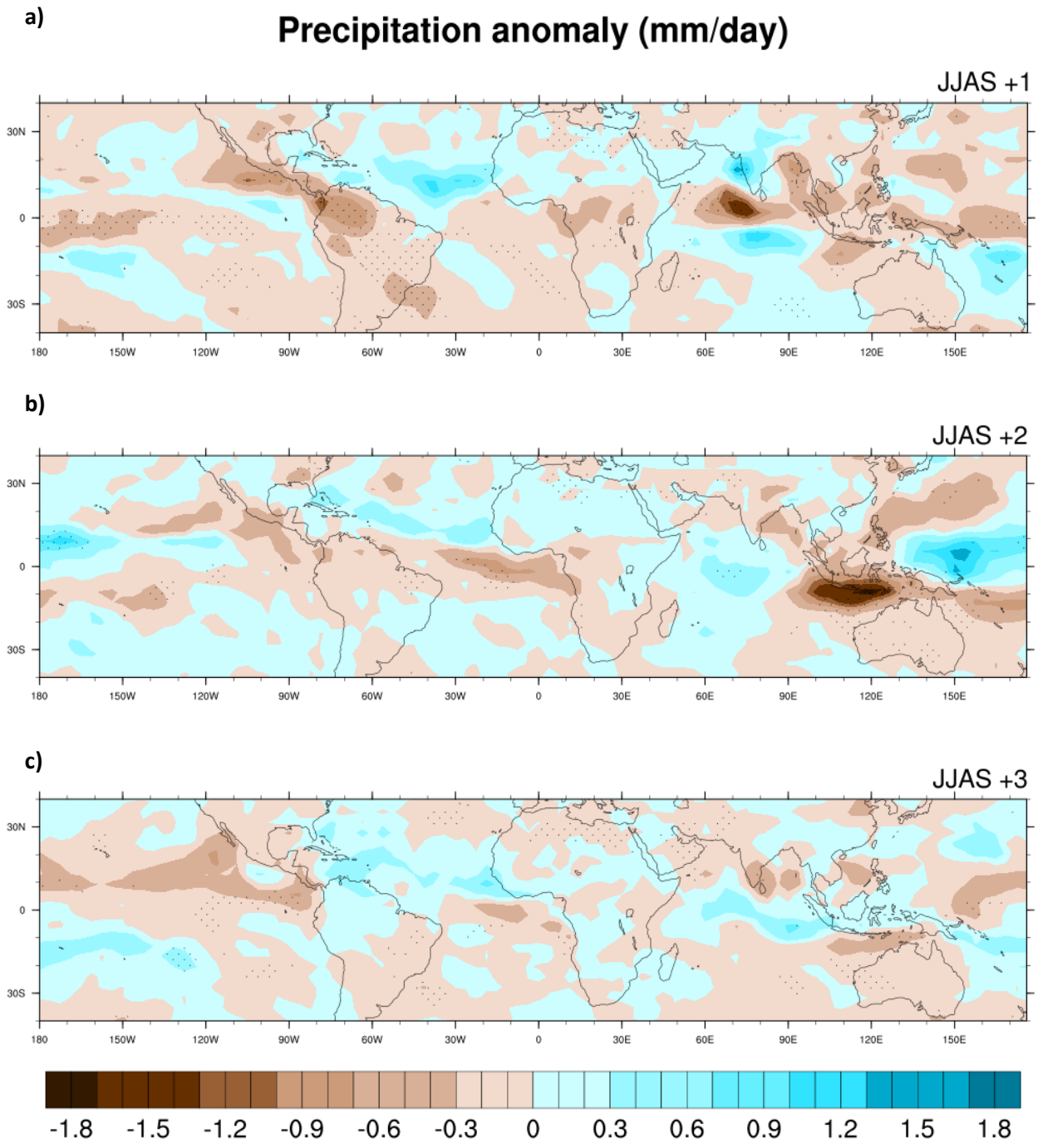

***Fig 4.28**: Averaged precipitation (mm/day) anomalies for the **(a)** first, **(b)** second and **(c)** third boreal summer (JJAS) following the 13 major tropical volcanic eruptions (EnsembleL1L2 simulation). Dotted areas represent 95% inter-eruption confidence level for the precipitation.*

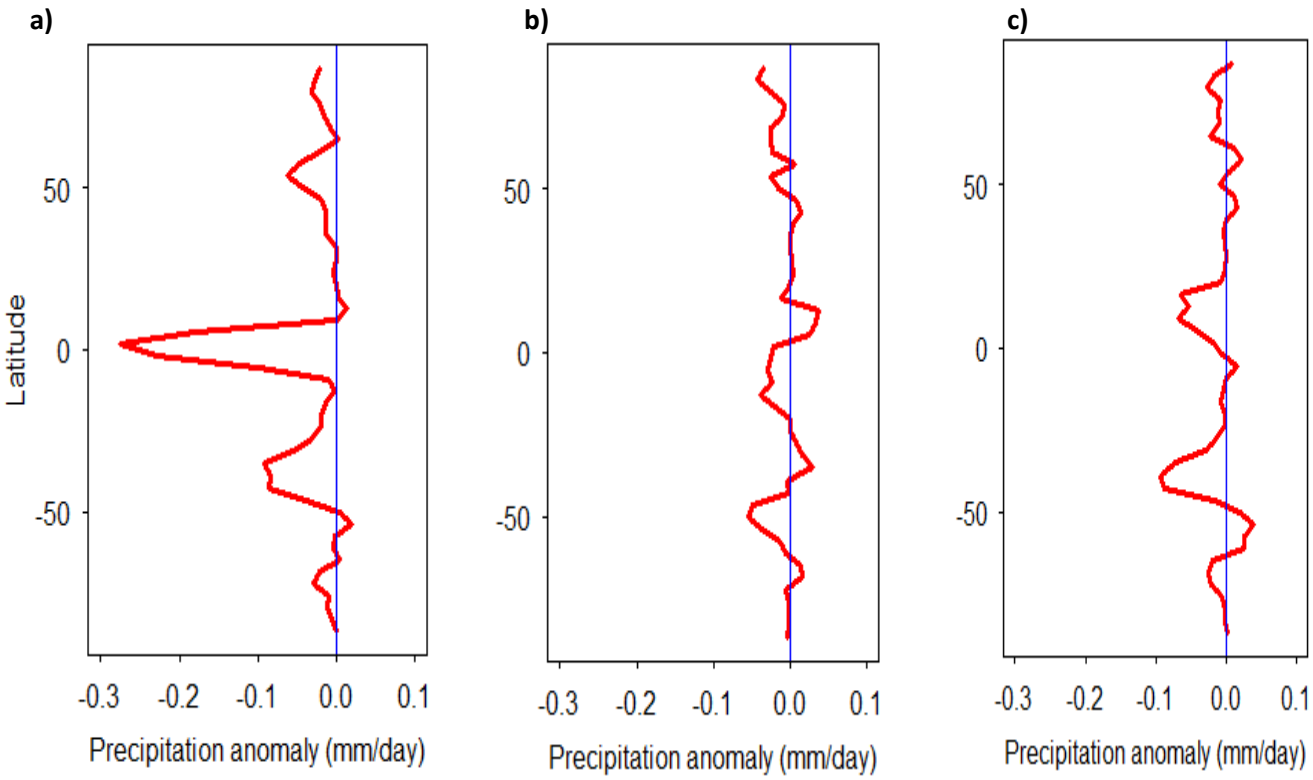

Fig 4.29: *Zonally averaged precipitation anomaly for the* ***(a)*** *first,* ***(b)*** *second, and* ***(c)*** *third summer following the 13 major volcanic eruptions in the EnsembleL1L2 simulation.*

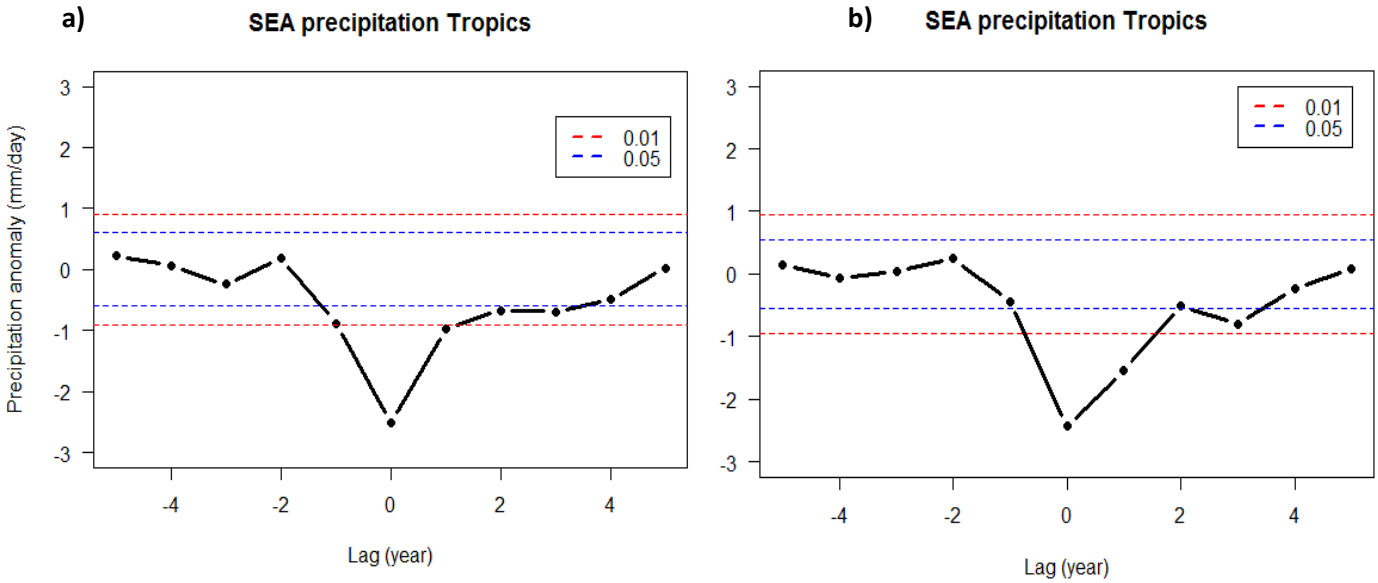

Fig 4.30*: SEA results of boreal summer temperature over the Tropics for the 13 major volcanic eruptions for* ***(a)*** *EnsembleL1L2 and* ***(b)*** *EnsembleM1M2. The lag 0 corresponds to the first summer following the eruption. The two dashed lines represent the p-values at 1% and 5%.*

In figure 4.31 the scope of the analysis has been reduced and a focus has been set on the Asian continent. Once more number of significant drying patches can be found all over the southeast of Asia and Indonesia. The drying over Indonesia is significant in both simulations and reaches almost 2 mm/day during the second summer. The northern parts of the continent, as well as the regions distant from the coasts, seem to be less affected. Over the Indian continent the situation is different. Both Ensemble simulations give approximately the same results and no significant drying patches can be observed during the two first boreal summers following a major tropical eruption. The only significant negative anomaly is produced by the EnsembleL1L2 simulation over Sri Lanka after 3 summers (Figure 4.31 c).

But surprisingly, the EnsembleL1L2 and EnsembleM1M2 simulations rather produce positive anomaly during the first and the second summer over India. It is interesting to look at the zonal wind anomaly at 850 hPa which have been added in figure 4.31. In the EnsembleL1L2 simulation, an increase in the strength of westerlies winds is jointly observed with a positive precipitation anomaly. During the second summer the wind anomaly decreases significantly and vanishes almost completely during the third summer. Precipitation follows more or less the same pattern and it seems that there is a link between these two variables over the Indian continent in the AOCCM SOCOL-MPIOM simulations. Indeed westerlies bring moisture from the Bay of Bengal and could explain a part of the precipitation variability over South of India. The same analysis was done for the EnsembleM1M2 simulation (not shown) and similar conclusion can be drawn: During the second summer a positive precipitation anomaly is jointly observed to the strengthening of the westerlies wind over the southern part of India. During the third summer, the magnitude of the wind anomaly is sharply reduced while the wetting patches completely vanished. The response of zonal winds to volcanic forcing will be carefully analyzed in a further section (Section 4.2.4)

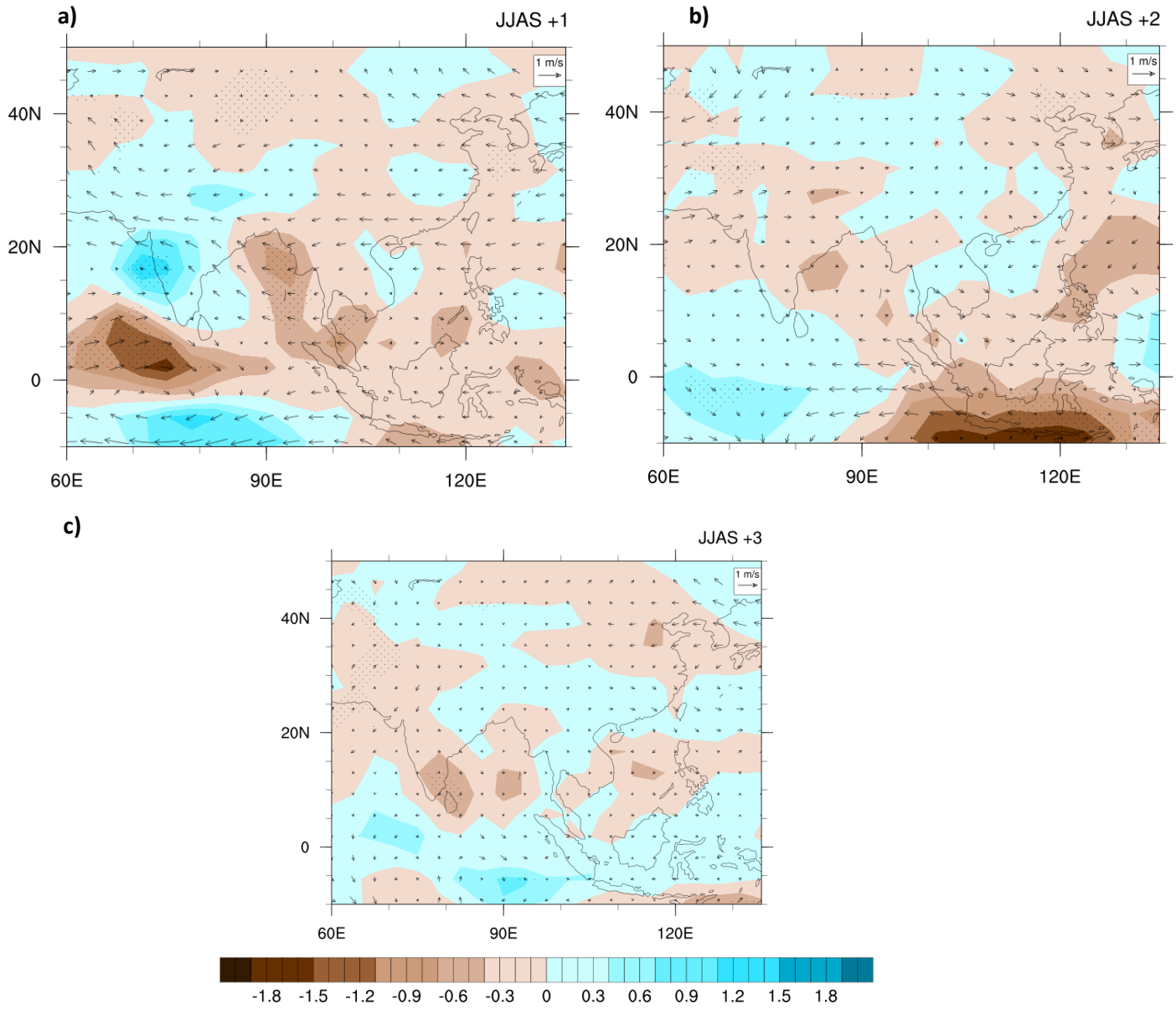

Fig 4.31*: Averaged precipitation (mm/day) and zonal wind at 850 hPa (m/s) anomalies for the* ***(a)*** *first,* ***(b)*** *second and* ***(c)*** *third boreal summer (JJAS) following the 13 major tropical volcanic eruptions (EnsembleL1L2). Dotted areas represent 95% inter-eruption confidence level.*

The superposed epoch analysis done in figure 4.32 confirms that no significant drying follows major tropical volcanic eruptions over India. The only significant value obtained with the EnsembleL1L2

simulation is a drying at lag +4 where a slight significant p-value is obtained (p-value = 0.05). On the other hand, we got an almost significant wetting a lag +1 (p-value= 0.055) for the second simulation.
The response of precipitation after a major eruption differs then completely between the tropical region and the Indian continent

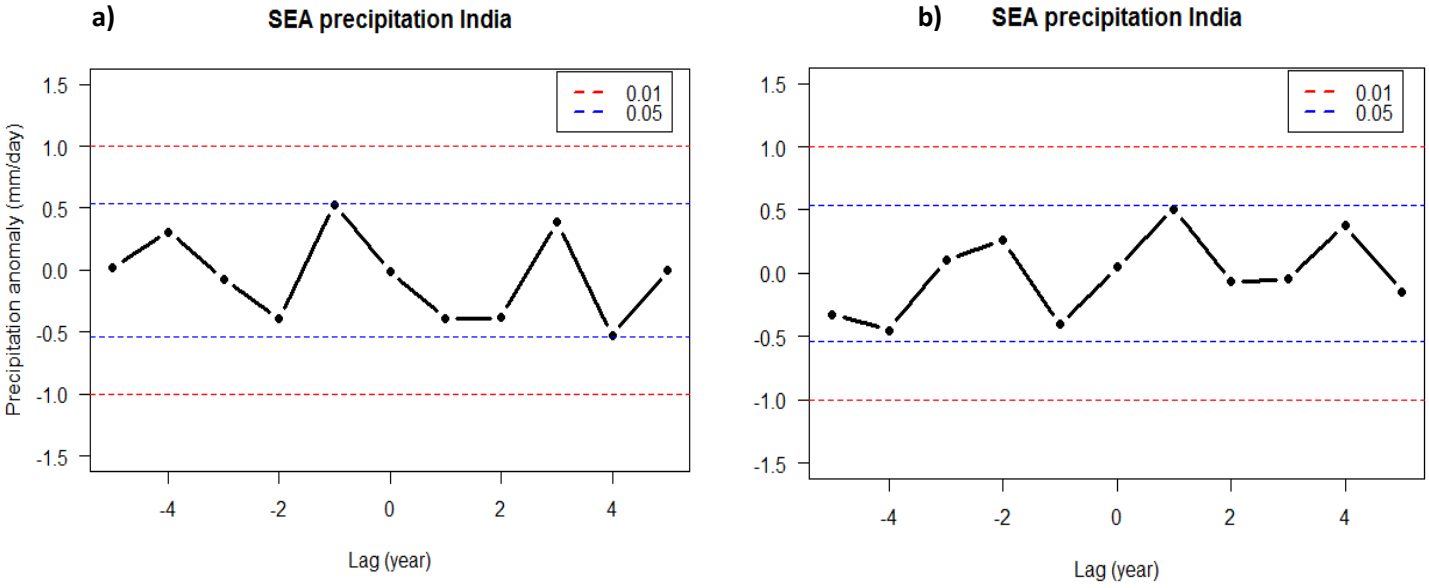

***Fig 4.32**: The SEA results of boreal summer temperature over the Indian continent for the 13 major volcanic eruptions chosen for **(a)** the EnsembleL1L2 and **(b)** the EnsembleM1M2 simulations. The lag 0 corresponds to the first summer following the eruption. The two dashed lines represent the p-values at 1% and 5%.*

It is interesting to note that the regions where precipitations are mainly convective and driven by incoming solar radiation undergo a clear drying after such an event. For the Indian monsoon responses, we can observe two interesting pattern: On one hand, over the Indian continent, where the summer precipitation is largely formed by dynamical monsoon, no clear response can be observed. Even though a clear cooling can be found over India, precipitation does not follow the same pattern. The tendency observed is rather a slight wetting during the first or second summer depending in which Ensemble simulations. As a first result, the Indian summer monsoon doesn't seem to be significantly affected after major volcanic tropical eruptions in the AOCCM SOCOL-MPIOM model. On the other hand, the Southeast Asian monsoon seems to be affected by volcanic forcing and a pronounced drying can be observed at summer 1 and 2 (Figure 4.31) in both Ensemble simulations.

4.2.4: Wind

Volcanic eruptions are also expected to exert an influence on dynamical factor such as the zonal winds, the vertical winds, the Intertropical Convergence Zone (ITCZ) or different dynamical monsoon indices. Due to the stratospheric temperature gradient generated after volcanic eruption (chapter 4.2.2), thermal winds are generated and can then be propagated downward, perturbing thus the global atmospheric circulation. In this section, the effects of major tropical volcanic eruptions on different dynamical variables in the AOCCM SOCOL-MPIOM are investigated.

4.2.4.1: Vertical wind

Due to the reduced incoming solar radiation in the tropical regions, one would expect a reduction in the strength of the convective cells near the equator. A significant reduction of the tropical precipitation has already been found in chapter 4.2.3 and should be relatively well correlated with the vertical wind anomaly.

Fig 4.33 shows the evolution of the mean vertical wind anomaly (mPa/s) around the equator at 500 hPa for the 24 months following a major tropical volcanic eruption. Note that in the AOCCM SOCOL-MPIOM simulations, a negative number indicates upward motion, whereas a positive number indicates downward motion. Therefore a negative anomaly implies a stronger upward movement than normal. A positive anomaly indicates a stronger downward movement than normal. Even if the pattern is less clear than for tropical temperature and precipitation evolution, the vertical wind seems to be affected and the convective cell around the equator reduced, since a positive anomaly can be observed after most of the 13 tropical volcanic eruptions. In both Ensemble simulations, the eruption of Mount Tambora is relatively distinguishable and positive wind anomalies follow this event. Anomalies equal to about 6 mPa/s are reached and the upward wind motion around the equator is weakened during about 10 months. After about one year, the anomaly is completely reversed and extremely high negative anomalies are observed during a short period of time (Figure 4.33, b). This unexpected drop cannot really be physically explained but is surprisingly observed in both model simulations.

In contrary to what was observed for precipitation and temperature, the vertical wind responses after extra and tropical volcanic eruption can hardly be distinguished from another. In both cases, the mean stays around 0 mPa/s and it is hard to draw any conclusion. But by looking at the individual members (Fig. 4.34), we can note that the biggest tropical volcanic eruptions in term of AOD are followed by a non-negligible positive anomaly. After the Unknown eruption of 1809, the eruption of Huaynaputina and Parker, positive wind anomalies higher than 5 mPa/s are observed. This is not really the case for the 4 extra tropical eruptions picked for this study. The eruption of the Mount Laki for example, does not generate anomalies higher than 2 mPa/s.

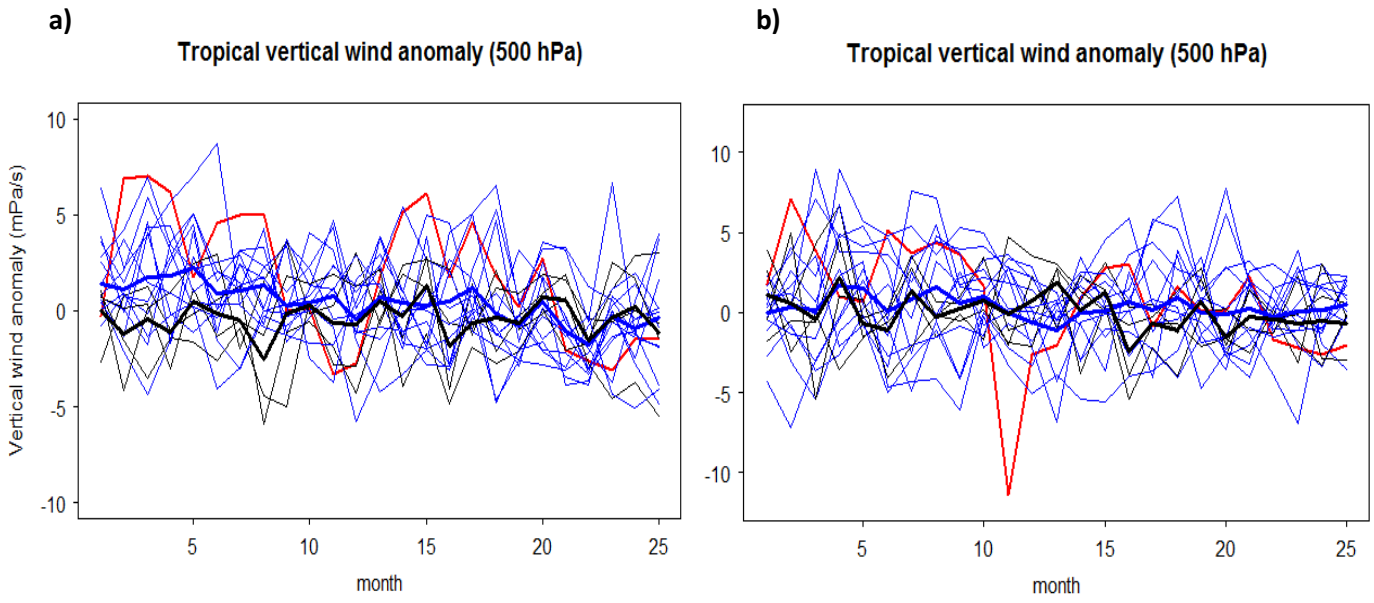

***Fig 4.33**: Monthly averaged evolution of vertical wind (mPa/s)after the 13 tropical and 4 extra-tropical eruption around the equator (5S-5N; 180W-180E) for the **(a)** model EnsembleL1L2 and **(b)** model EnsembleM1M2. The thick red line shows the evolution of the vertical wind after the eruption of the Tambora. The blue lines represent the tropical eruptions whereas the black lines represent the extra-tropical eruptions. The two thick lines (black and blue) are the mean for extra and tropical eruptions.*

For the tropical volcanic eruptions, a significant correlation is obtained between the AOD following the event and the magnitude of the vertical wind anomaly. By using the same linear regression model as used in the previous sections, significant R-squared have been found and are illustrated in the Figure 4.34. For the Ensemble L1L2 simulation, the AOD can already explain 41% of the averaged vertical wind anomaly during two years (Fig 4.34 a). The R-squared decreases a bit if we select only the boreal summer month (Figure 4.34 b) but still reaches 33%. Both R-squared are significant at the 0.05 level. For the winter, the R-squared obtained is not significant and is only equal to 0.18 (plot not shown here). Indeed, during the boreal winter the convection cell and the intertropical Convergence Zone (ITCZ) move a bit southward. By selecting a different region comprised between 10° south and 5° south we also found a significant weakening of the vertical wind (not shown).

Thus according to the L1L2 simulation, the upward vertical winds significantly decrease after a volcanic eruption and the magnitude of the anomaly is linearly correlated to the strength of the AOD. It is also interesting to note that out of the 13 volcanic eruptions, only 3 are followed by a mean strengthening of the upward winds (negative anomaly) during the 24 following months (Fig 4.34 a).

By looking at the second model simulation, the results are similar. The R-squared obtained for the whole year and the summer are both significant at the 0.05 level and are equal to 0.45 and 0.57 respectively. Once more, the same linear regression applied for the winter season did not give any significant results. The R-squared obtained is not significant and only equal to 0.008. In this second simulation, 7 out of 13 tropical eruptions are followed by a mean strengthening of the upward winds.

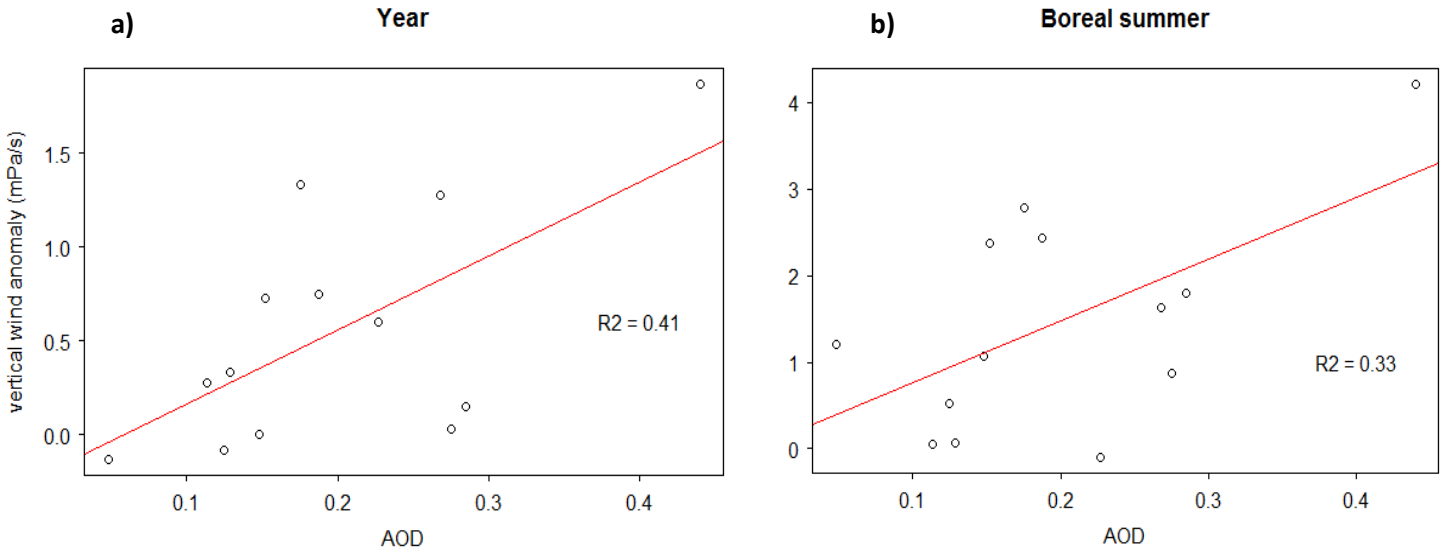

***Fig 4.34**: Simple linear regression model explaining vertical wind anomaly through AOD (EnsembleL1L2 simulation). The dots represent the 13 different tropical volcanic eruptions, and the red line is the regression line. In **(a)** the 24 months following the eruptions have been chosen whereas in **(b)** only the summer (JJAS) months have been selected.*

Figure 4.35 shows the geographical repartition of the vertical wind anomaly for the three first summers following a major tropical volcanic eruption as well as the zonal mean. In contrary to the precipitation or temperature response, the anomaly observed in this figure is harder to analyze and no clear pattern can be distinguished.

As expected and shown by the previous analysis, significantly weakened upward vertical winds can be observed around the equator. Green patches above the north of South America, the East of Africa and Indonesia are indeed well distinguishable. During the second summer (Figure 4.35 b), the anomaly decreases sharply and the only patches where the convective cells seems to be weakened are found over the tropical Pacific Ocean. After the second summer, the significant anomaly vanishes completely (Figure 4.35 c).

A bit further from the equator, it is interesting to note that there are many places where upward winds are strengthened (red patches), namely above India, Australia and the tropical Atlantic Ocean. These anomalies persist until the second summer and then vanish. Around 30° North and South, we find the descending branches of the Hadley cell. If the Hadley cell is weakened, the downward motion of air parcels should be reduced and we should observe a negative anomaly over these areas. Thus the weakening of the Hadley cell could relatively well explain the negative zonally anomaly around the 30th parallel north and south (Figure 4.35). Similar results are obtained when using the EnsembleL1L2 simulation, therefore the results are not presented in this section (Appendix A7).

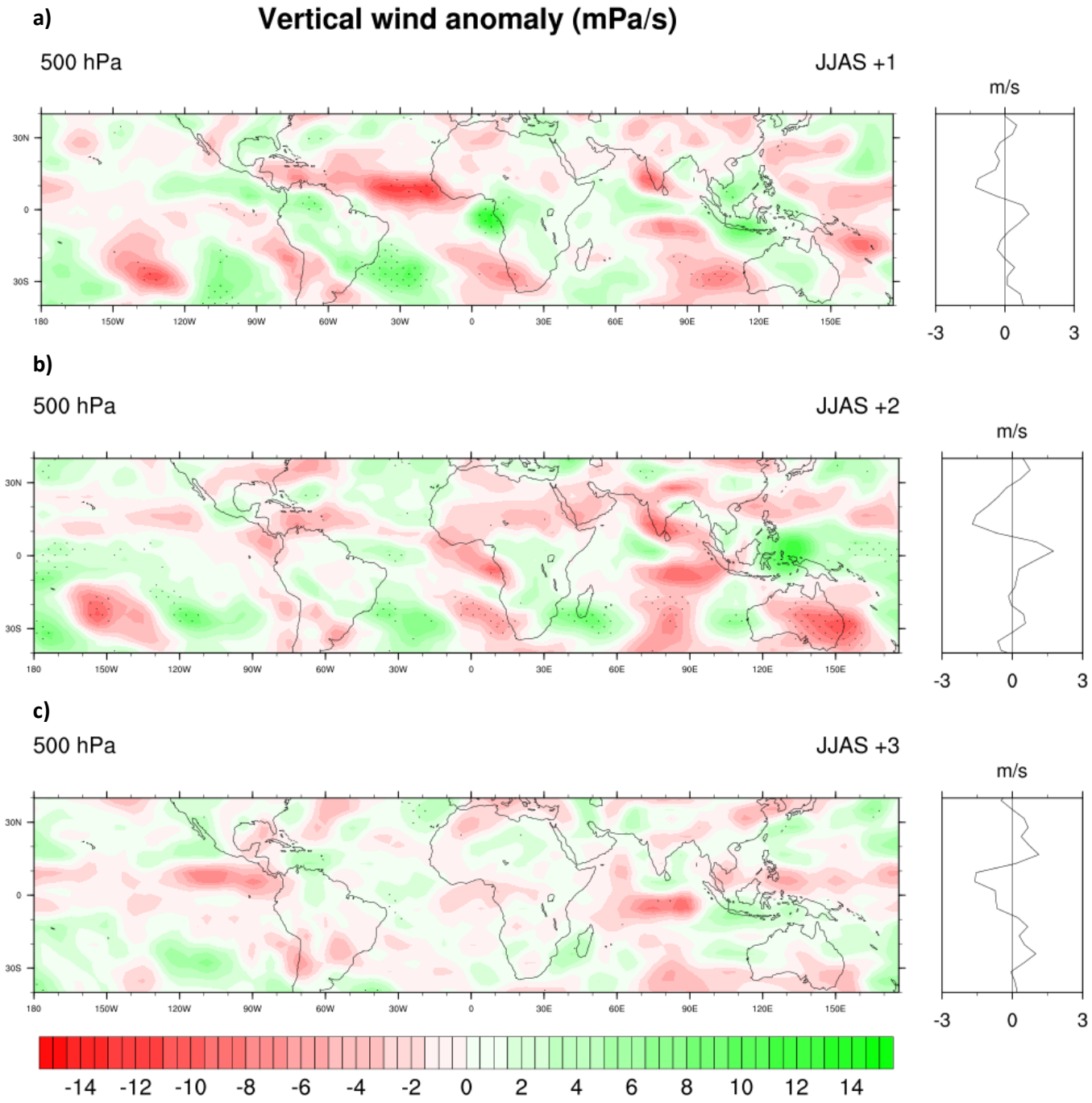

***Fig 4.35**: Averaged vertical wind anomaly (mPa/s) for the **(a)** first, **(b)** second and **(c)** third boreal summer (JJAS) following the13 major tropical volcanic eruptions (EnsembleM1M2 simulation). Dotted areas represent 95% inter-eruption confidence level.*

This positive anomaly around the equator is not only seen at 500 hPa level and several eruptions weakened the upward winds all along the troposphere. Figure 4.36 shows wind profiles of the troposphere which describe well the distribution of vertical wind anomalies during three boreal summers. By and large, even if the response is not homogeneous after each major volcanic eruption, a

weakening of the vertical winds (positive anomaly) is rather observed after the first summer (Figure 4.36 a). The mean of the 13 eruptions (red line) is in both cases always positive (above 0 mPa/s) all along the wind profile. Only 3 eruptions (Huaynaputina, Gamkonora and Babuyan Claro) out of 13 do not generate a general weakening of the upward winds during the first summer. The eruption of the Tambora (green line) affects largely this variable and is once more well distinguishable. For the second and third summer (Figure 35 b and c), the wind profile is less clear and heterogeneous between the different volcanic eruptions. But the mean stays approximately around 0 mPa/s and no significant variations can be perceived. The effects of volcanic eruptions on vertical wind anomaly seem thus to vanish after the first summer and last only one year according to the AOCCM SOCOL-MPIOM.

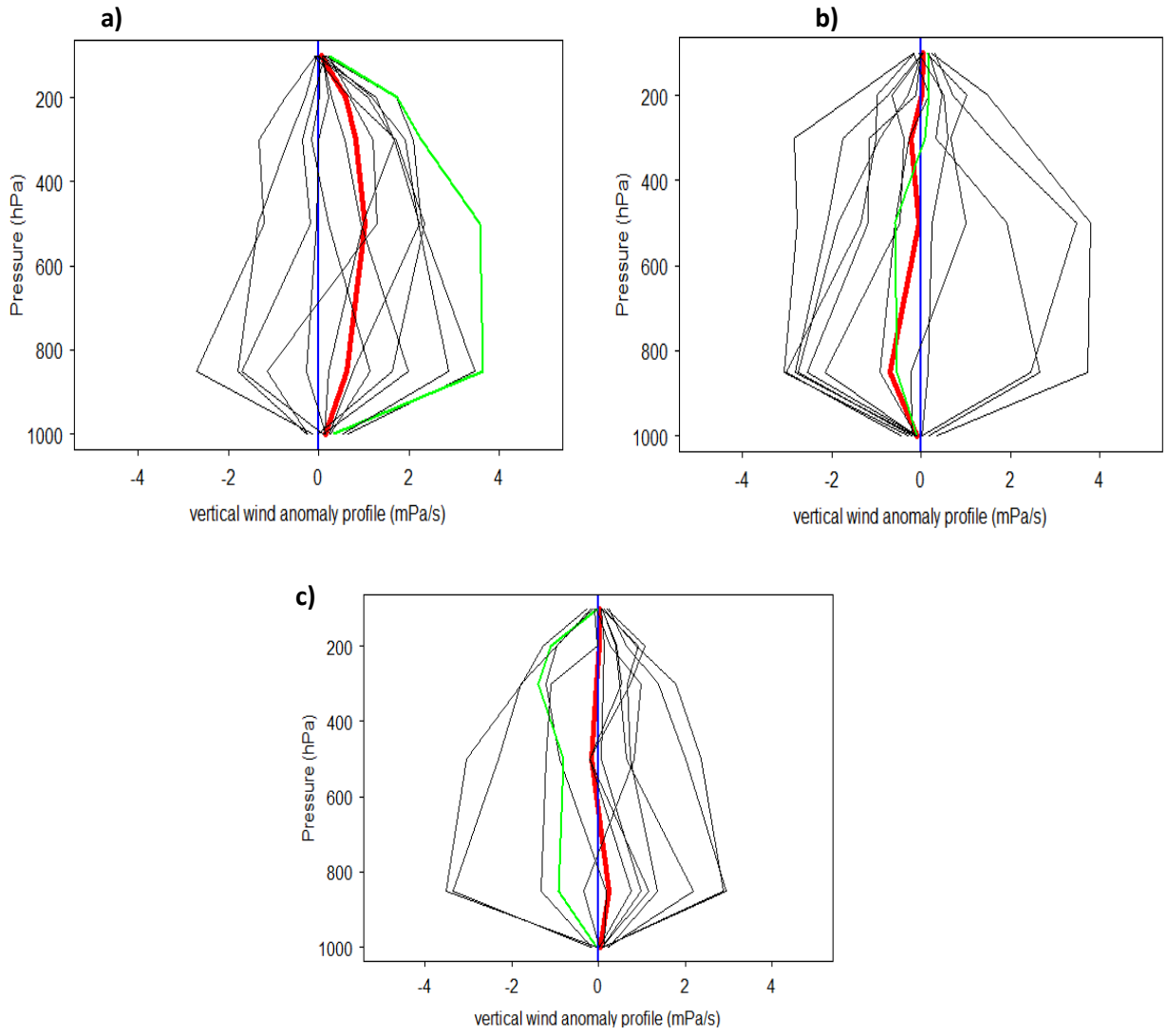

Fig 4.36*: Vertical wind profile around the equator (5°N-5°S,180°W-180°E) for* ***(a)*** *the first,* ***(b)*** *the second and* ***(c)*** *the third summer following a tropical volcanic eruption (EnsembleL1L2 simulation). The red line represents the mean of the 13 tropical eruptions, the green line is the eruption of the Tambora and the 12 grey lines represent each one eruption. On the right side of the blue line, the anomaly is positive and the vertical winds are weakened.*

In the EnsembleM1M2 simulation, the pattern is less clear and 6 eruptions are already followed by a strengthening of the upwards vertical winds during summer 1. But the most powerful eruptions in term of AOD (Tambora, eruption of 1809, Pinatubo…) still generate a weakening of the ascending winds in this equatorial region. During summer 2 and 3, it is hard to discern any clear pattern and the strength of the vertical winds do not seem to be influenced (Figures not shown here).

It is also interesting to investigate the link existing between the strength of the upwards vertical winds around the equator and the reduction of tropical precipitation found and analyzed in Chapter 4.2.3.
As expected, a significant linear relationship exists between these two variables and is shown in Figure 4.37. According to this figure, the annual vertical wind anomaly around the equator could explain about 46% of the annual precipitation anomaly in the Tropics. If we look only at the boreal summer, the R-squared is reduced to 21% but still significant at the 0.05 level. The relation is not significant anymore during the boreal winter. This tends to prove that tropical precipitations are directly and significantly influenced by a weakening of the convective cells around the equator. With the EnsembleM1M2 simulation, the R-squared obtained are even higher and equal to 0.67 (year) and 0.75 (summer) (not shown).

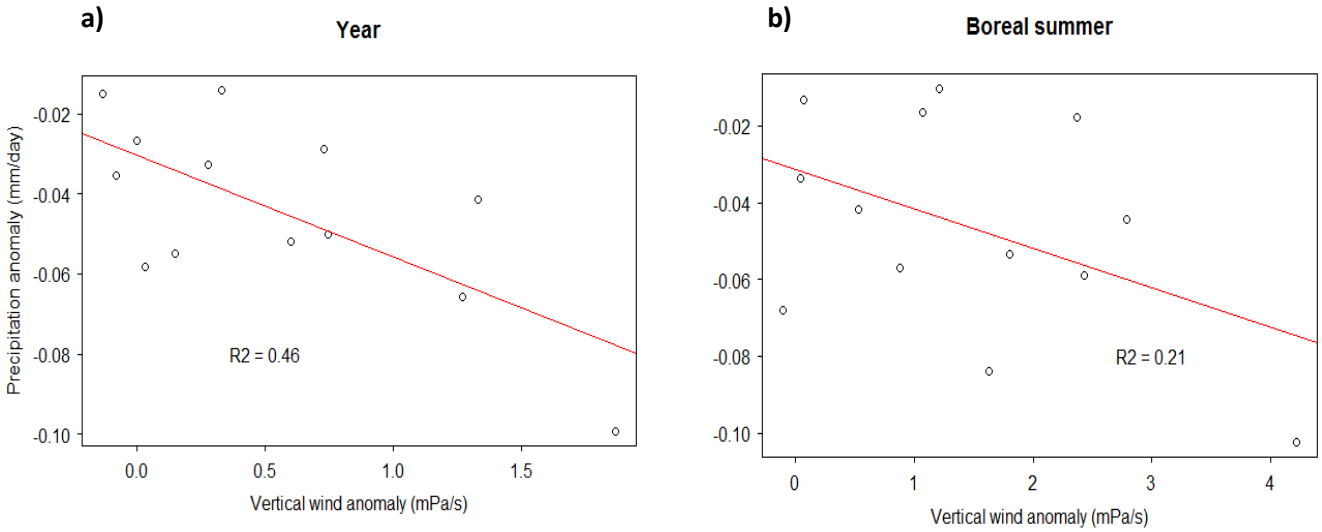

Fig 4.37*: Simple linear regression model explaining the tropical precipitation anomaly through the vertical wind anomaly (5°N-5°S, 180°W-180°E) for the EnsembleL1L2 simulation. The dots represent the 13 different tropical volcanic eruptions, and the red line is the regression line. In* ***(a)*** *the 24 months following the eruptions have been chosen, whereas in* ***(b)*** *the summer (JJAS) months have been selected.*

Thus, in the AOCCM SOCOL-MPIOM, the vertical winds as well as the convective cells around the equator seem to be weakened after major volcanic eruptions and could explain partially the drying undergone by tropical regions (chapter 4.2.3)

4.2.4.2: Intertropical Convergence Zone (ITCZ)

As mentioned by Ridley et al. (2015), the position of the ITCZ could move towards the less cooled hemisphere. In this section, we will check if similar conclusion can be drawn with the AOCCM SOCOL-MPIOM simulations. In this study, 11 out of 17 volcanic eruptions blew up in the northern hemisphere: Parker, Gamkonora, Serua, Unkonwn eruption 1729, Laki, Claro, Cosiguina, Unknown eruption of 1861, Santa Maria, El Chichón and Pinatubo. During the first boreal summer following these 11 events and according to the AOCCM SOCOL-MPIOM simulations, the cooling is more pronounced in the northern hemisphere. Indeed, the averaged anomaly between 5 and 80° north reaches -0.32 K. For an equivalent region over the southern hemisphere, the averaged cooling is less pronounced and is only equal to -0.20 K. If we select the 5 volcanic eruptions which occurred in the southern hemisphere (Huaynaputina, Serua, Tambora, Krakatau and Agung) and performed the same analysis, we obtain a northern cooling equal to about -0.30 K and a southern cooling of -0.23 K. In both cases, the temperature response in the southern hemisphere seems to be damped by the ocean. But we can also note that as expected, the volcanic eruptions occurring in the northern hemisphere exert a bigger influence over this region.

Thus, and according to the study of Ridley et al. (2015), we expect a southward shift of the ITCZ after the 11 volcanic eruptions which occurred in the northern hemisphere. Figure 4.38 shows the zonally averaged tropical precipitation during the two first boreal summers following these 11 volcanic events and allows us to determine the position of the ITCZ. The index used to calculate the exact position of the ITCZ is fully described in section 3.3.

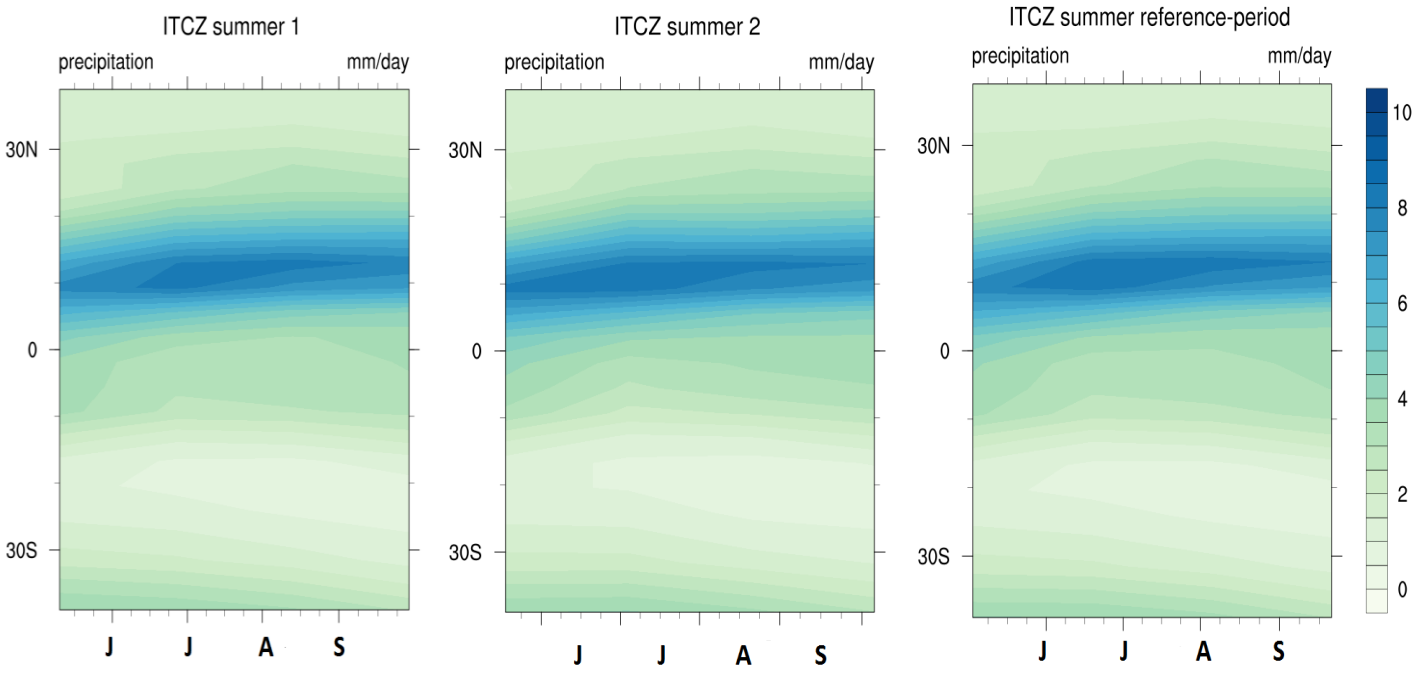

***Fig 4.38**: Zonally averaged precipitation (mm/day) for the first and the second boreal summer following 11 major volcanic eruptions (EnsembleL1L2 simulation) over the tropical regions (180W-180E, 40N-40S). The third plot shows the mean position of the ITCZ during the 11 reference period following each eruption.*

In contrary to what has been found and described by Ridley et al. (2015) the position of the ITCZ in the AOCCM SOCOL-MPIOM do not seem to be influenced by tropical volcanic eruption after this first analysis and stays fixed around 10° north. The same analysis has also been done for the boreal winter season and the mean position of the ITCZ stays around 10° south. If we zoom in on the Asian region (65E-135E, 50N-10S) the results are similar. The ITCZ do not seem to significantly move towards the less cooled hemisphere for the summer season. The same analysis can be done for the winter season (Figure not shown)

In Fig 4.39 the zonally averaged precipitation difference between the first, second and third summer and the reference period is shown. This allows to discern more precisely the motion of the ITCZ.

During the first summer, a slight drying is observed around the equator. The intensity and the strength of the tropical convergence zone seem then to be weakened. At summer 2, it is interesting to note a clear positive anomaly around 10° North and a dry anomaly around 10° South. During the third summer, no clear pattern can be distinguished. Thus Figure 4.39 would rather betray a non-significant northward motion of the ITCZ. These results are in opposition with the well documented proxy-based study of Ridley et al. (2015) and the robustness of the model can thus be reasonably call into question.

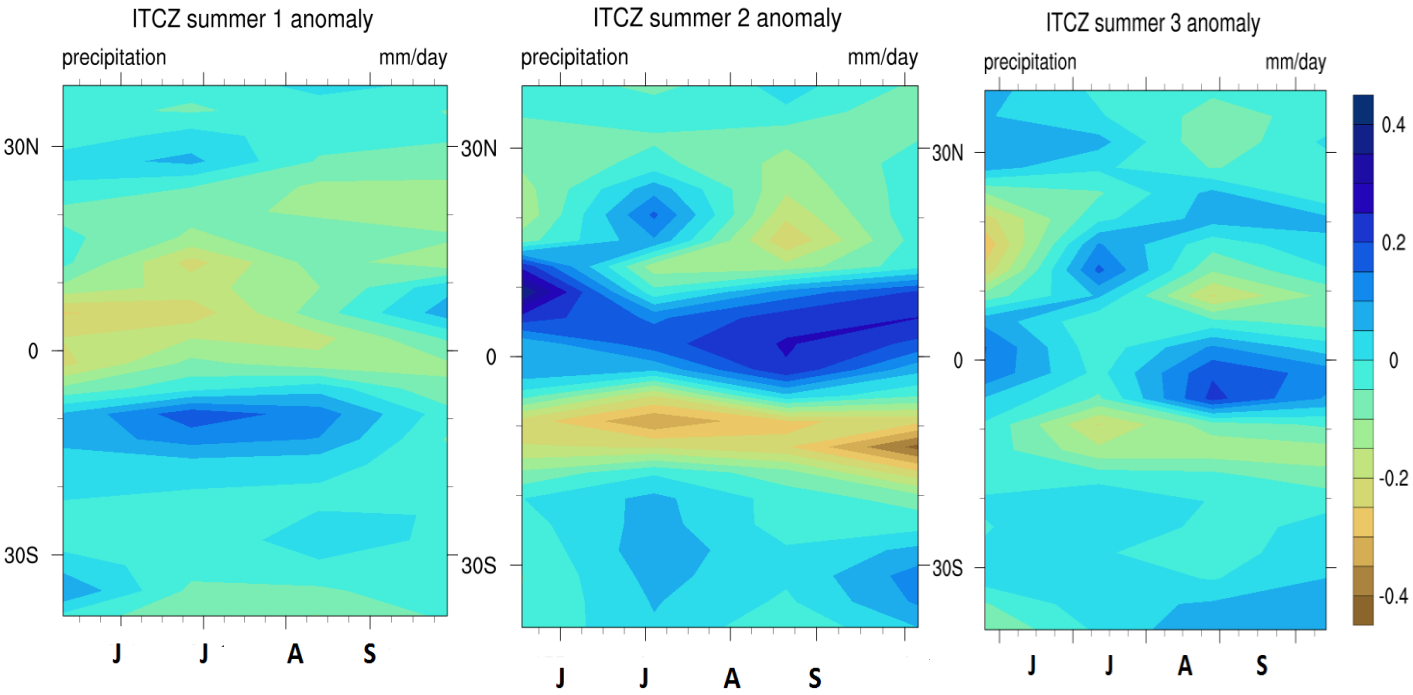

***Fig 4.39**: Zonally averaged precipitation anomaly for the first, second and third summer following 11 major volcanic eruptions (EnsembleL1L2 simulation).*

4.2.4.3: Zonal wind

The stratospheric temperature gradient generated after volcanic eruption and described in section 4.2.2, generates thermal winds which can then be propagated down into the troposphere. In this section, we try to determine whether or not the zonal winds in the troposphere are significantly affected by tropical volcanic eruption in the AOCCM SOCOL-MPIOM. Given the vertical resolution of the AOCCM SOCOL-MPIOM, the zonal wind response at 200 and 850 hPa are analyzed here. At these two levels and with the help of wind profiles we should be able to determine if and how the surface wind as well as the tropical jet are affected. Note that in the model used for this study, a negative number indicates westward motion of air masses whereas a positive number describes an eastward movement. A negative anomaly indicates thus a stronger east to west component than normal.

4.2.4.3.1: Zonal winds at 200 hPa

Firstly, the behavior of the tropical easterly jet after different volcanic eruptions is analyzed. This tropical jet is indeed one of the drivers of the Asian monsoon and influences precipitation over the Indian continent. To analyze the response of this easterly jet, we looked at the zonal wind at the 200 hPa level and over the following region: 13-17°N and 50-80°E.

Figure 4.40 shows the evolution of the zonal wind over this region for 3 summers directly following one of the 13 major tropical volcanic eruptions. Once more, the response is less clear than for tropical precipitation and temperature. Nevertheless, the tropical easterly jet seems to be significantly affected by tropical eruptions. Indeed, most of the tropical eruptions are followed by a negative anomaly, meaning that the easterly jet at this level is strengthened. In both model simulations, the anomaly is rather high during the first summer and decreases then slightly. During the third summer, the anomaly vanishes almost completely and the volcanic influence seems to have vanished. Once more, and especially in the EnsembleM1M2 simulation, we observe a discrepancy between the effects of the tropical and extratropical volcanic eruptions. Indeed, during the first and second summer, the mean for the tropical eruptions is always below the extratropical mean, which does not seem to significantly influence the easterly tropical jet.

Figure 4.40 also shows the linear relationship which exists between the AOD (explanatory variable) and the summer zonal wind anomaly (dependent variable) and confirms our first impression. The link is particularly well seen in the EnsembleM1M2 simulation, where the magnitude of the eruption can explain about 47% of the zonal wind variability after the eruption. The R-squared obtained is significant at the 0.01 level.

It is also interesting to note that a strengthening of the tropical easterly jet follows the majority of the events picked for this study. Among the 13 tropical eruptions, only the eruptions of Santa Maria and Babuyan Claro generate a weakened tropical easterly jet. In the EnsembleL1L2 simulation, even though the linear relationship is not significant at the 0.1 level (R-squared = 0.12), we still observe a positive correlation between the strength of the easterly jet and the AOD. Indeed only 4 eruptions, namely Santa Maria, Babuyan Claro, Gamkonora and Cosiguina are followed by a weakening of the tropical jet whereas the 9 others tropical volcanic eruptions are followed by a negative zonal wind anomaly (fig 4.40 c).

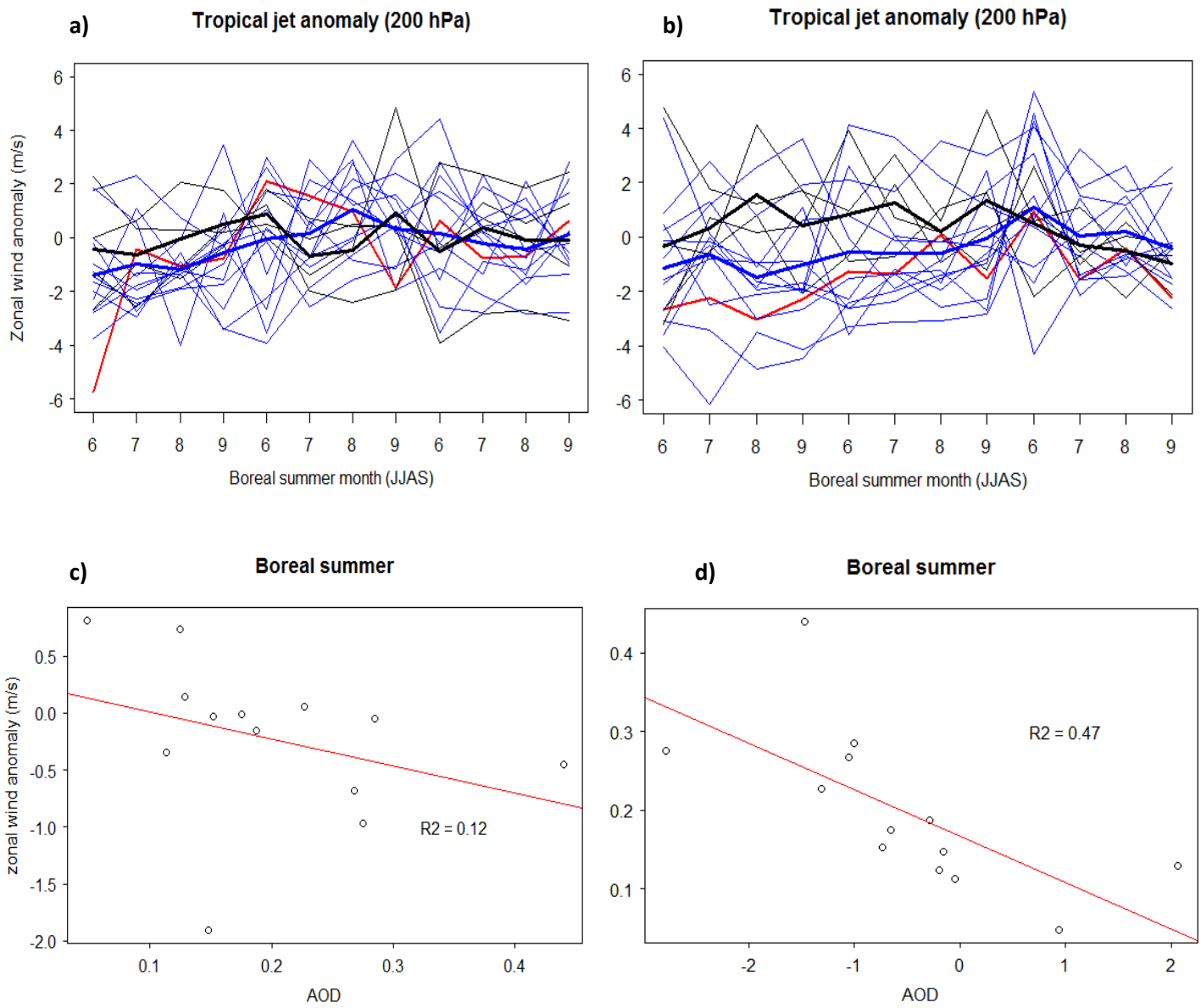

***Fig 4.40**: Monthly averaged evolution of the zonal wind (m/s) after the 13 tropical and 4 extra-tropical eruptions (13N-17N; 50E-80E) for the **(a)** model EnsembleL1L2 and **(b)** model EnsembleM1M2. The thick red line shows the evolution of the vertical wind after the eruption of the Tambora. The blue lines represent the tropical eruptions, whereas the black lines represent the extra-tropical eruptions. The two thick lines (black and blue) are the mean for extra and tropical eruptions. On **(c)** and **(d)** simple linear regression model explaining summer zonal wind anomalies through AOD for the EnsembleL1L2 and EnsembleM1M2 simulations are shown respectively.*

Furthermore, in both cases, the eruption of Mount Tambora affects significantly and strengthens the tropical easterly jet. But in the linear regression model, we also note that the zonal wind response after the eruption of the Tambora is weaker than expected and the link between AOD and zonal wind anomaly is not perfectly linear.

The SEA presented in figure 4.41 confirms that for both Ensemble simulations, a significant strengthening of the tropical easterly jet is observed. This strengthening is still significant at year +2 for the EnsembleM1M2 simulation. It is not the case in the EnsembleL1L2 simulation and the anomaly vanishes already one summer after the eruption. After the second summer, the significance of the anomaly decreases sharply and no volcanic influence can be seen. In the AOCCM SOCOL-MPIOM, the tropical easterly jet seems thus to be significantly perturbed by major tropical volcanic eruptions during one or two year.

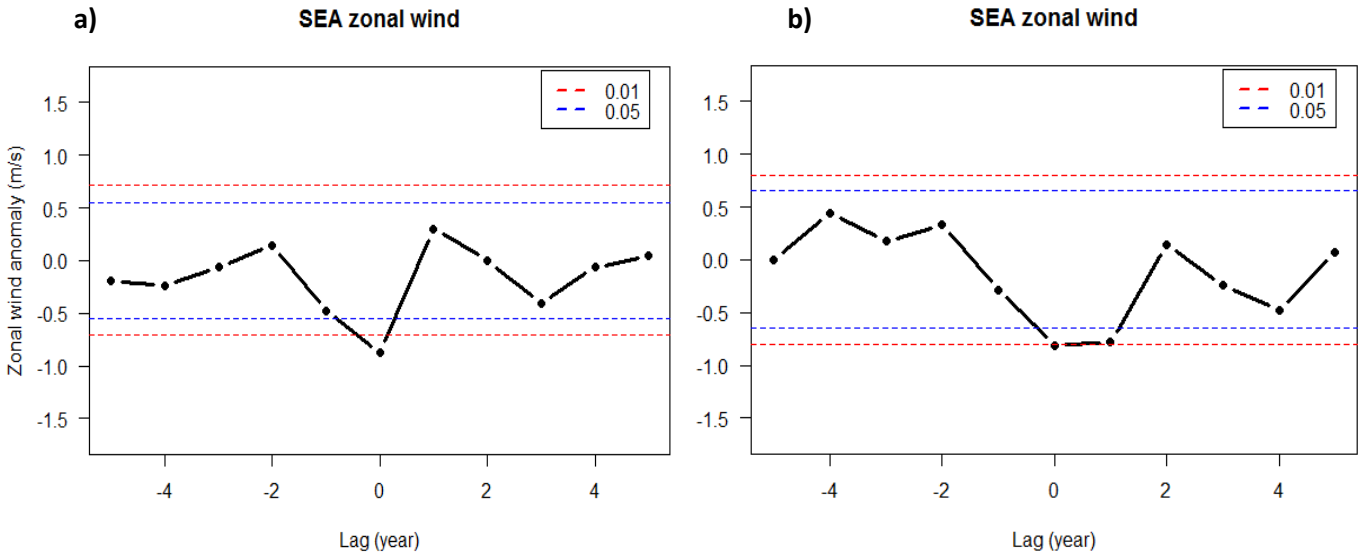

***Fig 4.41**: The SEA results of summer tropical zonal wind for the 13 major volcanic eruptions chosen for **(a)** EnsembleL1L2 and **(b)** EnsembleM1M2. The lag 0 corresponds to the first summer following the eruption. The two dashed lines represent the p-values at 1% and 5%.*

It is interesting to note that at 200 hPa, the eastward zonal wind anomaly is not confined to the tropical easterly jet region bus is found all over the tropics. Figure 4.42 shows the geographical repartition of the anomaly for the EnsembleM1M2 simulation.

Surprisingly the easterly zonal winds are significantly enhanced over the Tropics and no significant positive anomaly is registered. The zonally averaged anomaly is indeed negative for each latitude at summer 1 and 2. At summer 2, the eastward anomaly is still high and significant (Figure 4.42 b) but decreases already slightly. Yellow significant patches begin to appear over the south of Africa or Australia. But by and large, the mean anomaly largely stays negative. During the third summer (figure 4.42 c), the magnitude of the anomaly decreases and the only eastward significant anomaly is observed over central Africa. Significant weakening of the easterly winds is also computed by the model over South East Asia and all along the 30th South parallel.

The response of the model is quite problematic and there is no physical evidence which could explain the large strengthening of the easterly winds computed by the model after volcanic eruptions. The model seems indeed to react to volcanic forcing but in an unexpected way. We would rather have expected a strengthening of the westerly winds. This unexpected response could then be due to the imperfections of the model (Figure 4.58) but further investigations are necessary.

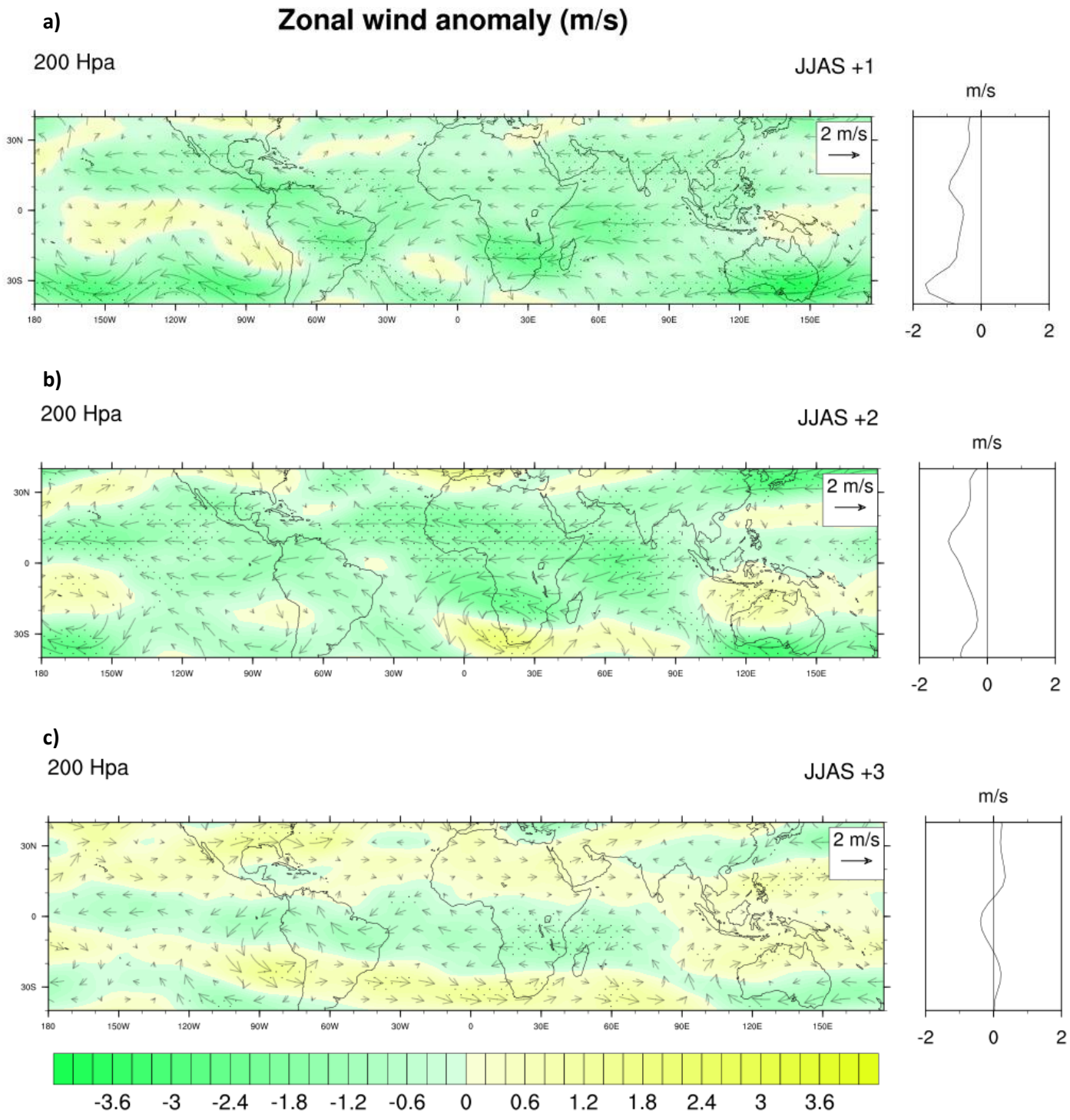

***Fig 4.42**: Averaged zonal wind anomaly at 200 hPa (m/s) for the **(a)** first, **(b)** second and **(c)** third boreal summer (JJAS) following the 13 major tropical volcanic eruptions (EnsembleM1M2 simulation). Negative anomalies indicate a stronger east to west component than normal. Dotted areas represent 95% inter-eruption confidence level.*

The decrease in the magnitude of the anomaly is well visible in Figure 4.43. It is also interesting to note that the increase of the eastward wind component is not restricted to the low latitude and is also visible in the middle latitudes, namely in the southern hemisphere towards the latitude 40°S.

In contrary, over the Southern Ocean we observe a strengthening of the westerly winds which could correspond to a strengthening of the Southern Annular Mode (SAM). This would lead to a higher isolation of the Antarctica and limit the exchanges of air masses and could explain the stratospheric cooling observed in Figure 4.21. Figure 4.44 shows the evolution of the SAM index (Ho et al. 2012) after 17 volcanic eruptions for the EnsembleM1M2 simulation. No significant signal is really seen in the first plot but it is interesting to look at the correlation between the volcanic forcing and the strength of the SAM. Even though none of the correlation obtained are significant, they still indicate a slight positive correlation between the power of the eruption and the magnitude of the SAM following these volcanic events (Figure 4.44). The results are therefore relatively well in agreement with the study of Krüger et al 2014. According to this study, a Pinatubo-size eruption would not significantly strengthen the SAM but after the eruption of Los Chocoyos (VEI =7) a positive up to 10x SAM phase is simulated.

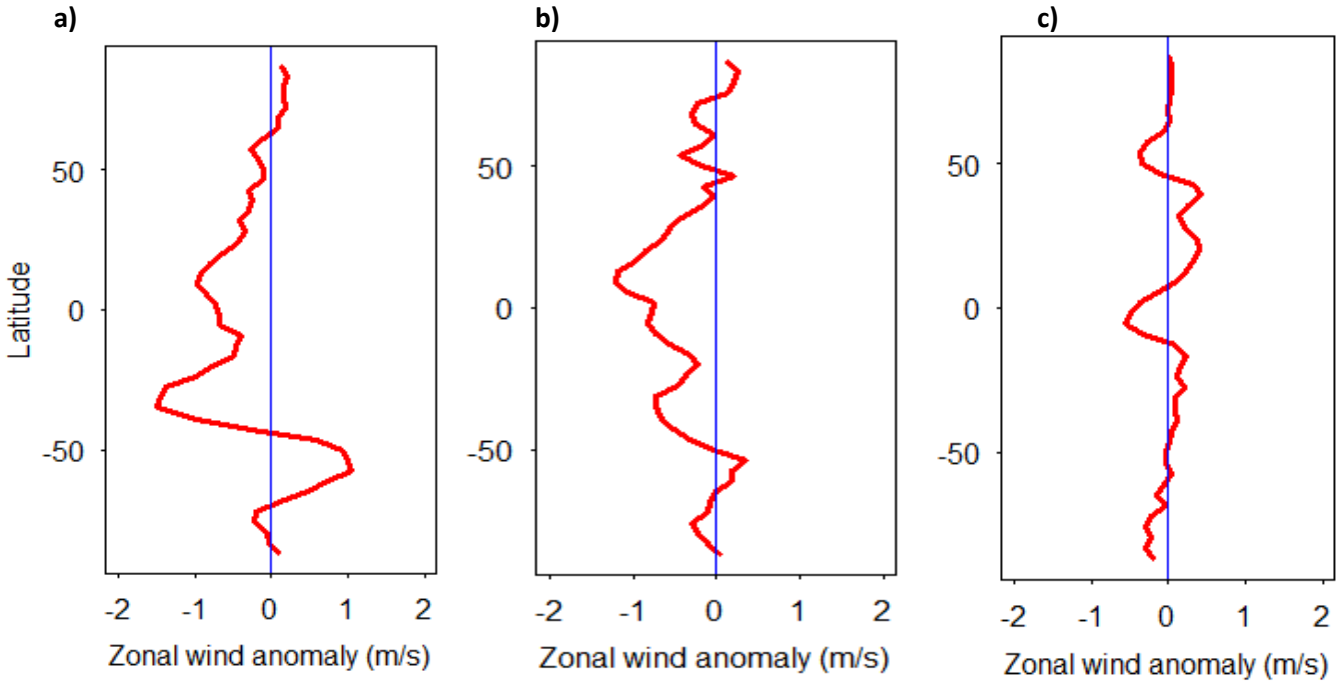

***Fig 4.43**: Zonally averaged zonal wind anomaly at 200 hPa for the first **(a)**, second **(b)**, and third **(c)** summer following 13 major volcanic eruptions in the EnsembleM1M2 simulation.*

a) **SAM anomaly (Pa)** **b)**

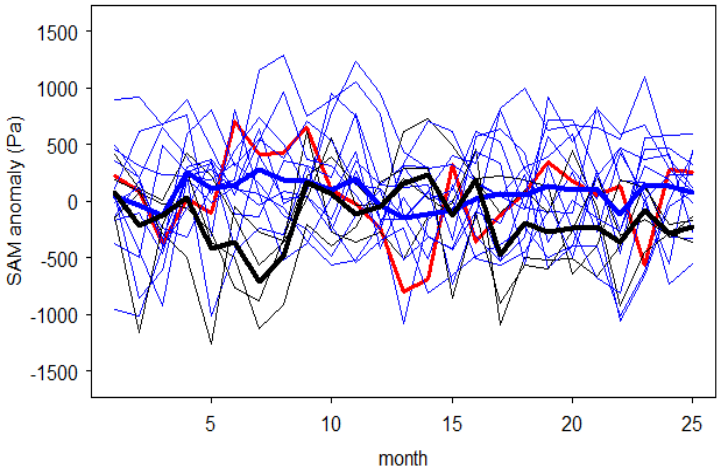

R-squared	Year	JJAS	DJF
EnsembleL1L2	**0.01 +**	**0.13 +**	**0.04 +**
EnsembleM1M2	**0.10 +**	**0.01 +**	**0.02 +**

Fig 4.44*: Monthly averaged evolution of the SAM index (Pa) after the 13 tropical and 4 extra-tropical eruptions* ***(a)*** *(M1M2). The thick red line shows the evolution of the vertical wind after the eruption of the Tambora. The blue lines represent the tropical eruptions whereas the black lines represent the extra-tropical eruptions. The two thick lines (black and blue) are the mean for extra and tropical eruptions. The table* ***(b)*** *contains the R-squared for the linear regression model explaining the SAM anomaly through AOD.*

The wind profiles presented in Figure 4.45 show the mean zonal wind anomaly at different pressure levels. The upper troposphere seems to be the most affected region. Lower in the troposphere and at the surface, the anomaly decreases sharply and it is hard to detect any clear pattern. The response of tropical surface winds will be carefully investigated later on but they do not seem to be affected at first glance. By and large, a negative anomaly and the strengthening of the easterlies are found at 200 hPa even if the response diverges completely between some of the 13 tropical volcanic eruptions. It is interesting to note that the biggest eruptions in term of AOD (Tambora, Unknown 1809,…) are all followed by a negative anomaly at this level (Figure 4.45 a and b). By zooming in on the Indian continent, a similar pattern can be observed. During the first two summers, the tropical easterly jet is strengthened and winds blow with a stronger west to east component than normal (Figure 4.45 c and d).

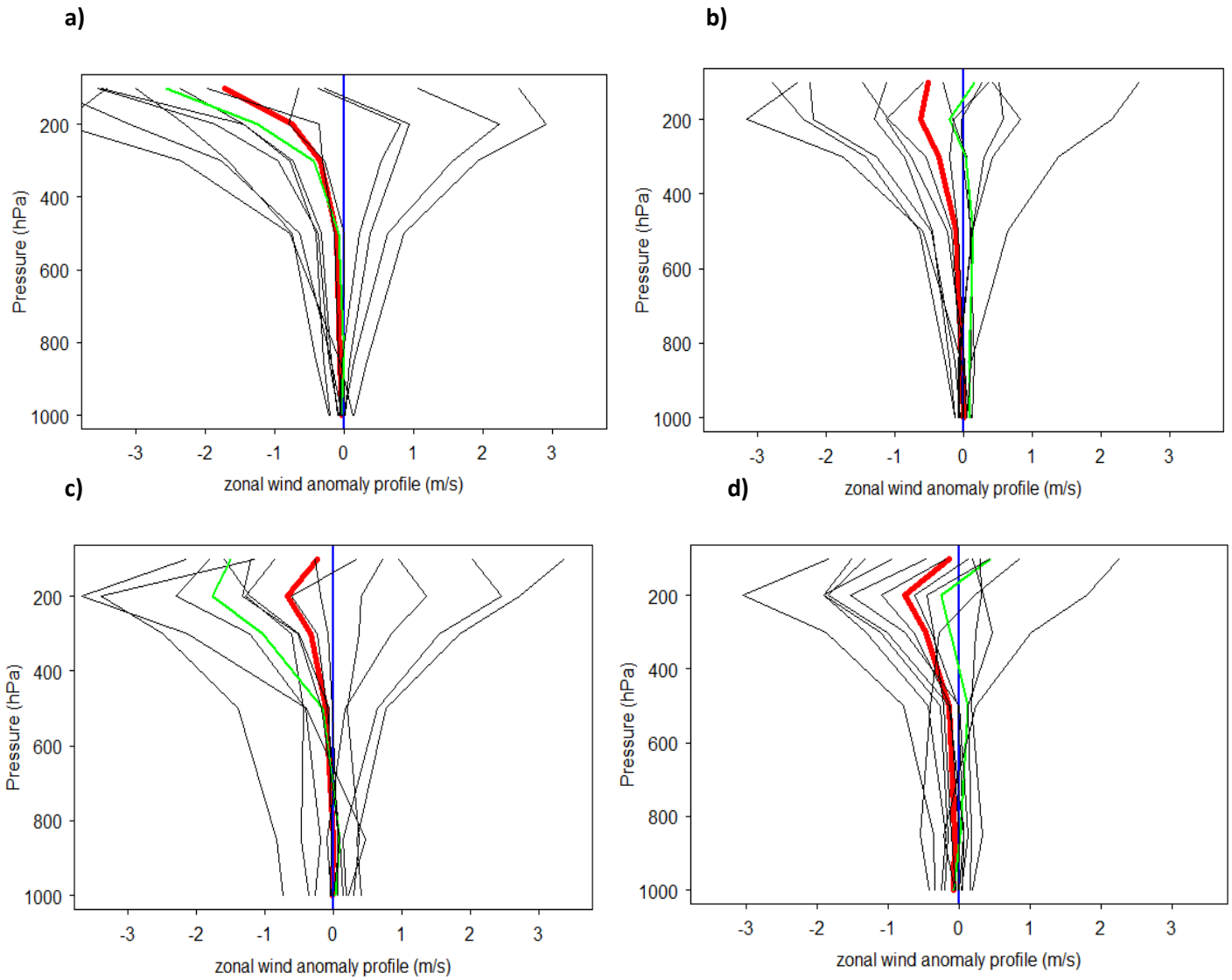

***Fig 4.45**: Zonal wind profile around the equator (10°N-10°S,180°W-180°E) for **(a)** the first and **(b)** the second summer following a tropical volcanic eruption (Ensemble M1M2 simulation). In **(c)** and **(d)** we zoomed in on the Indian continent (65E-95E, 40N-10N).The red line represents the mean of the 13 tropical eruptions, the green line is the eruption of the Tambora and the 12 grey lines represent each one eruption. On the right side of the blue line, the anomaly is positive and the vertical winds are weakened.*

4.2.4.3.2: Zonal winds at 850 hPa

At a lower level, the surface zonal winds could also be influenced and the response is analyzed in this section.

On Figure 4.46 the evolution of zonal wind over the Tropics and the Indian continent during the boreal summer months following volcanic eruption is shown. According to this figure, the zonal winds in the AOCCM SOCOL-MPIOM simulations do not react significantly after the volcanic eruption and the

response is heterogeneous between each events. With the linear regression model used previously, no significant linear relationship can be found between the AOD and the zonal wind anomaly. None of the R-squared found for the whole Tropics or the Indian continent are significant (Figure not shown).
The same analysis can be done for the EnsembleM1M2 simulation, and here as well, no significant changes in the zonal wind are seen after volcanic events.

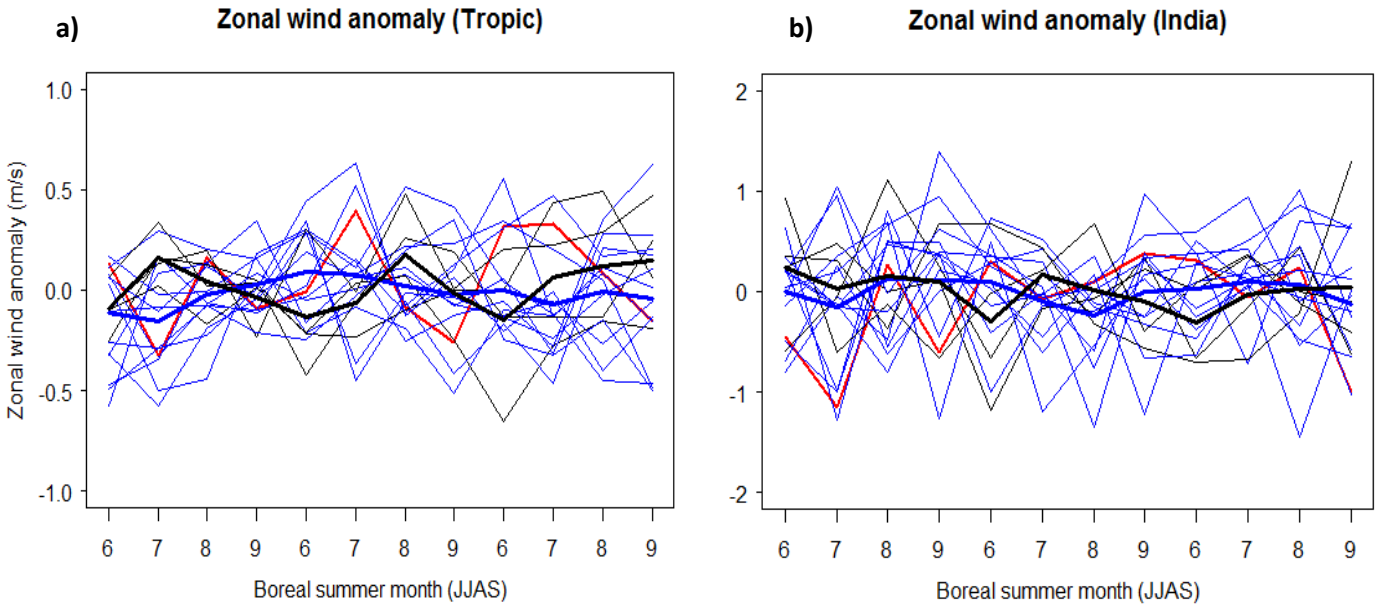

***Fig 4.46**: Monthly averaged evolution of zonal wind (m/s) at 850 hPa after the 13 tropical and 4 extra-tropical eruptions over **(a)** the Tropics and **(b)** the Indian continent (45N-10N; 65E-95E) for the model EnsembleL1L2. The thick red line shows the evolution of the vertical wind after the eruption of the Tambora. The blue lines represent the tropical eruptions whereas the black lines represent the extra-tropical eruptions. The two thick lines (black and blue) are the mean for extra and tropical eruptions.*

But by looking at figure 4.47 some local interesting pattern can be seen.

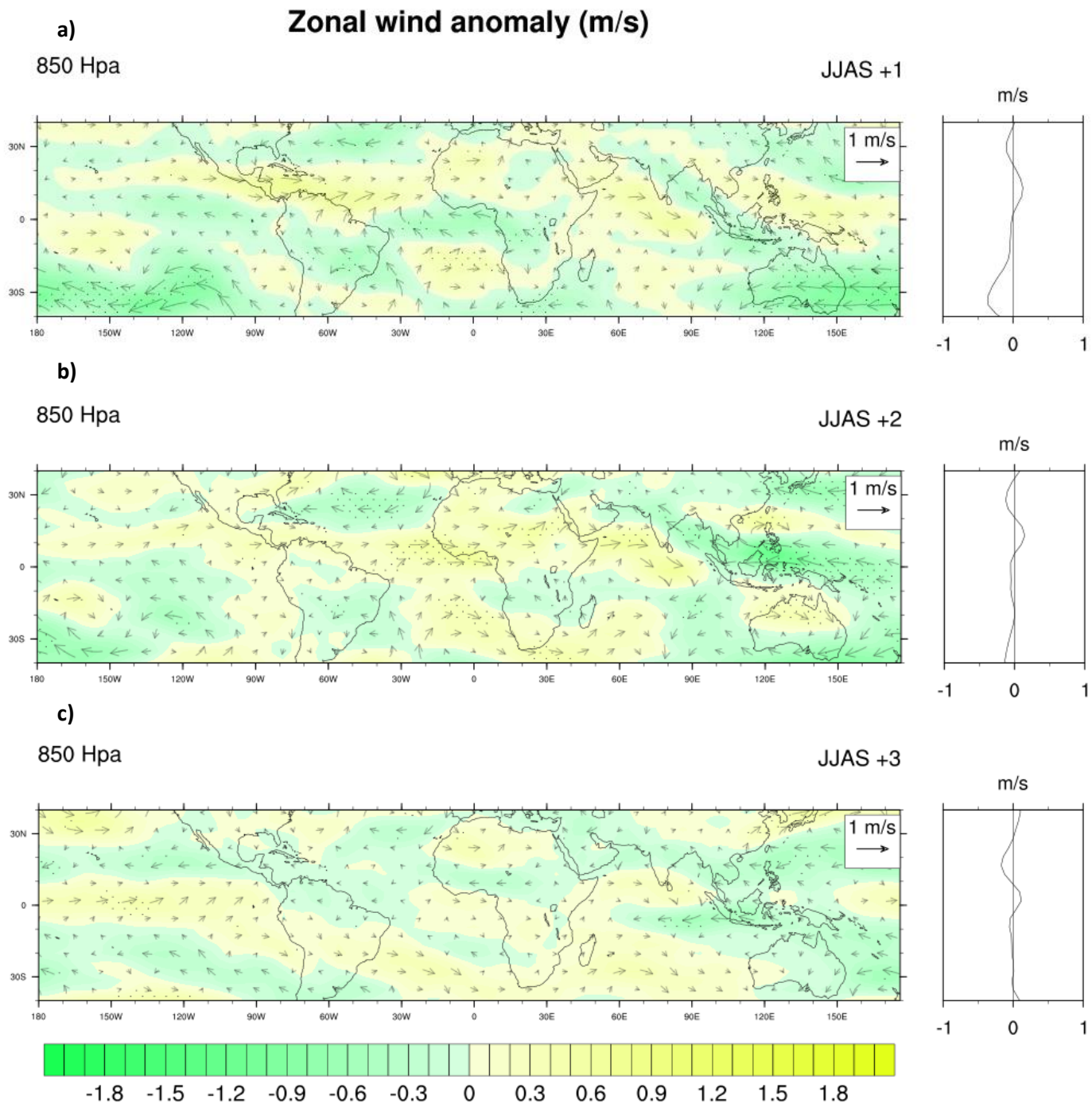

***Fig 4.47**: Averaged zonal wind anomaly (m/s) at 850 hPa for the **(a)** first, **(b)** second and **(c)** third boreal summer (JJAS) following 13 major tropical volcanic eruptions (EnsembleM1M2 simulation). Negative anomaly indicates a stronger east to west component than normal (and vice versa). Dotted areas represent 95% inter-eruption confidence level.*

During the first boreal summer (Figure 4.47 a), surface zonal winds with a significant higher east to west component can be found all over the 5-10°N latitude. This significant anomaly is especially seen over the Arabian Sea, the west part of Africa and the northern part of South America. This significant anomaly can still be found after the second summer (Figure 4.47 b). In the contrary, over South East Asia, we observe a significant strengthening of the easterly winds. After the third summer (Figure 4.46 c), the magnitude of the anomaly generally decreases and almost no significant patches are left.

Thus, as already shown in Figures 4.46 and 4.47, the magnitude of the surface wind anomaly is relatively small and disparate all over the Tropics. Locally we do find significant signals but, taken as a whole, the tropical regions do not undergo any major change. The zonal mean stays indeed always 0 m/s for every latitude and is not significant.

This is confirmed by Figure 4.48 which shows the zonally averaged surface wind anomaly. It is hard with this graphic to draw any robust conclusion even if the magnitude of the anomaly seems to decrease slightly after summer 1. At summer 3, the zonal averaged wind anomaly is almost equal to 0 m/s. Once more over the Southern Ocean, we do see a slight strengthening of the westerly winds which could be the result of the strengthened SAM index (Figure 4.33).

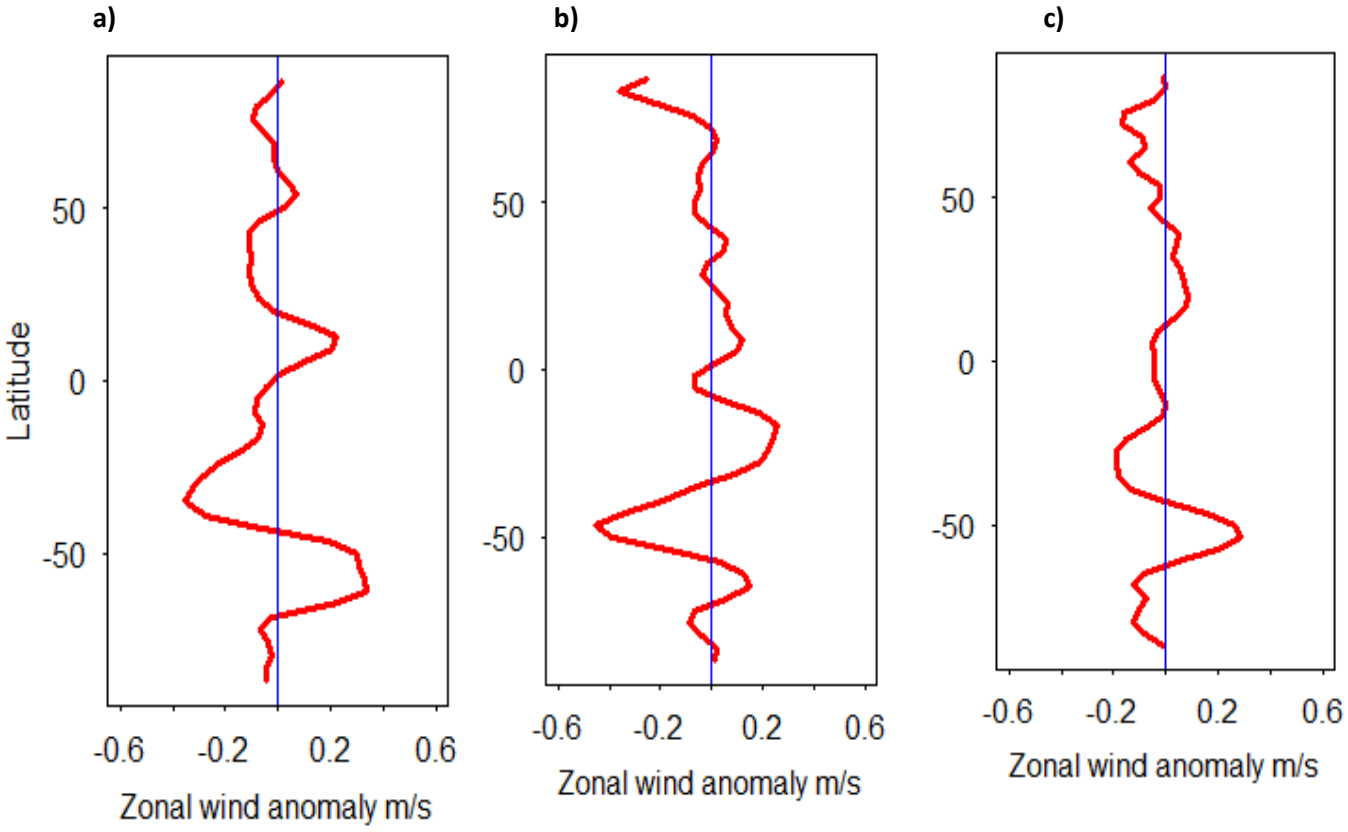

***Fig 4.48**: Zonally averaged zonal wind anomaly at 850 hPa for the **(a)** first, **(b)** second and **(c)** third summer following the 13 major volcanic eruptions in the EnsembleM1M2 simulation.*

4.2.4: Dynamical monsoon indices

In this section, we investigate more carefully the evolution of the 4 different dynamical monsoon indices presented and fully described in Chapter 3.3 after major volcanic eruptions.
Figure 4.48 gives a first overview and shows the monthly evolution of these 4 indices in the EnsembleM1M2 simulation. As for the wind analysis, the variability is high and no robust conclusion can be drawn based on these graphics. According to this figure, the monsoon systems over Asia do not seem to be sharply affected by volcanism activity. Nevertheless on Figure 4.49 (c) and (d) one can note interesting patterns. In both figures, the eruption of Mount Tambora is followed by a relatively high and pronounced positive anomaly. According to the M1M2 model simulation, this extremely powerful volcanic eruption is thus rather followed by a strengthening of the Asian monsoon systems. The patterns found after running the EnsembleL1L2 simulation are relatively similar and therefore not shown here.

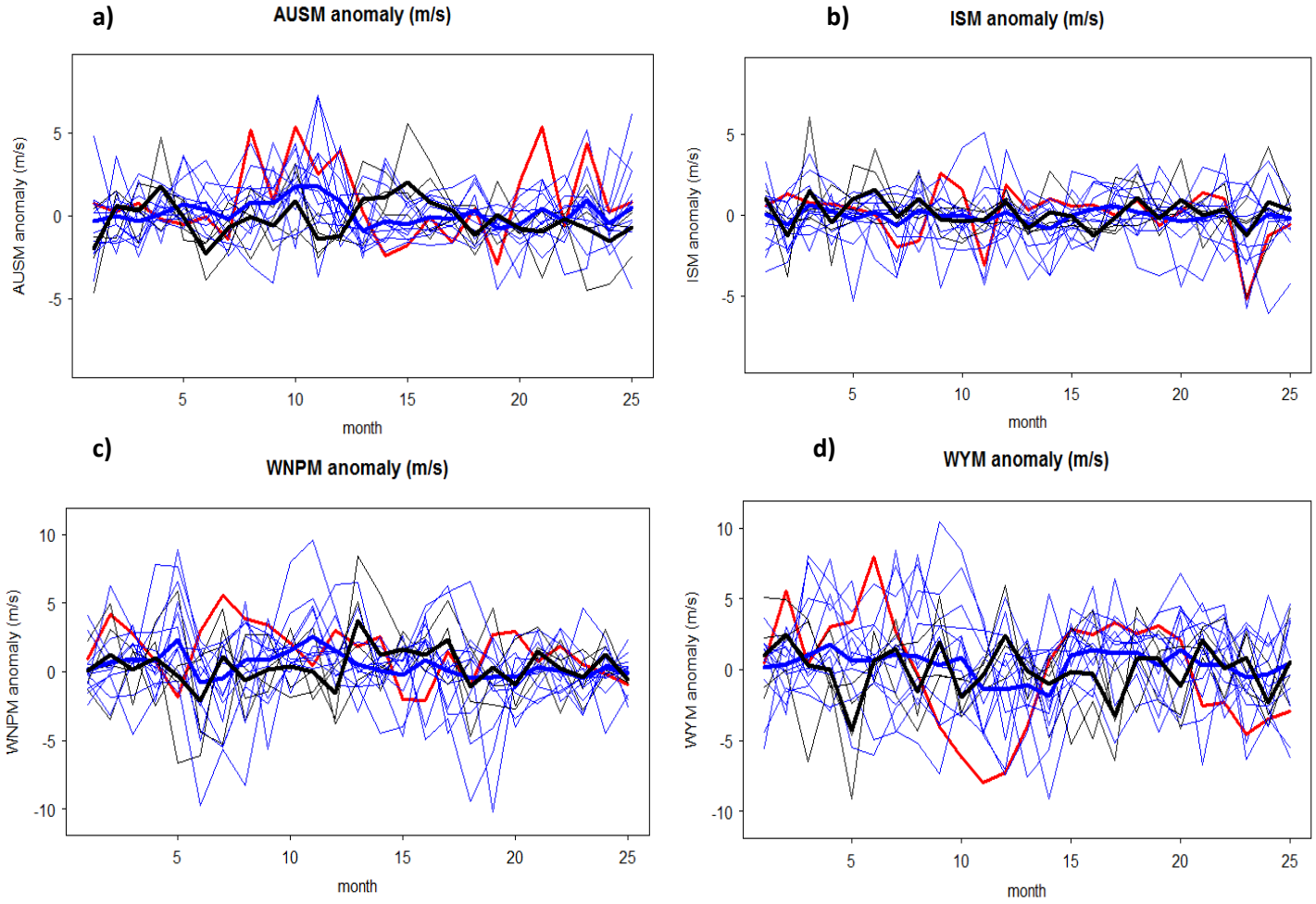

Fig 4.49: *Monthly averaged evolution of 4 dynamical monsoon indices (m/s) after the 13 tropical and 4 extra-tropical eruptions for the EnsembleM1M2 simulation:* ***(a)*** *AUSM,* ***(b)*** *ISM,* ***(c)*** *WNPM,* ***(d)*** *WYM. The thick red line shows the evolution of the index after the eruption of the Tambora. The blue lines represent the tropical eruptions whereas the black lines represent the extra-tropical eruptions. The two thick lines (black and blue) are the mean for extra and tropical eruptions.*

By looking more carefully at the linear relationship which exists between the AOD following each eruption and the dynamical monsoon indices anomalies, we found interesting results presented in Figure 4.50. Out of the 4 indices, 2 seem to react after volcanic events in the AOCCM SOCOL-MPIOM simulations. Indeed, the AUSM as well as the WYM indices seem to be strengthened after volcanic eruptions and a significant and positive correlation is found in both Ensemble simulations. This tends to prove that the monsoon system over Asia and Oceania is affected by such events. Over the Indian continent, the situation is different as no significant link can be drawn between the ISM index and volcanic eruptions. The same analysis can be done for the WNPM index.

For the AUSM index, we observe a positive and significant correlation with the AOD for the whole year as well as for the boreal winter season. For the EnsembleM1M2 simulation, these correlations are equal to 0.33 and 0.40 respectively (Figure 4.50). The numbers obtained are slightly lower for the EnsembleL1L2 simulation and reach 0.22 and 0.29 (not shown). It is also interesting to note that none of the eruptions are followed by a weakening of the AUSM index in winter. For the yearly mean, the situation is different and the eruptions of Huaynaputina, B. Claro, Cosiguina as well as Krakatau generate a global negative AUSM anomaly (Figure 4.50 b)

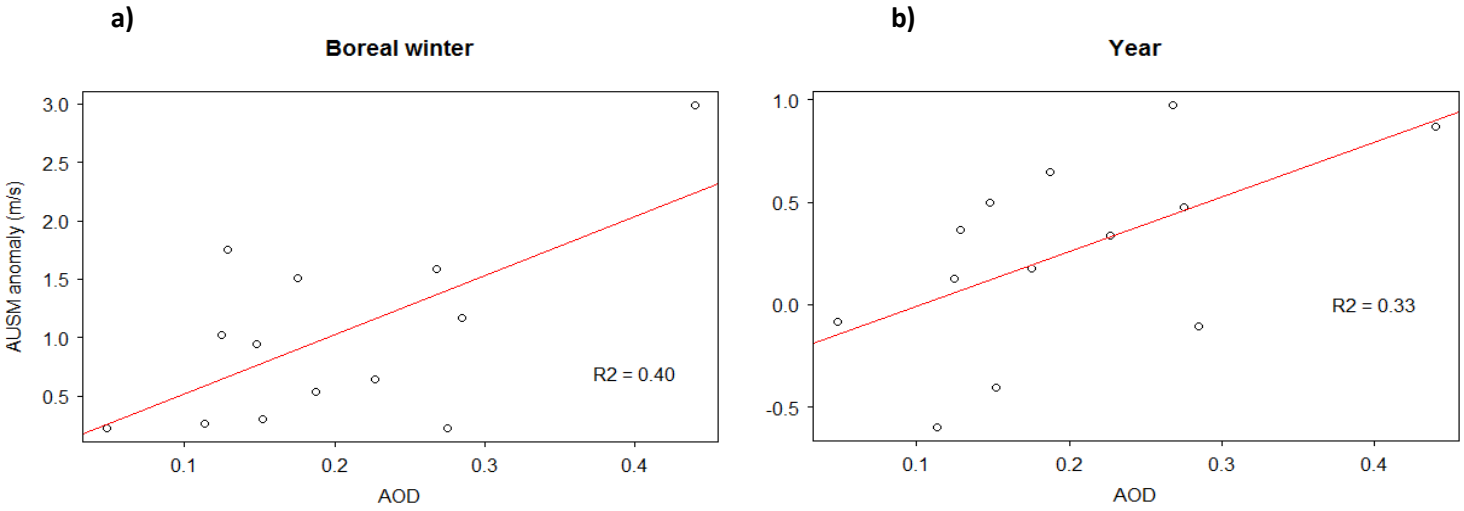

Fig 4.50*: Simple linear regression model explaining the averaged AUSM index anomaly through AOD (EnsembleM1M2 simulation). The dots represent the 13 different tropical volcanic eruptions and the red line shows the regression line. In* ***(a)*** *the 24 months following the eruptions have been chosen whereas in* ***(b)*** *only the boreal winter months (DJF) have been selected.*

A similar analysis can be done for the WYM index after analyzing Figure 4.51. The correlation obtained for the whole year and the boreal summer season are equal to 0.24 and 0.52 respectively. In the second simulation (EnsembleL1L2), the correlation obtained for the boreal summer is also significant (0.34). It is not the case if we look at the annual mean and the correlation obtained is only equal to 0.11 (p-value = 0.25). As for the AUSM, most of the eruptions are followed by a positive WYM summer index. Only the Unknown eruption of 1809 and the eruption of Mount Krakatau make exception.

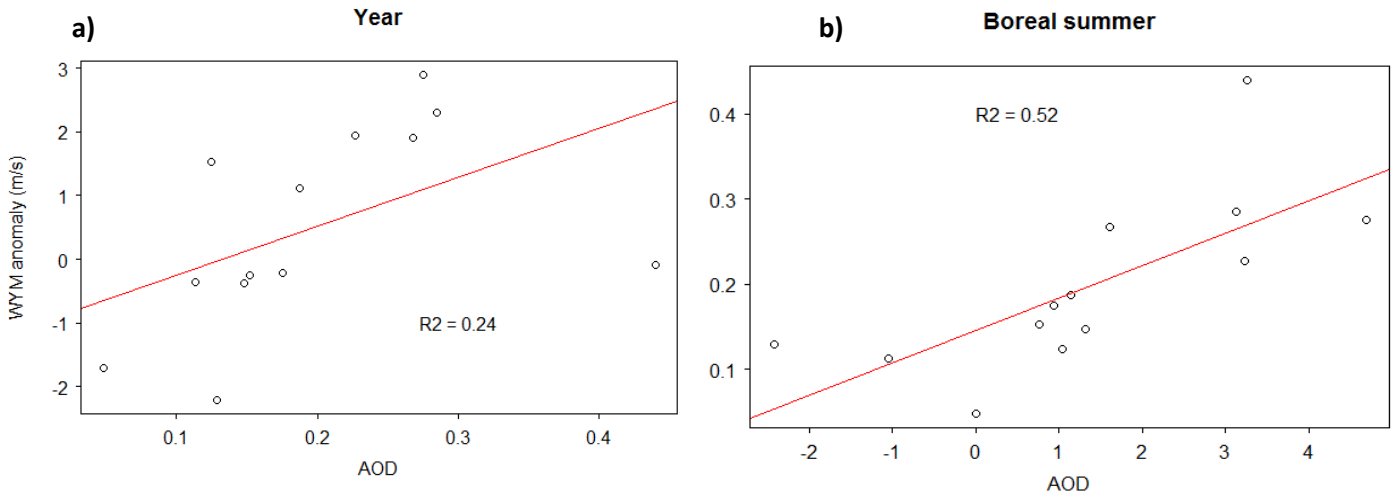

Fig 4.51*: Simple linear regression model explaining the averaged WYM index anomaly through AOD (EnsembleM1M2 simulation). The dots represent the 13 different tropical volcanic eruptions and the red line shows the regression line. In* ***(a)*** *the 24 month following the eruptions have been chosen whereas in* ***(b)*** *only the boreal summer months (JJAS) have been selected.*

Despite the promising results shown in figure 4.50 and 4.51, the results of the SEA (Figure 4.52) do not clearly confirm these first results. Indeed, even though we see a slight positive anomaly at lag 0 for AUSM index, the response is not clear and the volcanic influence seems to be negligible. For the WYM index (Figure 4.52 b), the AOCCM SOCOL-MPIOM do not seem to react to volcanic eruption neither. The same analysis has been performed with the EnsembleL1L2 simulation and for the two remaining dynamical monsoon indices but no significant anomaly were captured by the model (Figures not shown here).

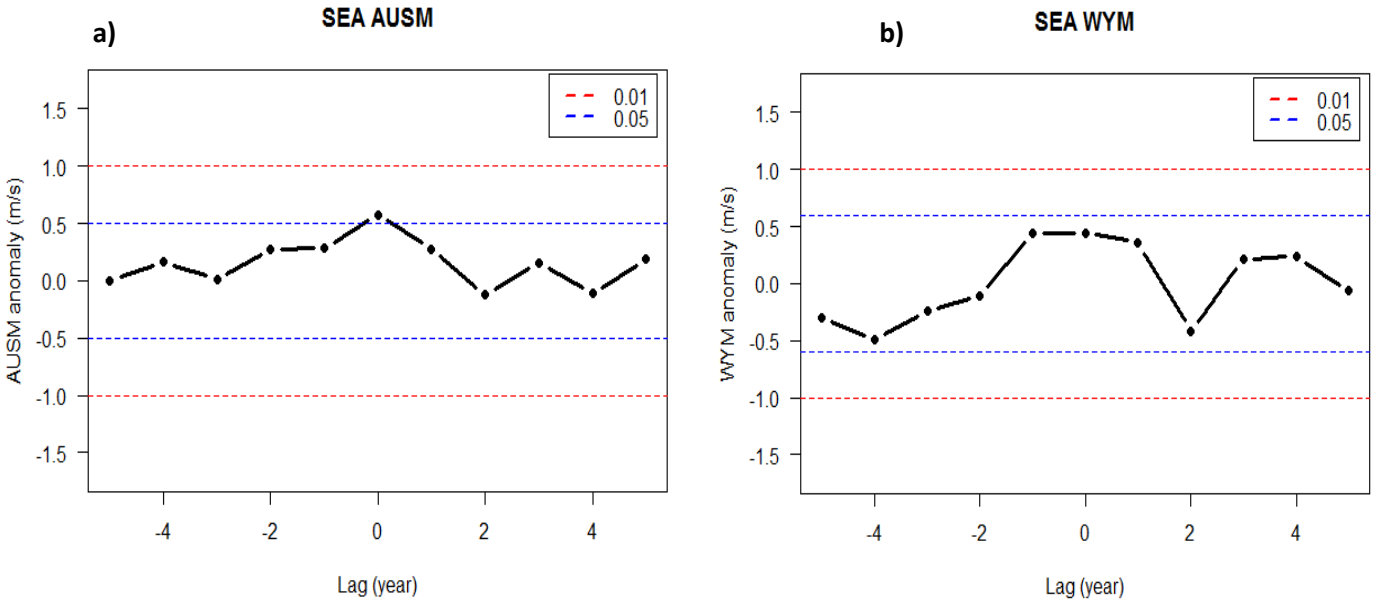

Fig 4.52: *The SEA results of* ***(a)*** *AUSM (boreal winter) and* ***(b)*** *WYM (boreal summer) for the 13 major volcanic eruptions for the EnsembleM1M2 simulation. The eruptions occur at lag 0. The two dashed lines represent the p-values at 1% and 5%.*

4.3: Comparison with 20CR and MADA

In order to validate the results obtained all along the chapter 4, we evaluate in this section the validity and the accuracy of the AOCCM SOCOL-MPIOM simulations. Because of the research questions and the scope of this thesis, we are mainly interested in tropical regions and on the Asian continent. To evaluate the GCM used in this study, we used the reconstructed and observational dataset described in Chapter 2.2.
Firstly, the surface temperature, the precipitation as well as the zonal wind data obtained after running the AOCCM SOCOL-MPIOM are compared to the 20th century reanalysis dataset. Then in order to evaluate the capability of the model to reconstruct precipitation over Asia, we compare the output of the model with the Monsoon Asia Drought Atlas (MADA) (Chapter 2.2.2).

4.3.1: AOCCM SOCOL-MPIOM surface temperature

Firstly we looked at the mean boreal summer surface temperature averaged over the period 1900-1999 AD for the 20th century reanalysis dataset and for the two model simulations. The comparison is then done by subtracting the model simulation to the 20th century reanalysis dataset (SOCOL-20CR) and the results are presented in Figure 4.53.

Generally, at the tropical level (Figure 4.53 a), the EnsembleM1M2 simulation of the AOCCM SOCOL-MPIOM overestimates the mean boreal summer temperature. The discrepancy between the model and the reconstructed dataset is rather high and reaches for certain regions 5 K. This positive anomaly is particularly high over the landmasses while its magnitude decreases over the ocean. The model even underestimates the surface temperature over the equatorial Pacific and the El Niño region.

By zooming in on the Asian continent, significant discrepancy between the global climate model and the reconstructed dataset are also clearly visible. The model seems to have trouble to predict the surface temperature over mountainous area and high anomalies are visible over the Himalaya and the Western Ghats. The model mainly overestimates the surface temperature over these regions and is not really appropriate to reconstruct historical climatic variations over highlands. Apart from these mountainous regions, the EnsembleM1M2 simulation simulates reasonably well the boreal summer surface temperature and the discrepancy is rarely above 2 K over the Indian continent and Asia. By comparing the EnsembleL1L2 simulation and the 20th century reanalysis dataset, the figure obtained did not significantly differ from the Figure 4.53 and is therefore not presented here.

Figure 4.54 shows more precisely how the AOCCM SOCOL-MPIOM EnsembleL1L2 simulation can reconstruct the effects of major volcanic eruptions on tropical summer surface temperature. As the 20th century reanalysis dataset starts only in 1871, we compared the surface temperature response after the 5 last tropical volcanic eruptions (Krakatau, Santa Maria, Agung, El Chichon and Pinatubo) with the output of the global climate model.

By looking at this figure, we can see a relative large discrepancy between the model and the reconstructed dataset. The temperature response in the model seems to be overestimated even though we still observe a general cooling of the landmasses in 20CR.

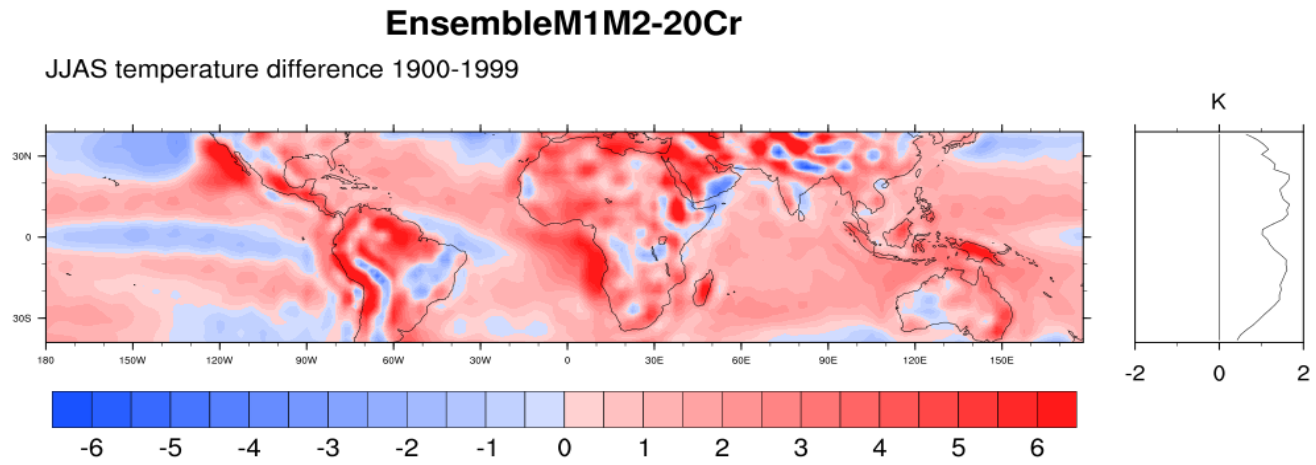

***Figure 4.53**: Mean boreal summer surface temperature difference (K) between the EnsembleM1M2 simulation and the 20th century reanalysis dataset (1900-1999 AD) for the tropical regions (SOCOL – 20CR).*

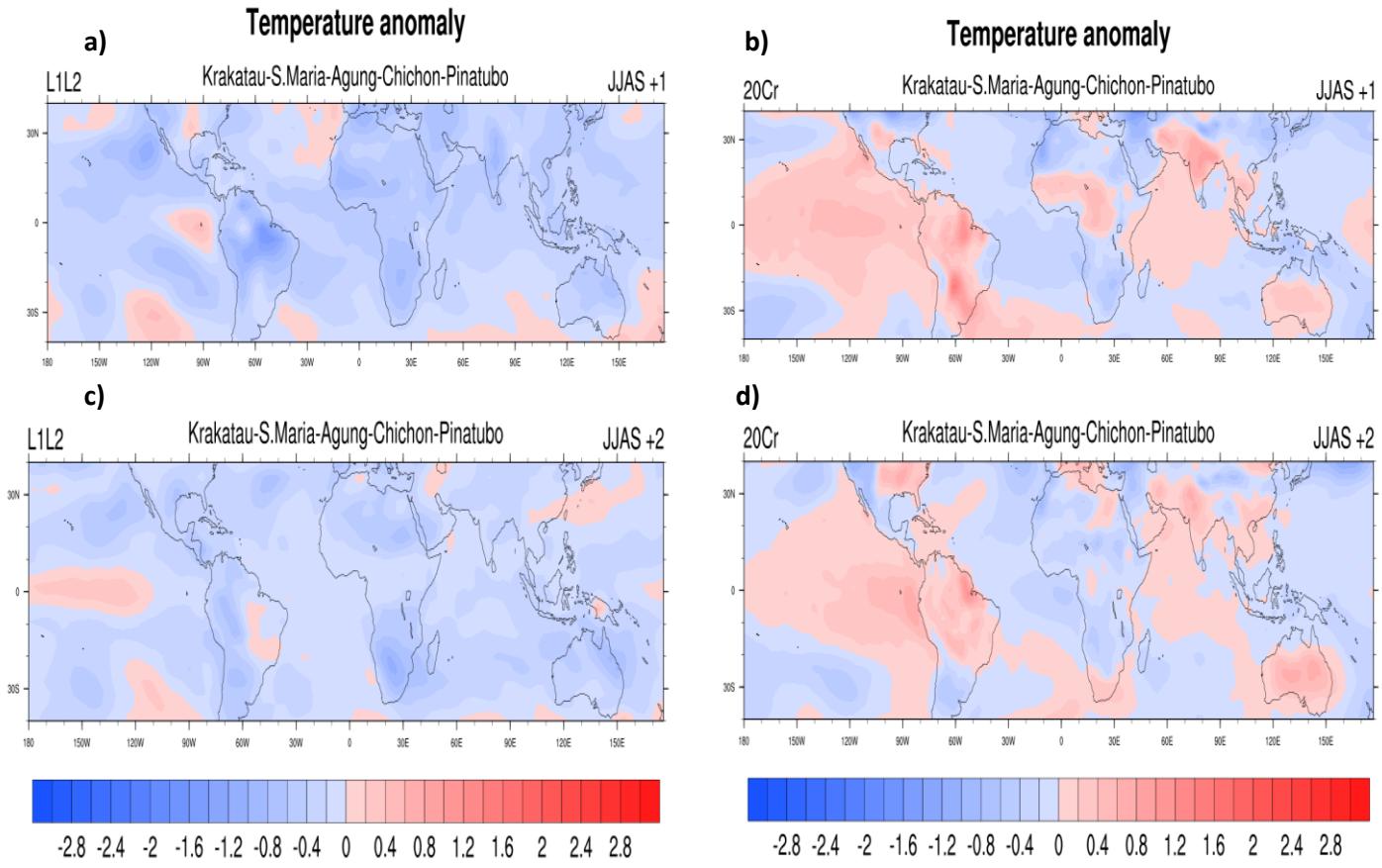

***Fig 4.54**: Averaged surface temperature anomalies (K) for the first boreal summer (JJAS) following 5 major tropical volcanic eruptions in **(a)** EnsembleL1L2 simulation and **(b)** 20CR. **(c)** and **(d)** show the second summer in EnsembleL1L2 and 20CR respectively.*

This cooling (Figure 4.54 b) is simply less pronounced (especially over the ocean). Disappointingly, the model and the observational dataset do not agree about the temperature response over the Indian continent and South America where the sign of the anomaly is reversed. For the second summer (Figure 4.54 c and d), approximately the same analysis can be done. We still observe a general cooling and the discrepancy observed for the Indian continent and South America persist. At summer +3, as in the AOCCM SOCOL-MPIOM simulations, the 20CR surface temperature anomaly vanishes gradually (not shown here).

4.3.2: AOCCM SOCOL-MPIOM precipitation

As for the temperature, a similar analysis can be done for the precipitation modelled by the AOCCM SOCOL-MPIOM. At the tropical scale, the model captures relatively well the distribution of precipitation and no major discrepancy are observed (Figure 4.55). Nevertheless, around the equator, we may note a slight underestimation of the amount of boreal summer precipitation of the model (Especially over the Pacific). As for the temperature, the global climate model used in this study seems to be experiencing difficulty in reconstructing precipitation over mountainous area. Indeed over the Himalayan region and the Western Ghats, the model sharply underestimates the strength of the Asian monsoon and the discrepancy between the model and the 20th century reanalysis dataset even reaches 14 mm/day over those regions. The results obtained by comparing the EnsembleL1L2 simulation and the reanalysis dataset were not significantly different and therefore are not shown here.

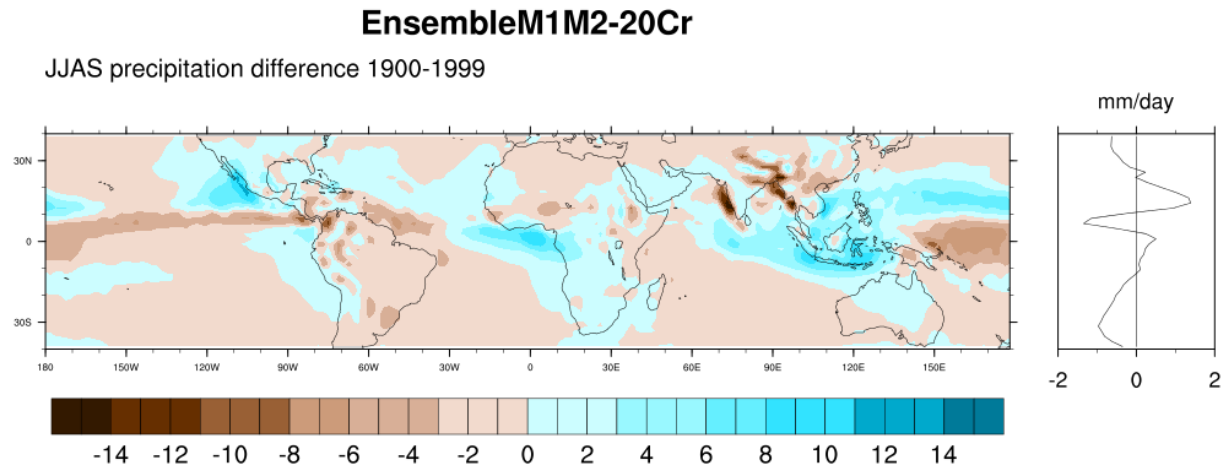

***Figure 4.55**: Mean boreal summer precipitation difference (mm/day) between the EnsembleM1M2 simulation and the 20th century reanalysis dataset (1900-1999 AD) for the tropical regions.*

On Figure 4.56, we looked more precisely at the capability of the model to reconstruct boreal summer precipitation response after the 5 last tropical eruptions picked for this study. The precipitation response after those 5 events looks relatively similar in both datasets. Indeed a general drying is observed all over the landmasses and we notice a stronger signal just around the equator. It is also interesting to note that the magnitude of the anomaly observed in the EnsembleL1L2 simulation is weaker compared to the 20CR dataset. Thus the model seems to underestimate the drying effect of major tropical volcanic eruptions.

For India the results are not that good. Indeed, during the first summer (Figure 4.56 a and b), an opposite signal is observed over the Indian continent: Whereas the model shows rather a wetting over the continent and a drying over Bangladesh and the Arabian sea, the signal is reversed in the 20th century reanalysis dataset where the Indian continent undergoes a drying and a wetting is recorded over Bangladesh. For the second summer (Figure 4.56 c and d) the analysis is relatively similar. At the tropical scale, the model is relatively good even if the magnitude of the anomaly is reduced compared with 20CR. At a local scale, we still can observe a large number of significant differences between the model and the reconstructed dataset. The 5-volcanic eruptions composite pictures obtained after handling the EnsembleM1M2 simulation did not bring anything new to the analysis and are therefore not shown here.

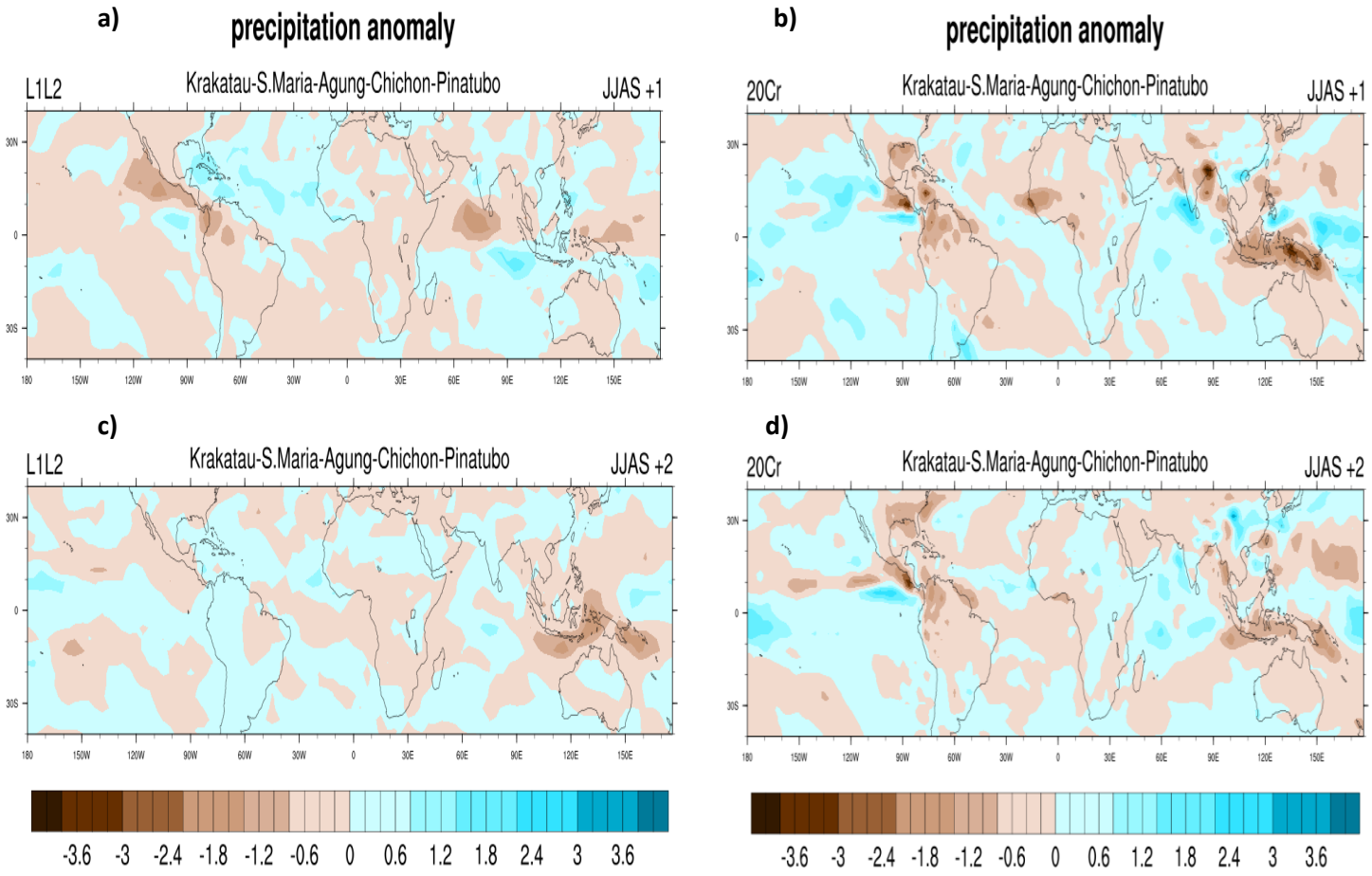

***Fig 4.56**: Averaged precipitation anomalies (mm/day) for the first boreal summer (JJAS) following 5 major tropical volcanic eruptions in **(a)** EnsembleL1L2 simulation and **(b)** 20CR. **(c)** and **(d)** show the second summer in EnsembleL1L2 and 20CR respectively.*

4.3.3: AOCCM SOCOL-MPIOM zonal winds

As for the two previous climate variables, we discern significant discrepancy between the model simulations and the 20th century reanalysis dataset. By and large, at the tropical level winds with a

stronger east to west component are observed in the model. The strength of the tropical easterly jet at 200 hPa is thus probably exaggerated in both Ensemble simulations (Figure 4.57 a). This difference is relatively homogeneously distributed and it is hard to detect any local pattern. But we can still note the large discrepancy over the Asian continent where anomaly of +5 m/s can be observed. There also the strength of the easterlies winds seems to be underestimated in both model simulations.

At 850 hPa (Figure 4.57 b) the pattern is less clear and more heterogeneous. In comparison with 200 hPa, the differences are reduced and the AOCCM SOCOL-MPIOM agrees relatively well with the 20th century reanalysis dataset. However, we do note a positive anomaly all along the 10th parallel North. Over this region the model seems to overestimate the west to east zonal wind component in the lower troposphere and especially over the South of the Indian continent.

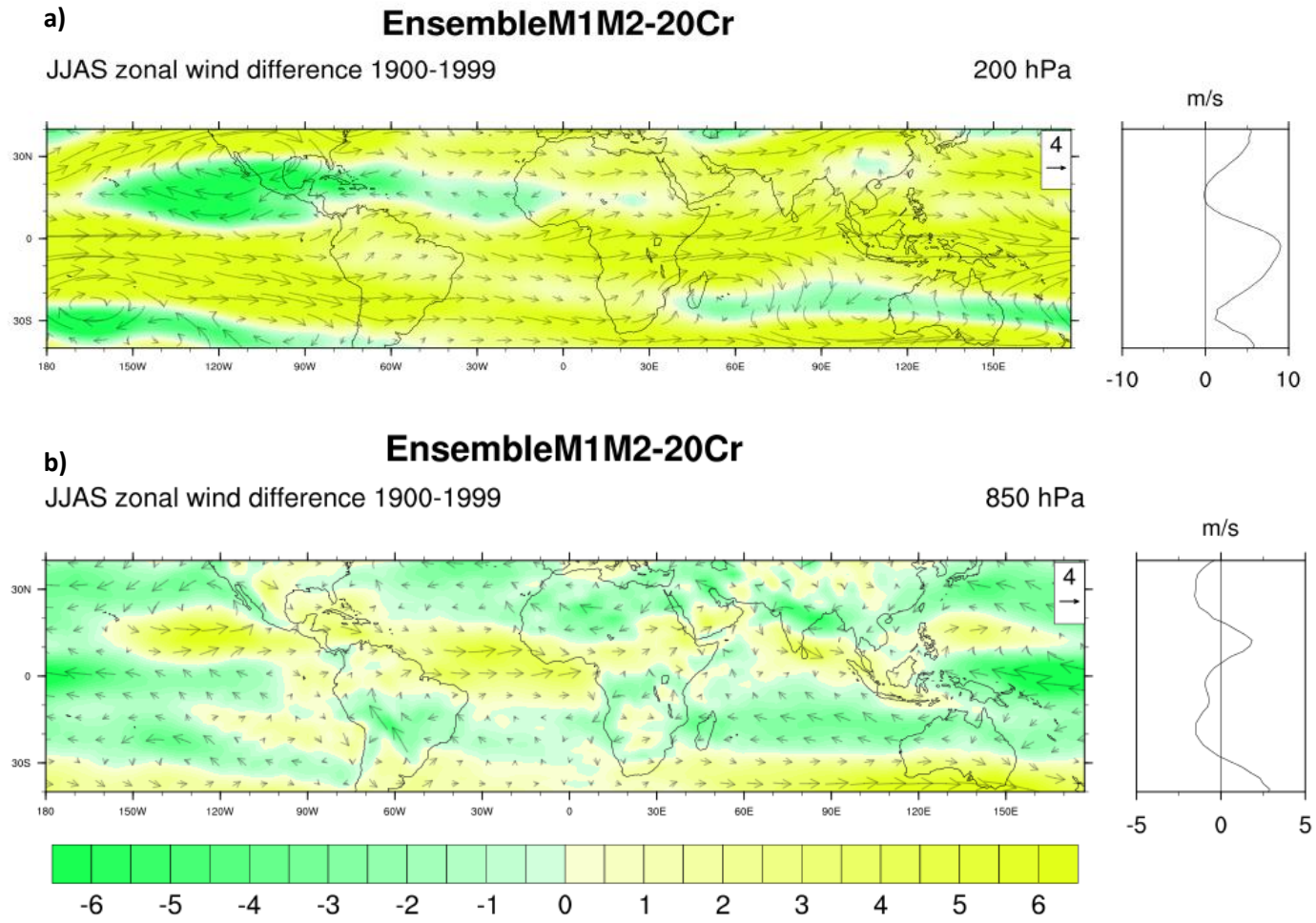

Figure 4.57*: Mean boreal summer zonal wind difference (m/s) at* ***(a)*** *200 hPa and* ***(b)*** *850 hPa between the EnsembleM1M2 simulation and the 20th century reanalysis dataset (1900-1999 AD) for the tropical regions. Negative anomalies indicate a stronger east to west component than normal (and vice versa).*

Surprisingly, the response of zonal wind at 200 hPa after the last 5 tropical volcanic eruptions is completely different in the AOCCM SOCOL-MPIOM and in the 20CR. In our model, volcanic eruptions create rather a strengthening of the tropical easterlies as we do observe a negative anomaly all over the

Tropics (Figure 4.58 a). The signal is completely reversed if we use the 20CR dataset where we observed a general weakening (Figure 4.58 b). Then unfortunately, the model used in this study seems to have problems to reconstruct the zonal winds response at 200 hPa after major volcanic eruptions. We have to keep that fact in mind before drawing any conclusions. During the second summer, the agreement is better between the two datasets. We still observe local discrepancy but the general pattern is by and large much better. In both case, we observe a sharp weakening in the magnitude of the anomaly which is not higher than 3 m/s anymore.

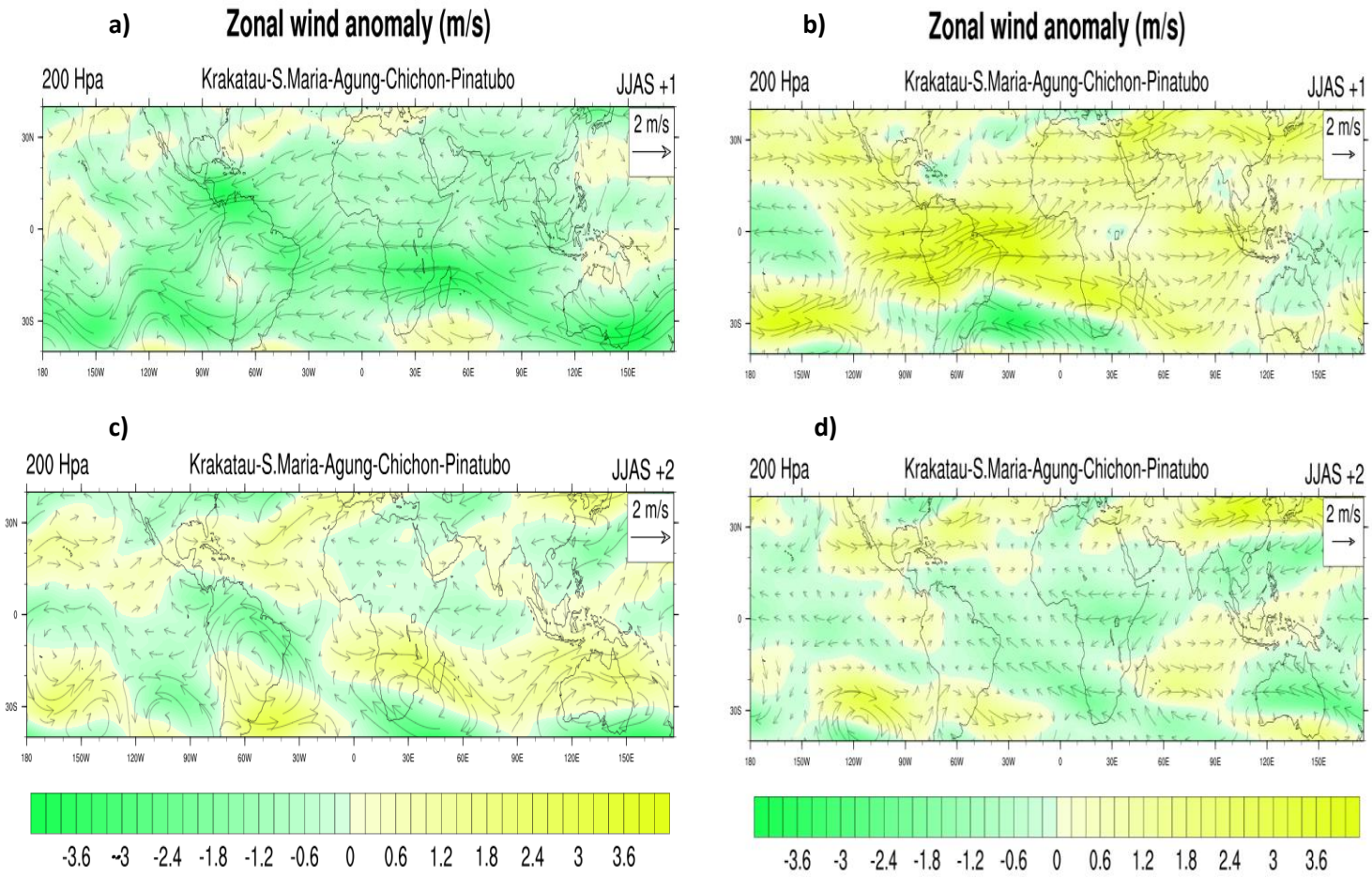

Fig 4.58*: Averaged zonal wind anomaly (m/s) at 200 hPa for the first boreal summer (JJAS) following 5 major tropical volcanic eruptions in* ***(a)*** *EnsembleL1L2 simulation and* ***(b)*** *20CR.* ***(c)*** *and* ***(d)*** *show the second summer in EnsembleL1L2 and 20CR respectively.*

Lower in the troposphere (Figure 4.59) the signal is much better and the AOCCM SOCOL-MPIOM and the 20CR dataset agree relatively well. Even though we can discern some local discrepancy the model seems to perform much better at this pressure level. During the first boreal summer following an eruption (Figure 4.59 a) and b)) we do observe a general weakening of the zonal easterly winds (yellow patches) around the equator. As for temperature and precipitation, the response simulated over India in the model does not really correspond to what is observed in 20CR. Once more we have over this region an

opposite signal. At summer +2 (Figure 4.59 c) and d)), the magnitude of the anomaly decrease in both cases and the agreement between the climate model and the reconstructed dataset is rather good.

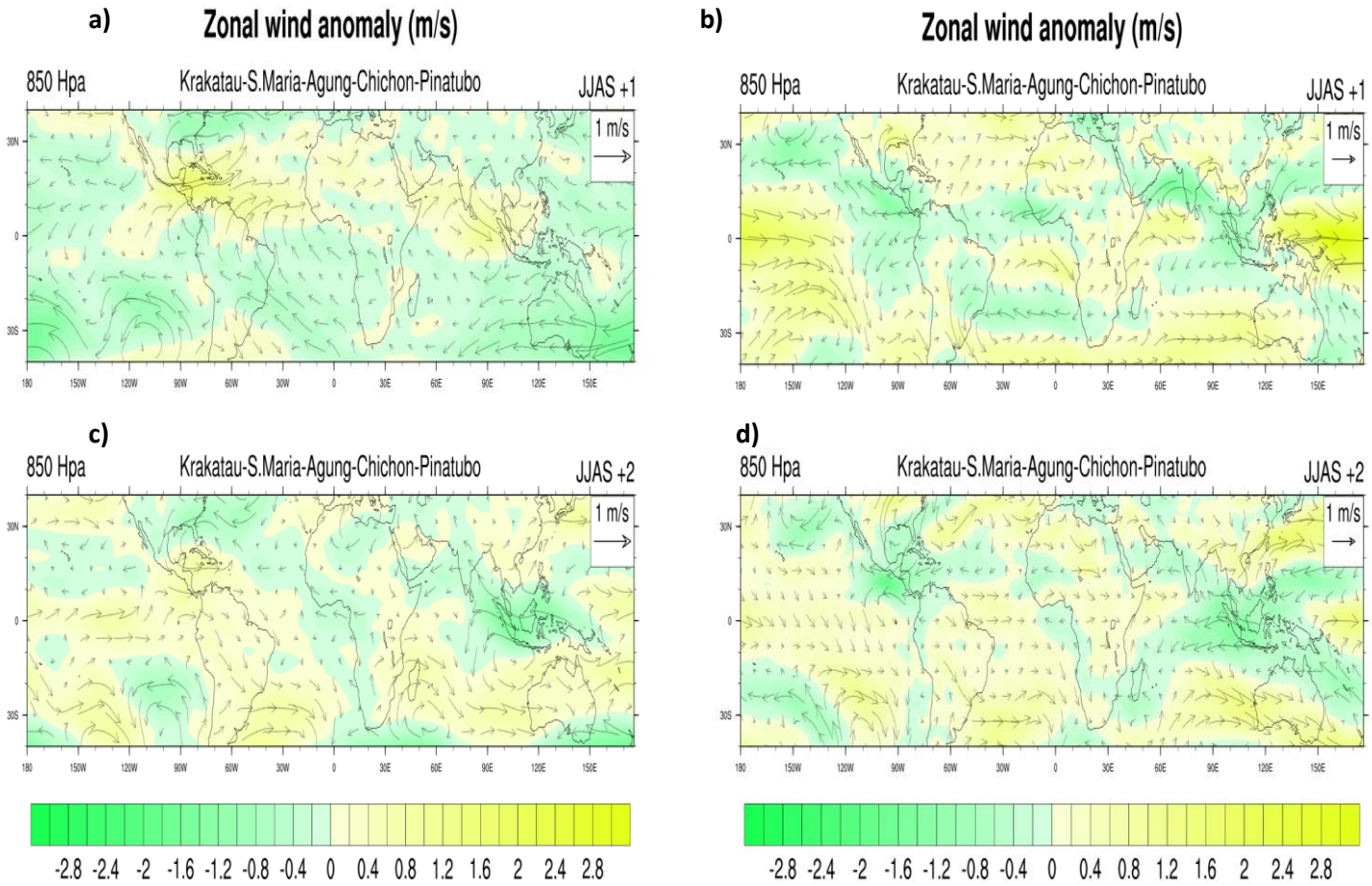

***Fig 4.59**: Averaged zonal wind anomaly (m/s) at 850 hPa for the first boreal summer (JJAS) following 5 major tropical volcanic eruptions in **(a)** EnsembleL1L2 simulation and **(b)** 20CR. **(c)** and **(d)** show the second summer in EnsembleL1L2 and 20CR respectively.*

4.3.4: AOCCM SOCOL-MPIOM PDSI

As one the aim of this study is to assess the effects of volcanic eruptions on Asian monsoon, it is important to evaluate more precisely the outputs of the AOCCM SOCOL-MPIOM over this region. For the evaluation, we used the Monsoon Asia Drought Atlas (MADA; Cook et al. 2010) fully described in section 2.2.2. We compared then the Palmer Drought Severity index (PDSI) obtained after running the model with the tree rings proxy. Unfortunately, as many others global climate models, the AOCCM SOCOL-MPIOM do not capture all the parameters and there is an obvious mismatch between the proxy and the model outputs (Especially over India). On one hand the model computes a drying over Southeast Asia in reaction to volcanic forcing but on the other hand, a wetting is observed over the Indian continent. If we look at the proxy data, we indeed see a clear drying over Southeast Asia during the first summer following the eruption. This drying seems to last and persist at summer +2 and +3. In the model this

drying is also seen but the magnitude of the anomaly seems to be underestimated. Over the Indian continent, we observe an obvious mismatch. Whereas the model simulates a slight wetting during the 3 first summer, the tree ring proxy suggests a pronounced drying which lasts during at least three summers. These results suggest then a deficiency in the AOCCM SOCOL-MPIOM model which is not really able to capture the effects of volcanic forcing over Asia. The same conclusion has been drawn by Cook et al. (2010) when they try to evaluate the accuracy of other climate models such as the NCAR CSM 1.4 model for example.

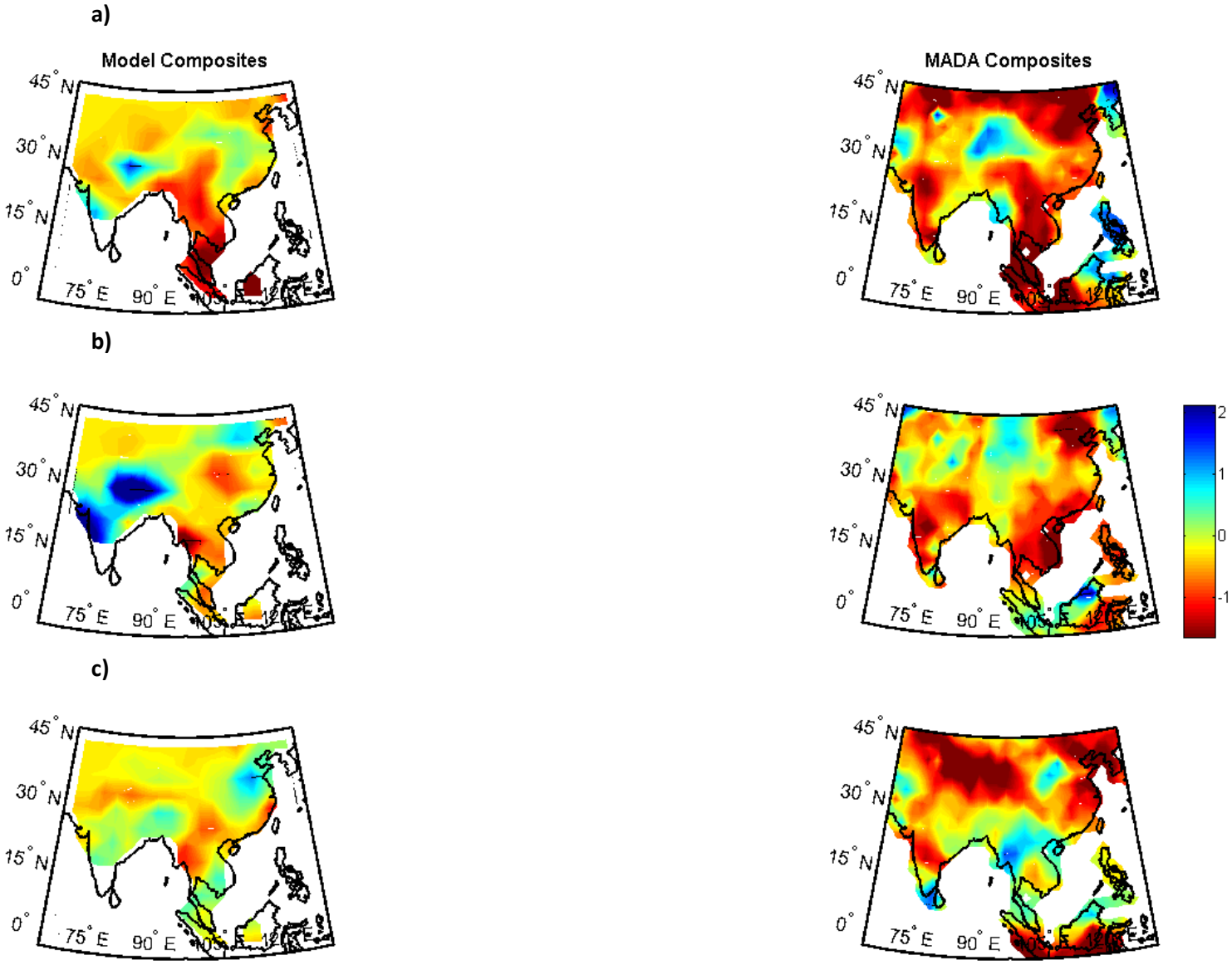

***Figure 4.60**: PDSI anomaly for the **(a)** first boreal summer (JJA), **(b)** second boreal summer and **(c)** third boreal summer following the 13 major tropical volcanic eruptions in EnsembleM1M2 simulation(left) and MADA (right).*

Chapter 5: Discussion

In this study, we tried to assess the effects of volcanic forcing on tropical regions and Asian monsoon regions. In order to reach that goal, the global climate model AOCCM SOCOL-MPIOM (Muthers et al. 2014) as well as a various set of reconstructed dataset have been used. Then the climatic response following 17 eruptions (4 extra-tropical and 13 tropical volcanic eruptions) which occurred during the last 400 years have been investigated.

Even though several similar studies (Wegmann et al. 2014; Joseph and Zeng. 2011) have been led, the present master thesis can still shed some light on this topic because of three specific points. Firstly, the aforementioned studies have been led using global climate models without dynamic oceans. Therefore the sea surface temperature (SST) and the sea ice had to be prescribed. This is not the case in this study thanks to the MPIOM ocean model fully described in section 2.1. Thus this model could be able to reproduce patterns which did not appear because of the prescribed ocean parameters and better reconstruct anomaly generated by volcanic forcing. Secondly, some basics points are still not clear for the scientific community such as the time duration of the tropical temperature and precipitation anomaly following a major volcanic eruption. This thesis brings interesting results on this specific topic and is not only focused on the short-time effects. Thirdly, the geographical scope of the present study is interesting and also could bring something new. Indeed, we did not only focus our analysis on the tropical regions but the effects of volcanic forcing on the Indian monsoon also were carefully analyzed and investigated. According to Schneider et al. (2009), major volcanic eruptions alter significantly the hydrological cycle of the monsoon and the eruption of Mount Tambora could have been the main driver of the unprecedented cholera epidemic outbreak in Bengal in 1817 (D'Arcy Wood 2014). Therefore, it is interesting to analyze carefully the climatic variations triggered by volcanic eruptions over these highly populated areas.

First of all, it is crucial to evaluate the accuracy and the performances of the AOCCM SOCOL-MPIOM model (see section 4.3). Indeed this global climate model is the most important tool and source beyond this thesis. Firstly the mean boreal summer surface temperature (1900-1999 AD) is relatively well reproduced by the model even though it generally overestimates the value of this variable. But at a local scale, significant discrepancies are observed and the AOCCM SOCOL MPIOM failed to reconstruct properly temperature over mountainous area. For example, the model overestimates the boreal summer surface temperature over the Andes, the Himalaya, the Rocky Mountains or the Western Ghats. This can be explained by the relative low horizontal resolution of the model (approximately 65km by 65km) and the orography in AOCCM SOCOL-MPIOM which do not corresponds to the one used in 20CR. Secondly, major volcanic forcing in 20CR and in both Ensemble simulations creates more or less similar surface temperature anomaly. It is interesting to note that our model do not show any warm anomaly over Africa. This warm anomaly has been modelled in many others study and is also well seen in the 20CR dataset but is missed by the AOCCM SOCOL-MPIOM. This warm anomaly detected by Robock et al. (2010) is probably due to the local reduction in cloud cover which lets more shortwaves radiations reaching the ground and trigger then a warming.

After the 13 volcanic eruptions, the model reconstructs a clear and extended cooling all over the Tropics. Note that the anomaly is particularly significant over the landmasses during the first summer and vanishes then gradually during the second summer but is still significant. The SEA performed supports this theory and shows that the significant cold anomaly persists until the second boreal summer and disappears then. Similar results had already been found by Robock (2000) where it had been

demonstrated that an immediate global cooling follows major tropical volcanic eruptions. This cooling according to the aforementioned study lasts between one to three years. In both Ensemble simulations, similar conclusion can be drawn and the global cooling following an eruption lasts in average 24 months with a pick after 10 to 12 months.

It is also interesting to note that the anomaly becomes linearly stronger with the power of the tropical volcanic eruption. With the Aerosol Optical Depth (AOD) derived from Gao et al. (2008), one can explain already more than 50% of the anomaly. This high linear correlation can easily be explained because the AOD and the Total Solar Irradiance (TSI) reaching the ground surface are closely linked. Indeed, the amount of solar radiation which cannot reach the ground because of aerosol back-scattering and absorption is directly proportional to the quantity of aerosol injected in the stratosphere. It could also be interesting for a further analysis to control if different others parameters such as the month of the year where the eruption occurred, could improve the linear regression model. As expected, after each individual tropical eruption a strong negative temperature anomaly is observed over the Tropics. Among those 13 events, the Mount Tambora is followed by the highest averaged tropical surface temperature anomaly which reaches 0.9 K after 13 months. This study also shows particularly well that the influence of extra-tropical eruptions on tropical climate is negligible. The mean anomaly following the 4 extra-tropical eruptions is never significant and stays around 0 K. In comparison, the 13 tropical eruptions generate a maximum anomaly of about -0.4 K. To sum up, the AOCCM SOCOL-MPIOM captures well the cooling generated by volcanic eruption and the magnitude of the anomaly is similar to what has been found by Wegmann et al. (2014) with the CCC400 simulations.

Over India, the performances of the model are less good. Indeed, if we compare the averaged effects of the 5 last tropical eruptions in the two Ensemble simulations and in the 20CR dataset, the response diverge largely. Indeed we observe a cooling in the model whereas a warming is obtained in the reconstructed dataset. Even though the 5 eruptions taken in account in the 20CR are not the most powerful (Pinatubo, El Chichon, Agung, Santa Maria and Krakatau), the differences seen between the model and the reconstructed dataset constrain us to remain prudent before drawing any conclusions. But if we rely on the AOCCM SOCOL-MPIOM simulations, the temperature response is relatively clear. As for the Tropics, a significant cold anomaly is observed during the first and the second boreal summer following an eruption and disappears then. Once more, the extra-tropical eruptions do not generate any significant temperature variations. It is also interesting to note that even though most of the tropical eruptions are followed by a negative anomaly, there is no clear link between the power of the eruption and the magnitude of the anomaly. On one hand, in the EnsembleL1L2 simulation no significant R-squared are found whereas in the second simulation (EnsembleM1M2), AOD could explain approximately 45% of the Indian boreal summer temperature anomaly. Therefore, according to the AOCCM SOCOL-MPIOM, major volcanic eruptions should trigger a cooling over the Indian continent. The model used by Wegmann et al. (2014) would rather suggest a warming whereas the study of Joseph and Zheng (2009) draw comparable conclusions.

Higher in the atmosphere the AOCCM SOCOL-MPIOM computes a highly significant warming. Indeed, after the emission of sulfur species, aerosols are formed in the stratosphere and absorb and scatter the incoming shortwave and outgoing longwave radiations. The absorption of Infrared and near-Infrared radiations caused by the aerosols is naturally followed by a warming of this atmospheric layer. This stratospheric warming remarkably described by Robock (2000) is also well captured in the AOCCM SOCOL-MPIOM simulations. Robock (2000), based on microwave sounding (Spencer et al. 1990) estimated the average stratospheric warming following the El Chichón (1982) eruption and the Pinatubo (1991) eruption to approximately 1 K and 1.5 K respectively. The AOCCM SOCOL-MPIOM computes for

the same eruptions and in the lower stratosphere (100hPa) a similar response: A maximal anomaly of about 1.2 K is reached 7 months after the eruption of El Chichón. After the eruption of the Mount Pinatubo, a maximal anomaly of 2 K is reached after 8 months. Despite a slight overestimation of the magnitude of the anomaly, the influence of volcanic forcing on stratospheric temperature is thus remarkably well captured by the model. But the overestimation is relatively small in comparison with others models and AOCCM SOCOL-MPIOM performs rather well in this domain.

In this model, the maximum temperature anomaly is computed at 100 hPa and is extremely clear. For example, 6 months after the eruption of month Tambora, the temperature increased sharply and the anomaly exceeds 6 K. Contrary to the surface temperature, the anomaly disappears quickly and is almost not seen one year after the eruption. The evolution of the temperature anomaly is similar for the 12 others volcanic eruptions. This is not really the case for the extra-tropical eruptions. Indeed even though we can see a slight warming after each event, none of them are significant. This was expected and can be explained by the global atmospheric circulation which reduces the interhemispheric exchanges of air masses (Newell et al. 1968). This fact combined to the reduced residence time of sulfuric acid in the stratosphere does not allow a general warming. The warming is thus confined to the hemisphere where the eruption took place and is not seen when we analyze the Tropics (40°N-40°S) as a whole. This explains why we do not see any global warming after the eruption of Mount Laki (Island) which is one of the biggest in term of aerosol masses generated (Gao et al. 2008).

The AOCCM SOCOL-MPIOM model also computes well the stratospheric temperature gradients evocated by Robock (2000). Indeed, as the tropical regions receive more incoming shortwave and outgoing longwave radiation, the heating is enhanced over those regions. This generates then thermal winds and amplifies the polar vortex. Such a change in the dynamic of the atmosphere is then propagated downwards and could influence other dynamical factors such as the monsoon system or the SAM. The AOCCM SOCOL-MPIOM also generates a gradient which is clearly seen when we looked at zonally averaged temperature. Around the equator, the zonally averaged anomaly is approximately equal to 2.5 K whereas in the higher latitude (50°N) the anomaly is only equal to 1 K. The model even products a cooling at around 50°S which could be explained by a strengthening of the SAM which limits the exchanges of air masses between Antarctica and the rest of the world. The temperature gradient disappears quickly and one year after the eruption, the temperature anomaly at 100 hPa stays at any latitude around 0 K. The SEA performed supports this analysis and in both Ensemble simulations, the influence of volcanic eruptions is only seen during one year. This conclusion had already been done by Robock (2000) where a stratospheric warming is already observed after one to three months. According to this study, the warming can last from one to two years. The AOCCM SOCOL-MPIOM agrees really well with the aforementioned study and similar conclusion can be drawn after an extensive analysis of both Ensemble simulations.

In contrary to the temperature evolution, the effects of volcanic forcing on water cycle have been less investigated and are less understood. Therefore, the present study could shed light on this topic. Moreover in contrary to many others studies, we did not only investigate the effects during the season directly following the eruption but the analysis has been led on a longer term. One of the strength of this study is then to evaluate the precipitation anomaly after the second and third summer following major volcanic eruptions and captures well the time duration of the anomaly.

As for the temperature, the AOCCM SOCOL-MPIOM model computes rather well the rainfall intensity over the Tropics but still shows some local discrepancies. For example, the model cannot really reconstruct properly the boreal summer precipitation over mountainous area. The precipitations over

those regions are largely underestimated. This problem is mainly seen over the northern part of Andes as well as the Western Ghats and the Himalaya where the discrepancy between the model and the reconstructed dataset can reach 12 mm/day. On one hand, the monsoon precipitation over large part of Asia is thus largely underestimated by the AOCCM SOCOL-MPIOM and we have to keep this fact in mind before drawing any conclusions. But in other hand, the coarse model used in this study is perfectly fitted to analyze precipitation anomaly at a tropical scale. We still have to note that over the equator the model slightly underestimates the boreal summer precipitations.

More precisely, after the five last eruptions picked for this study (Pinatubo, El Chichon, Agung, Santa Maria and Krakatau), the model reconstructs relatively well precipitation anomaly. In the 20CR reconstructed dataset as well as in the model, a drying is observed all over the Tropics. This drying is particularly pronounced around the equator in both cases but the magnitude of the anomaly differs. While the anomaly generally does not exceed -1 mm/day in the AOCCM SOCOL-MPIOM, it can reach -2 mm/day in the 20CR. The model used in this study seems then to slightly underestimate the effects of volcanic eruptions but agrees particularly well with the CMIP5 model used by Iles et al. (2014) and the CCC400 simulations employed by Wegmann et al. (2014).

Unfortunately, if we compare the performance of the AOCCM SOCOL-MPIOM with proxy dataset in Asia, we can see major discrepancies. Indeed, after the 13 tropical volcanic eruptions in the Monsoon Asia Drought Atlas (MADA), we observe a negative Palmer Drought Severity Index (PDSI) anomaly over India and South-East India. After calculating the PDSI for both Ensemble simulations, we did not get the same response. Indeed over India, the model computes a positive PDSI index (wetting) whereas South East Asia undergoes a clear drying. The model has then trouble to reconstruct the response of Indian monsoon to volcanic forcing. This discrepancy between global climate models and the MADA is not only unique to the AOCCM SOCOL-MPIOM but has been largely described by Cook et al. (2010). This obvious mismatch has already been observed in many models (For example the NCAR CSM 1.4 model) and should provide a way for modelers to improve theirs global climate models. This evident mismatch between the paleo dataset and the AOCCM SOCOL-MPIOM over this region forces us to interpret the results with prudence. In general global climate models fail to compute all the parameters driving the monsoon system and the AOCCM SOCOL-MPIOM simulation show the same weaknesses. However the model seems to be perfectly suited to analyze anomaly at larger geographical scale.

At the tropical scale, the response is perfectly clear and the model computes a large drop in tropical rainfall. This major drying is well distributed over the Tropics with some significant hot-spots over South-East Asia, the Arabian Sea and Central America. The negative anomaly over those areas can largely exceed -1 mm/day whereas in the study of Wegmann et al. (2014) values above -0.8 mm/day are barely computed. Thus precipitation anomaly in both Ensemble simulations seems to be highly sensitive to volcanic forcing and reacts rapidly after a tropical volcanic eruption. This was expected and has been largely described in the literature (Mitchell et al. 1961; Allen et al. 2002; Robock 2000). Indeed, as part of the solar radiation is blocked by the aerosol layer and cannot reach the Earth's surface, the energy available for the evaporation is reduced. This leads then to a drying of the air masses which reduces finally the formation of cloud and precipitation. This phenomenon should be typically present over the Tropics and the drying undergone by those regions much higher. Indeed, the tropical precipitations are closely correlated to the total solar irradiance (Agnihotri et al. 2011) and in contrast with some others regions, the importance of dynamical processes is reduced. This phenomenon is well captured by the model and a zonally averaged drying of about -0.3 mm/day is computed around the equator. A bit further from the equator, the zonally averaged anomaly stays negative but does not exceed -0.1 mm/day.

It is also interesting to note that, in contrary to the researches of Robock (2000), the negative anomaly computed by the model stays significant during at least three boreal summers directly following an eruption. Indeed, according to the aforementioned study, a tropical volcanic eruption begins to reduce the tropical precipitation through the blockage of shortwave radiations between one and three months after one eruption. This process continues then only during three to six months. According to the AOCCM SOCOL-MPIOM simulations, volcanoes also begin to have an influence on tropical precipitation after one or two months. However, for the time duration of the effects, the two Ensemble simulations show us completely different results. The SEA performed indicates that tropical averaged precipitations are still significantly weakened during the third summer following an eruption and persists when the cold surface temperature anomaly already vanished. This result is not really surprising. Indeed due to their thermal inertia, the oceans stay cold a bit longer in comparison with the landmasses. For this reason, the evaporation as well as the precipitation are reduced and the signal lasts longer. Indeed, a significant drying is for example still perceived at summer +2 over South-East Asia and Oceania. At summer +3, this drying stays significant over most of the equatorial regions. A consequent drying reaching -0.8 mm/day is notably seen over the Eastern Pacific and Central America. These results are thus more in agreement with the study of Trenberth and Dai (2007), where they investigated the effects of Mount Pinatubo eruption on hydrological cycle. According to this study, the water cycle has been negatively affected during a period of about 24 month.

As expected, and because tropical precipitation can be closely linked to the TSI (Agnihotri et al. 2011), we do have a clear link between the power of the eruption in term of AOD and the precipitation anomaly. In both Ensemble simulations, it is possible to explain more than 75% of the boreal summer precipitation anomaly with the strength of the eruption only. Hence, the biggest averaged tropical rainfall anomaly is observed 9 months after the eruption of Mount Tambora and reaches about -0.2 mm/day in both Ensemble simulations. As for the temperature, the anomalies caused by tropical and extra-tropical volcanic eruptions are clearly differentiated. Once more, the influence of the extra-tropical eruptions seems to be negligible on tropical climate. No clear patterns are distinguished and the mean anomaly stays always around 0 mm/day while the mean anomaly reaches -0.07 mm/day 10 months after a tropical eruption. Finally it is interesting to note that on one hand we observe a clear tropical precipitation effects and on the other hand, the global circulation seems to stay unchanged. Thus this would once more mean that tropical precipitation anomaly is directly driven by the reduced evaporation and the global cooling. Therefore, these three variables are interdependent and closely linked. Indeed, with a simple linear regression model, the temperature anomaly can already explain about 79% of the precipitation anomaly in the AOCCM SOCOL-MPIOM.

Over India and Asia, the model failed to reconstruct properly the dynamic of the monsoon system and for this reason, we have to stay prudent in our analysis. In contrary to the tropical regions, the global climate model does not compute any significant anomaly and no clear drying seems to be undergone by those regions. A significant wetting is even simulated at summer +1 over India, which would involve a strengthening of the monsoon system due to volcanic eruptions. The linear regression models performed with EnsembleM1M2 simulation supports this theory and suggests that precipitation over India is positively correlated with the strength of the eruption as the R-squared obtained is significant at the 0.1 level. But as the statistical test gave us only slight significant values and as a significant drying is observed at summer +1 over the Bay of Bengal, we can reasonably question the results obtained. The SEA performed consolidates this opinion by not showing any clear significant anomaly at any lags. No clear signal can then be seen in both Ensemble simulations. For the South East Asian monsoon, despite the imperfections of the model, the Figure 4.28 rather suggests a weakening of the monsoon system. The most common theory to explain this weakening may lie in the different heat capacity of the oceans and

the continents. Indeed, in theory the continents cool faster than the ocean and this reduced sea-land thermal contrast should weaken the monsoon dynamic.

In this study, we also checked if the Intertropical Convergence Zone (ITCZ) in the AOCCM SOCOL-MPIOM model moves towards the less cooled hemisphere. Indeed, Ridley et al. (2015) found that the anthropogenic emission of aerosol since the beginning of the industrialization may have caused a southward motion of the ITCZ. Most of the aerosol emissions due to human activities are released in the Northern hemisphere and the anthropogenic warming has then been muted there in comparison with the Southern hemisphere. Major tropical volcanic eruptions could have the same influence and generate a significant shifting of the ITCZ. In our set of volcanic eruptions, 11 out of 17 blew up in the Northern hemisphere and cooled therefore more this region of the globe. Indeed, after the eruption of Parker, Gamkonora, Krafla, Laki, Babuyan Claro, Cosiguina, Dubbi, Santa Maria, Katmai, El Chichón and Pinatubo, the model simulates a first averaged boreal summer anomaly equal to -0.31 K in the northern hemisphere (5°N-80°N) and -0.21 K in the southern hemisphere (5°S-80°S) . But after an extensive analysis, no clear and significant shifting of the ITCZ is seen in the AOCCM SOCOL-MPIOM simulations. The same analysis can be done after the 6 remaining volcanic eruptions occurring in the southern hemisphere. Unfortunately, not many studies dealt with this thematic so far and it is complicated to compare our results. Therefore it could be interesting to investigate more carefully this topic and check if a significant response is perceived in other global climate model. Because of a lack of time and resources, this comparison has not been done in this thesis, but could be an interesting starting point for future studies.

This thesis tries also to shed some light on the effects of volcanic forcing on zonal and vertical winds at different pressure level. As for the behavior of the ITCZ previously, not a lot of study have investigated this specific theme. To evaluate the robustness of the AOCCM SOCOL-MPIOM concerning the zonal winds, we compared the outputs of the model with the 20CR reconstructed dataset for the last century.
Surprisingly, in the low stratosphere (200 hPa) and for the boreal summer, the model is not really in agreement with 20CR. The discrepancies found are relatively high and can exceed 6 m/s. In both model simulations, we found a stronger tropical west to east component in comparison with 20CR. The tropical easterly jet seems then to be strongly underestimated in the AOCCM SOCOL-MPIOM simulations. Furthermore, the model does not seem to really capture all the parameters induced by volcanic forcing which perturbs the wind pattern. Indeed, after the 5 major volcanic eruptions occurring in the last century (Krakatau, Santa Maria, Agung, Chichon and Pinatubo), the model and the reconstructed dataset shows completely reversed responses. On one hand, in the 20CR dataset, a clear weakening of the tropical easterlies winds is observed. This supports the study of Wegmann et al. (2014) where the ECHAM5.4 atmospheric model computes a weakened African easterly jet. But on the other hand, the atmospheric model used in the present study simulates a clear strengthening of the tropical easterly jet.

During the second summer following an eruption, a much better agreement is found between both datasets. The magnitude of the anomaly is sharply reduced in both cases. Thus, our model seems to react to volcanic forcing and an abnormally high anomaly is perceived at summer 1. Nonetheless, the model must miss some parameters as the response is completely different in comparison with others studies or with 20CR and is hardly physically explainable. Further investigations are therefore necessary to explain the unexpected response of the global climate model. Lower in the troposphere (850 hPa) the model performs much better and the agreement with 20CR is better.

However, if we rely on the AOCCM SOCOL-MPIOM simulations, we observe a significant strengthening of the easterly jet at 200 hPa over most part of the Tropics. This strengthening is still present after the

second summer but vanishes afterwards. The significance is especially high over Asia and India. Indeed, over those regions, by using the power of the eruption as explanatory variable, we can already explain 12% and 47% of the zonal wind anomaly in EnsembleL1L2 and EnsembleM1M2 respectively. The SEAs support this theory and also show a significant strengthening of the easterly jet at summer +1 (and summer +2 in EnsembleM1M2 simulation). But this anomaly can hardly be physically explained and none of the study found in the literature show similar pattern. This is certainly due to the imperfections of the AOCCM SOCOL-MPIOM which cannot really properly model zonal wind at this height. It would be interesting in a further study to understand the zonal wind response of the model and this could help the modeler in the future.

Over the Southern Ocean, the model computes interesting results and a strengthening of the westerly winds is observed. This is the typical signature of a positive SAM index and after performing additional analysis we found a weak (non-significant) positive correlation between the magnitude of the SAM index and the volcanic forcing. Thus the model agrees relatively well with Krüger et al. (2014) where only a weak SAM signal is computed after a Pinatubo size eruption. However, in the same study, they found that the big eruption of Los Chocoyos (VEI =7) was followed by a significant and positive up to 10 times stronger SAM phase. In the AOCCM SOCOL-MPIOM model, even though the anomalies are not significant we observe slight positive SAM phases after the majority of the 13 tropical eruptions. For those reasons, the present study seems to confirm the influence of volcanic eruption on dynamical factors such as SAM.

Lower in the troposphere, where the model performs much better, it is hard to see any clear signal. Apart from a numbers of patches where the surface winds have a significant higher east to west component (notably over Africa, India and South America), no clear signal can be seen. It is also interesting to note that the magnitude of the anomaly do not really change between summer 1, 2 and 3. Thus in contrary to what was expected, the zonal surface winds (850 hPa) in the AOCCM SOCOL-MPIOM do not seem to react significantly to volcanic forcing and we do not see any strengthening of the surface westerly winds in the model.

Related to those results it is not surprising to note that the different monsoon indices do not really variate significantly after volcanic eruptions. Indeed, only the AUSM and the WYM react and are significantly correlated to volcanic forcing. As we use the zonal winds at 200 hPa to calculate these indices and as the AOCCM SOCOL-MPIOM has trouble to model this variable, we cannot draw any solid conclusion based on these results. For this reason, it would be interesting to perform the same analysis using a model with a better spatial resolution and try to see if as mentioned by different study, volcanic forcing is able to perturb the dynamic of the monsoon. Unfortunately, the AOCCM SOCOL-MPIOM which is perfectly suited to reconstruct climate at larger scale, is not the appropriate tool to carry out such a study.

Finally, the analysis of vertical winds in both AOCCM SOCOL-MPIOM simulations is interesting and gives promising results. As in the study of Wegmann et al. (2014) and Jones et al. (2005), we can discern a weakening of the ascending winds around the equator where we find the ascending branches of the Hadley cell (Figure 4.35). Due to the volcanic forcing, this dynamic atmospheric cell seems then to be significantly weakened. During the first and second summer, a lot of area with winds with a stronger downwards movement than normal are computed by the model. Significant patches are notably observed over South America, equatorial Africa and Indonesia. If we look a bit northward and southward of the equator an opposite signal is captured by the model. In those regions, corresponding to the descending branches of the Hadley cell, the descending vertical winds seem to be weakened. Those anomalies and according to the SEA performed (for both Ensemble simulations), remain during about 2

years and are still perceived at summer +2. Even if it is harder than with the other variables analyzed in this thesis, we also note a difference between the effects of extra-tropical and tropical eruptions. Whereas the equatorial vertical winds seem to be significantly weakened after tropical volcanic eruptions, the effects of extra-tropical volcanic events are negligible at a tropical level. It is also interesting to note that the magnitude of the vertical wind anomaly can be particularly well explained by the AOD generated by each volcano. Indeed, the R-squared obtained in both Ensemble simulations exceed 40%. Moreover, if we look at the vertical wind profile, the winds are weakened at all pressure levels. The Tambora eruption is particularly well seen and distinguished from the other eruptions and the vertical wind anomaly can reach 4 mPa/s between 800 hPa and 500 hPa. In comparison, the anomaly following the 13 eruptions selected for this study do not exceed 2mPa/s. Finally, the AOCCM SOCOL-MPIOM computes a clear link between the strength of the equatorial vertical winds and the temperature and precipitation. Indeed, in both simulations and as expected, the global tropical cooling can explain the weakening of ascending vertical winds (about 70%). Logically, the weakening of the convective cells explains then relatively well the tropical drying observed (about 50%)

To sum up and according to the AOCCM SOCOL-MPIOM, major tropical volcanic eruptions affect significantly the dynamic of the atmosphere. The Hadley cell seems then to react and be weakened after the global cooling generated by volcanic forcing. This weakening is then a major factor which can explain the reduction of tropical summer precipitation.

Chapter 6: Conclusion

In this study, a global climate model (AOCCM SOCOL-MPIOM) as well as different reconstructed and observed datasets have been used in order to assess the influence of major volcanic eruptions on the climate of the Tropics and Asia. Indeed, in the global climate model used, the response to volcanic forcing is clearly seen and we observe significant anomalies for several variables (temperature, precipitation, zonal winds…) all over the Tropics. Thus and despite the discrepancy observed between the AOCCM SOCOL-MPIOM simulations and the reconstructed datasets (20th century reanalysis datasets and MADA), this model is a suitable tool to analyze tropical climate response to volcanic forcing. If we look more carefully at the Asian monsoon system, the signal is harder to perceive and to interpret and we see significant differences between the model and the reconstructed and paleo dataset (Chapter 4.3 and 5). Therefore, to obtain robuster results, it would be useful to use another climate model with a higher spatial resolution and performing better over this region. Nevertheless, this model and this study still contribute to the research field of climate impact after volcanic forcing and interesting results have been found.

Firstly, it has been found that volcanic eruptions have considerable impacts on surface temperature and a negative anomaly lasting in average 2 years is observed after each of the 13 tropical events chosen for this study. For the 4 remaining extra-tropical eruptions, no clear and significant anomalies are observed. Last and not least, we found a clear linear relationship between the strength of the eruptions and the magnitude of the anomaly. Secondly, the model computes significant perturbation of the water cycle system over the Tropics due to volcanic forcing. As for the temperature, we observe a dry anomaly strongly correlated to the strength of the eruption which lasts more than three years. Once more, the extra-tropical eruptions do not generate any clear and significant anomaly. Over Asia, the response is less clear and we observe significant wetting over certain regions such as India. Furthermore, concerning the water cycle perturbation, we do not see any clear motion of the ITCZ. According to different studies, the ITCZ should slightly move towards the less cooled hemisphere but this phenomenon is not computed by the AOCCM SOCOL-MPIOM. Finally, if we look at some dynamical factors, interesting results have been found. The easterly tropical jet at 200 hPa is indeed significantly strengthened by volcanic forcing in the model. Lower in the atmosphere this anomaly disappears and is not clearly seen anymore. We also observe a significant strengthening of the upwards vertical winds around the equator which could indicate a strengthening of the Hadley cell. It is also interesting to note, that the model computes a slight strengthening of the SAM over the Southern Ocean. Those first results are encouraging and demonstrate the influence of volcanic forcing on dynamical factors. But, if we zoom in on the Asian region and consider several dynamical monsoon indices, the results are more disappointing. Indeed, in contrary to others similar studies, the AOCCM SOCOL-MPIOM do not compute any significant change and the monsoon dynamic do not seem to be really influenced by volcanic eruptions. But as already mentioned and described in chapter 4.3 and 5, our global climate model faces difficulties when it computes the zonal winds in the high troposphere. Therefore the previous results have to be carefully employed and can be easily criticized.

Nonetheless, and despite the weaknesses of the model, this study still brings interesting results and contribute to the research field of climate impact after volcanic eruptions. First of all it is one of the first studies of this type using a global climate model without fixed SSTs and simplified ocean circulation. The comparison with the outputs obtained after running others models is then particularly interesting and some differences can be noted. Furthermore, one of the strength of this study is to analyze the climate perturbation on longer-term. The effects due to volcanic forcing are still investigated 3-4 years after the

eruption in this study and we found interesting results. For example, in the AOCCM SOCOL-MPIOM, the precipitation anomaly lasts much longer in comparison with other study.

To sum up, our model computes well the climate perturbation due to major tropical volcanic eruptions on a large scale but faces some difficulties when the climate of specific local regions has to be reconstructed. Therefore, it would be interesting to investigate the variation of the Asian monsoon after a major volcanic eruption using another model which computes more effectively the climate over this region. For this reason, further research should be led to assess the effects of future major volcanic eruptions and potential future use of geoengineering option, on the climate of these highly populated areas.

Appendix

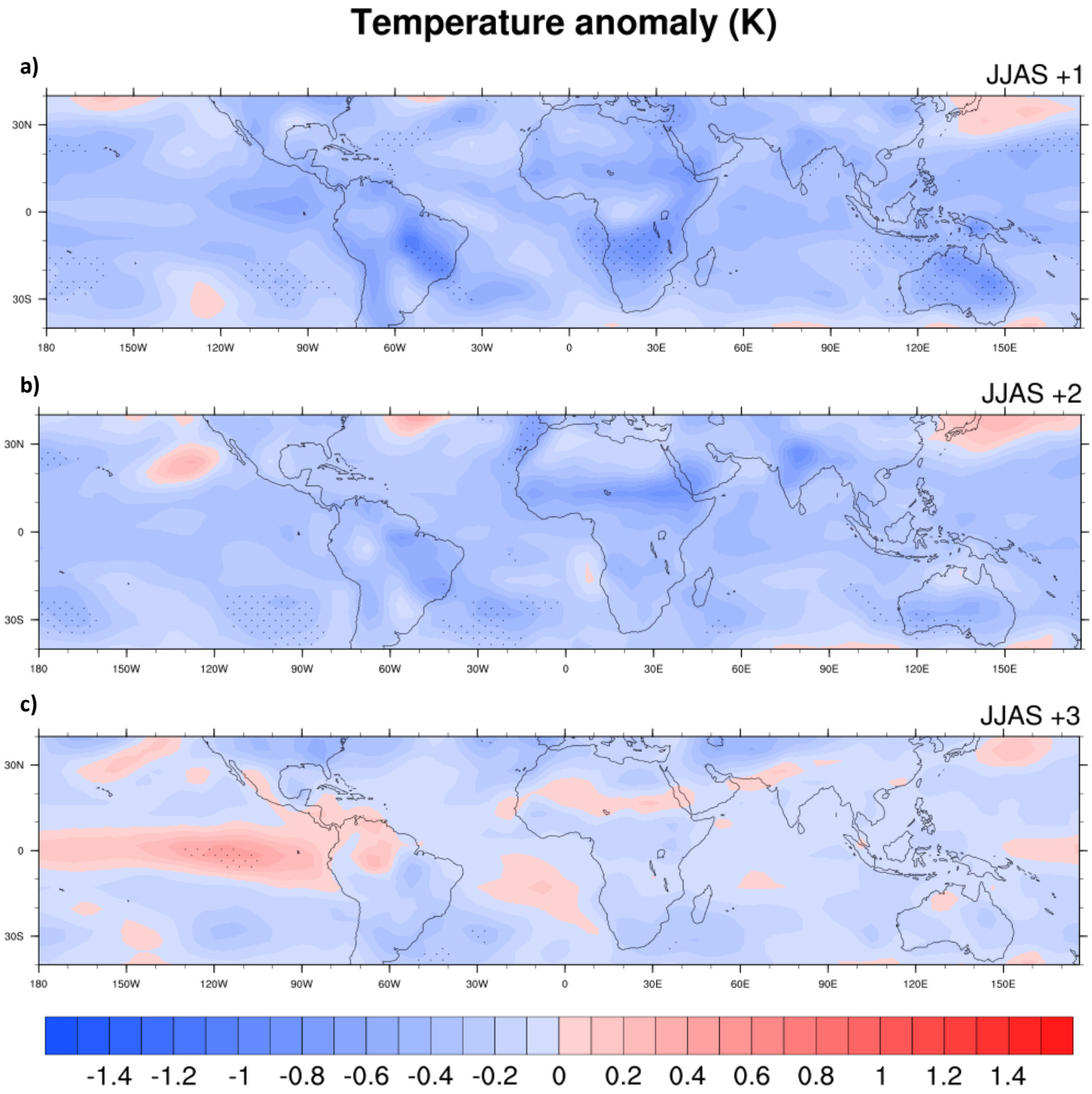

A1: Averaged surface temperature anomalies (K) for the (a) first, (b) second and (c) third boreal summer (JJAS) following the 13 major tropical volcanic eruptions (EnsembleM1M2 simulation). Dotted areas represent 95% inter-eruption confidence level.

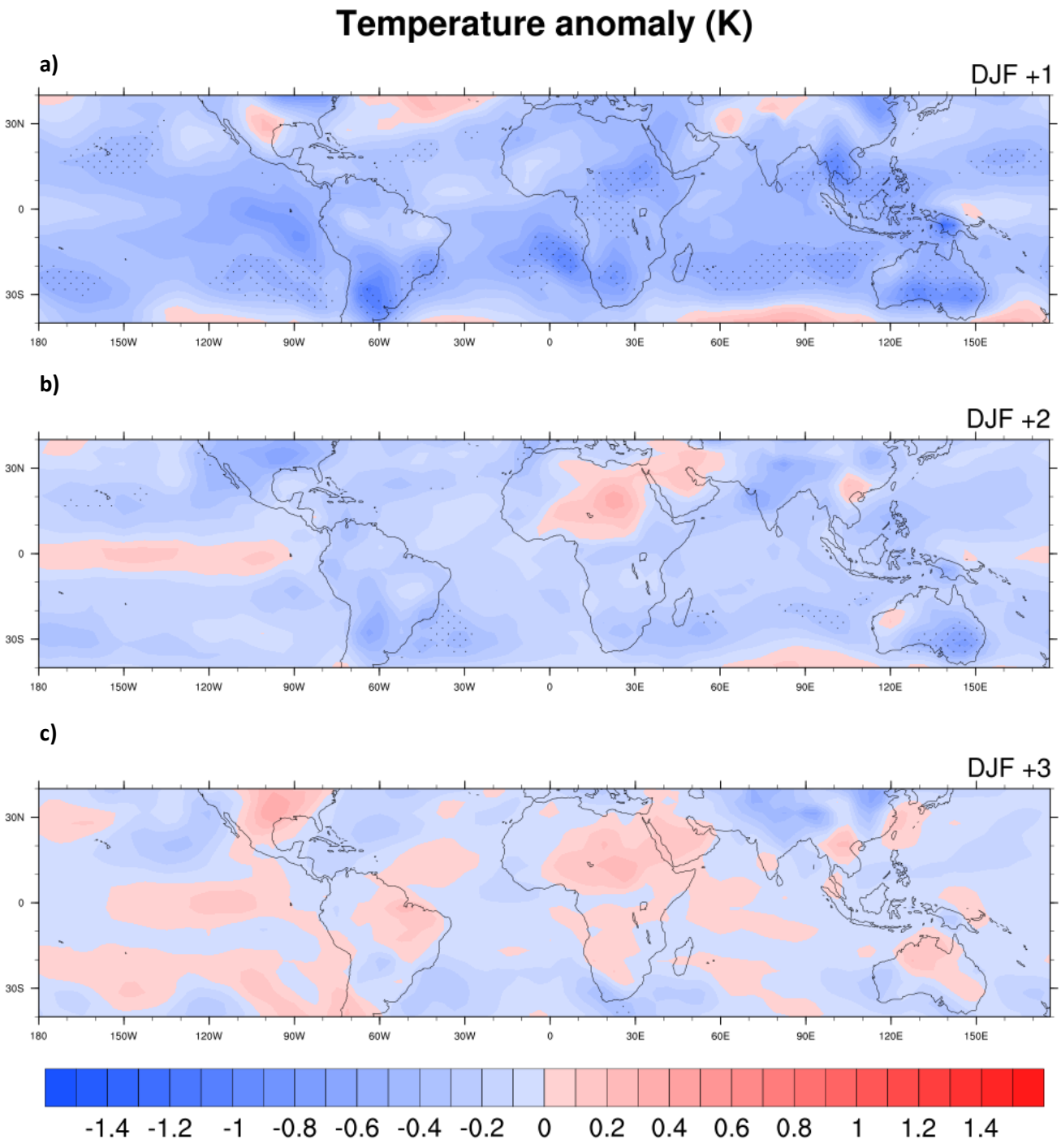

A2: Averaged surface temperature anomalies (K) for the (a) first, (b) second and (c) third boreal winter (DJF) following the 13 major tropical volcanic eruptions (EnsembleM1M2 simulation). Dotted areas represent 95% inter-eruption confidence level.

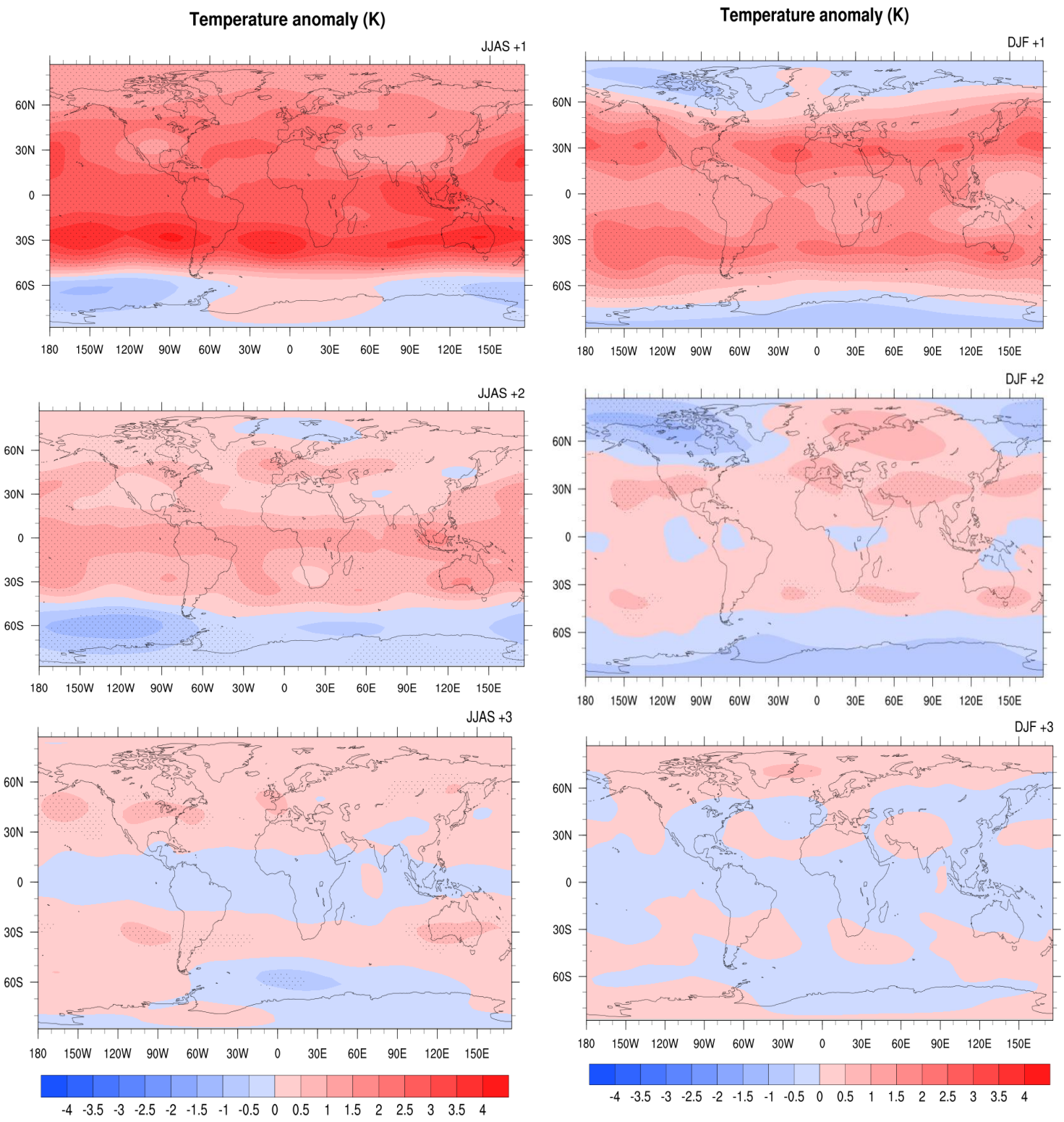

A3: Averaged temperature anomalies (K) at 100 hPa for the first, second and third boreal summer (JJAS) and winter (DJF) following the 13 major tropical volcanic eruptions (EnsembleM1M2 simulation). Dotted areas represent 95% inter-eruption confidence level.

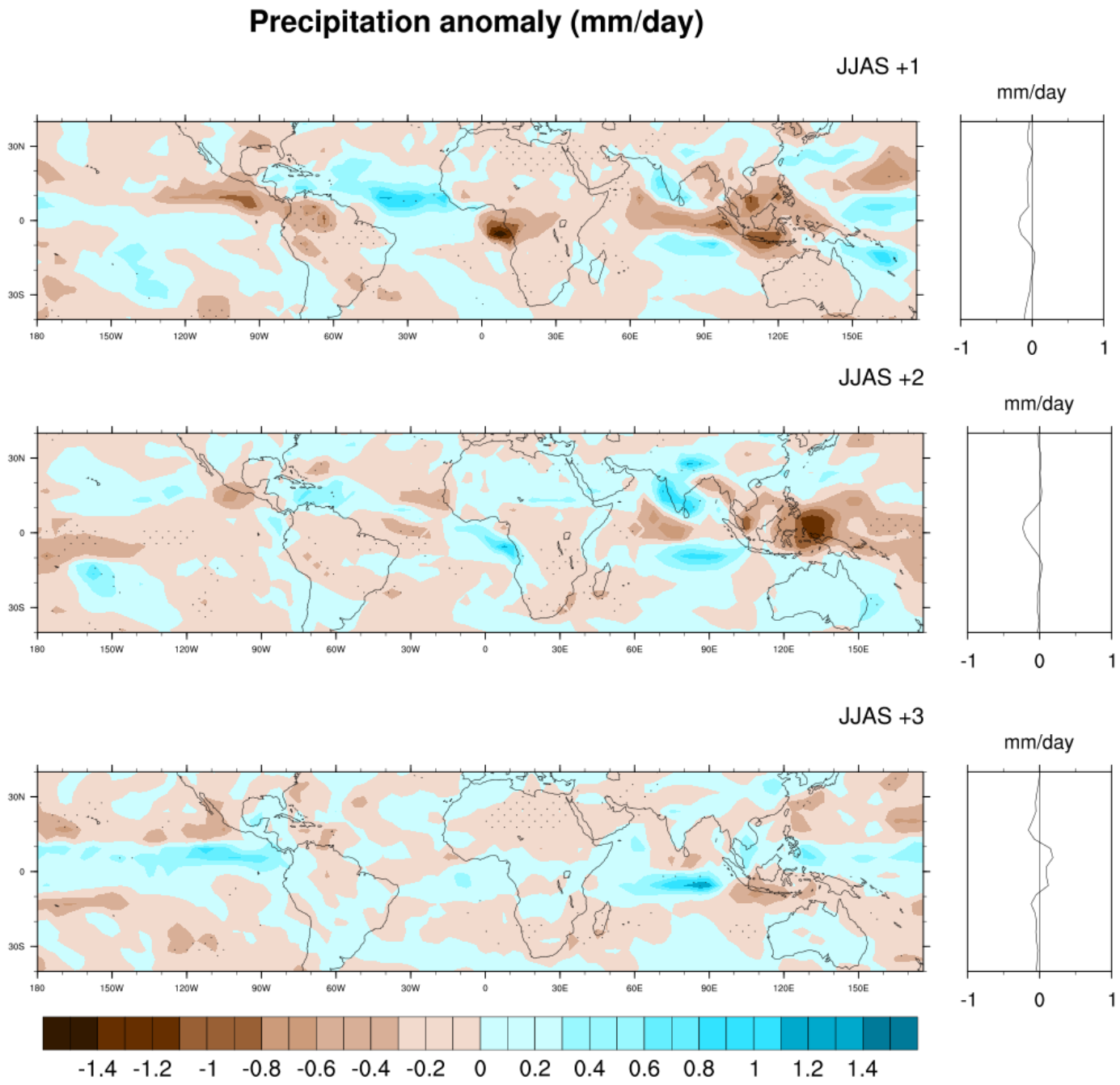

A4: Averaged precipitation (mm/day) anomalies for the first, second and third boreal summer (JJAS) following the 13 major tropical volcanic eruptions (EnsembleM1M2 simulation). Dotted areas represent 95% inter-eruption confidence level for the precipitation.

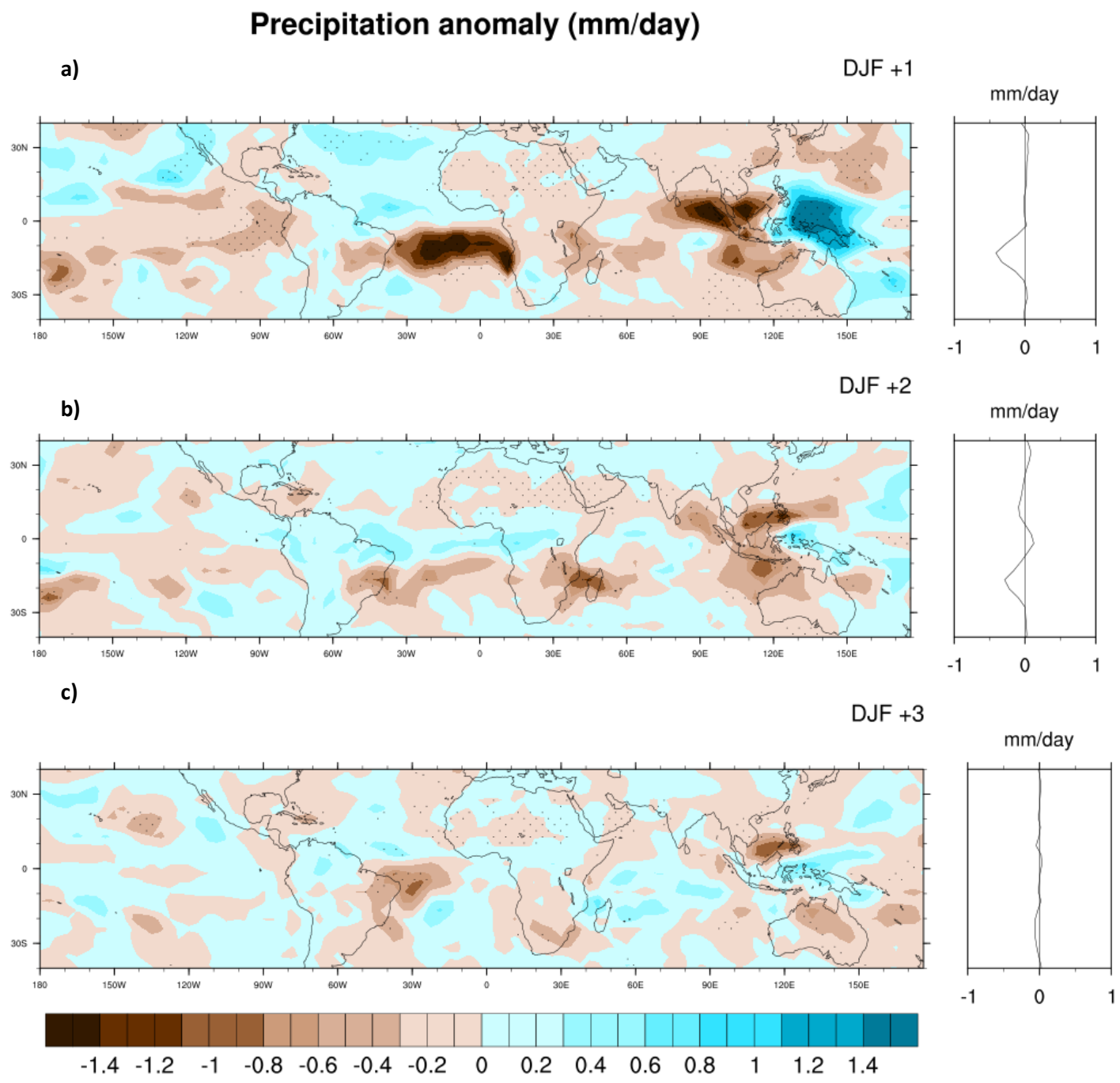

A5: Averaged precipitation (mm/day) anomalies for the first, second and third boreal winter (DJF) following the 13 major tropical volcanic eruptions (EnsembleM1M2 simulation). Dotted areas represent 95% inter-eruption confidence level for the precipitation.

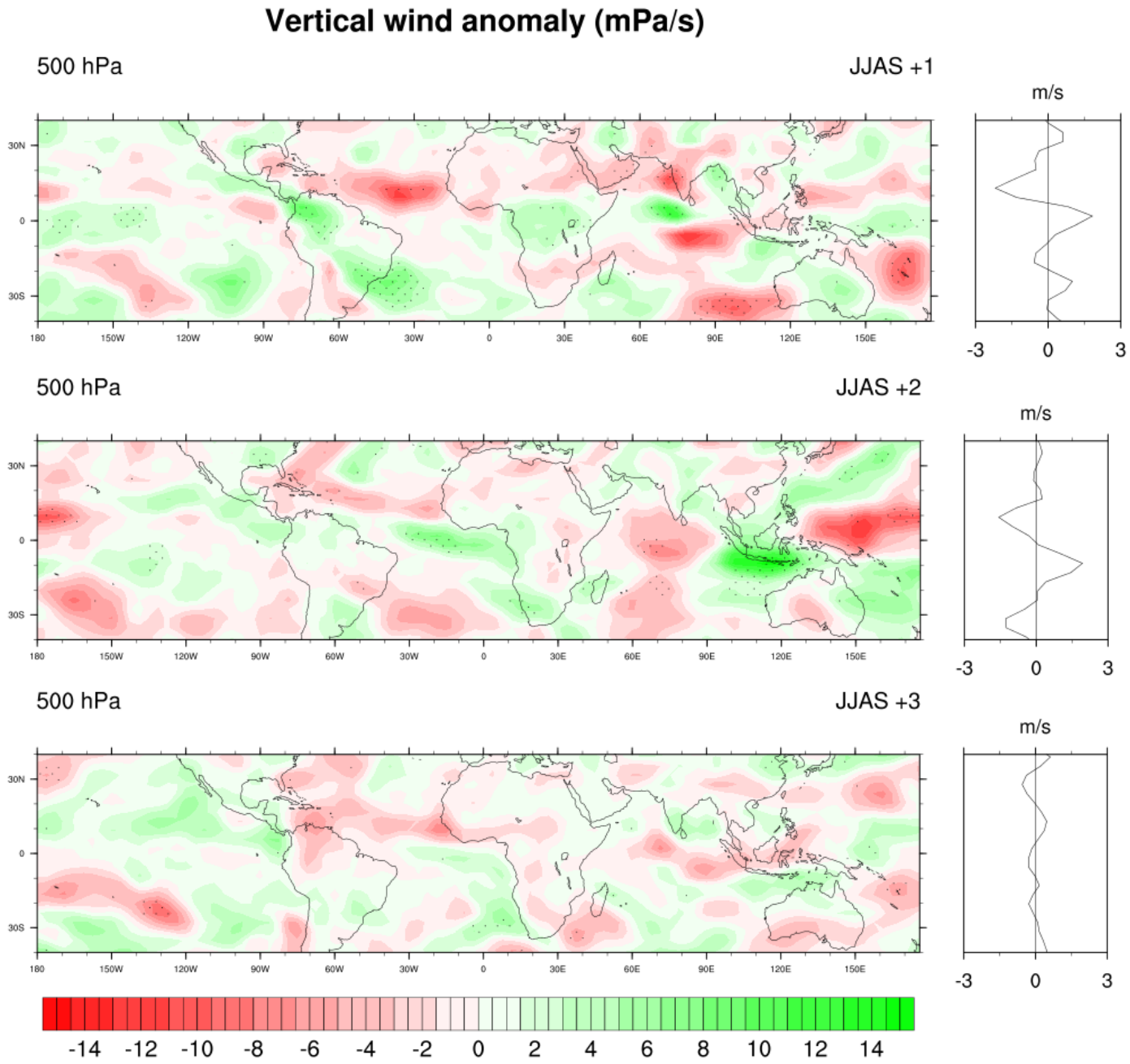

A6: Averaged vertical wind anomaly (mPa/s) for the first, second and third boreal summer (JJAS) following the13 major tropical volcanic eruptions (EnsembleL1L2 simulation). Dotted areas represent 95% inter-eruption confidence level.

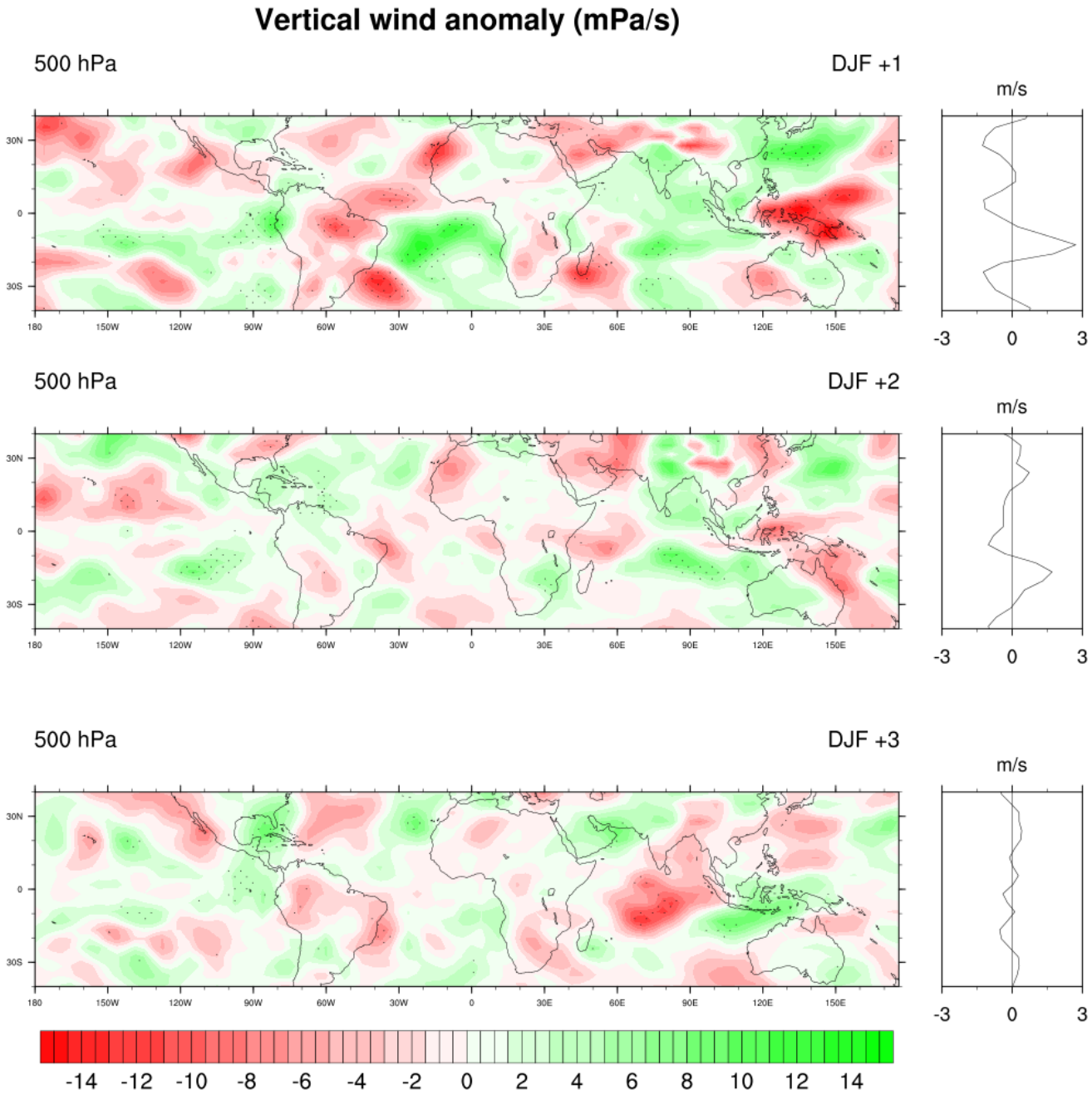

A7: Averaged vertical wind anomaly (mPa/s) for the first, second and third boreal summer (JJAS) following the13 major tropical volcanic eruptions (EnsembleL1L2 simulation). Dotted areas represent 95% inter-eruption confidence level.

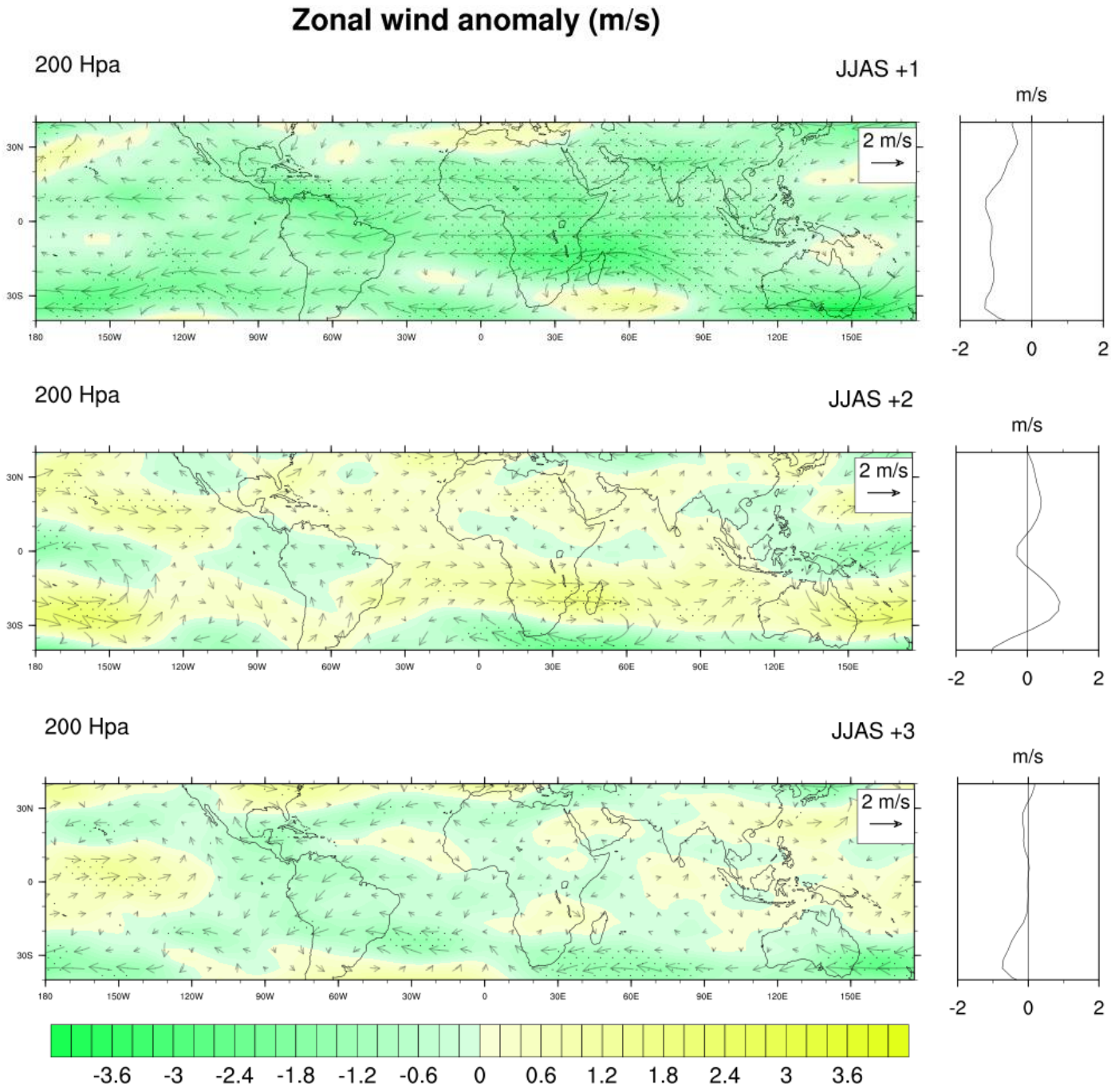

A8: Averaged zonal wind anomaly at 200 hPa (m/s) for the first, second and third boreal summer (JJAS) following the 13 major tropical volcanic eruptions (EnsembleL1L2 simulation). Negative anomalies indicate a stronger east to west component than normal. Dotted areas represent 95% inter-eruption confidence level.

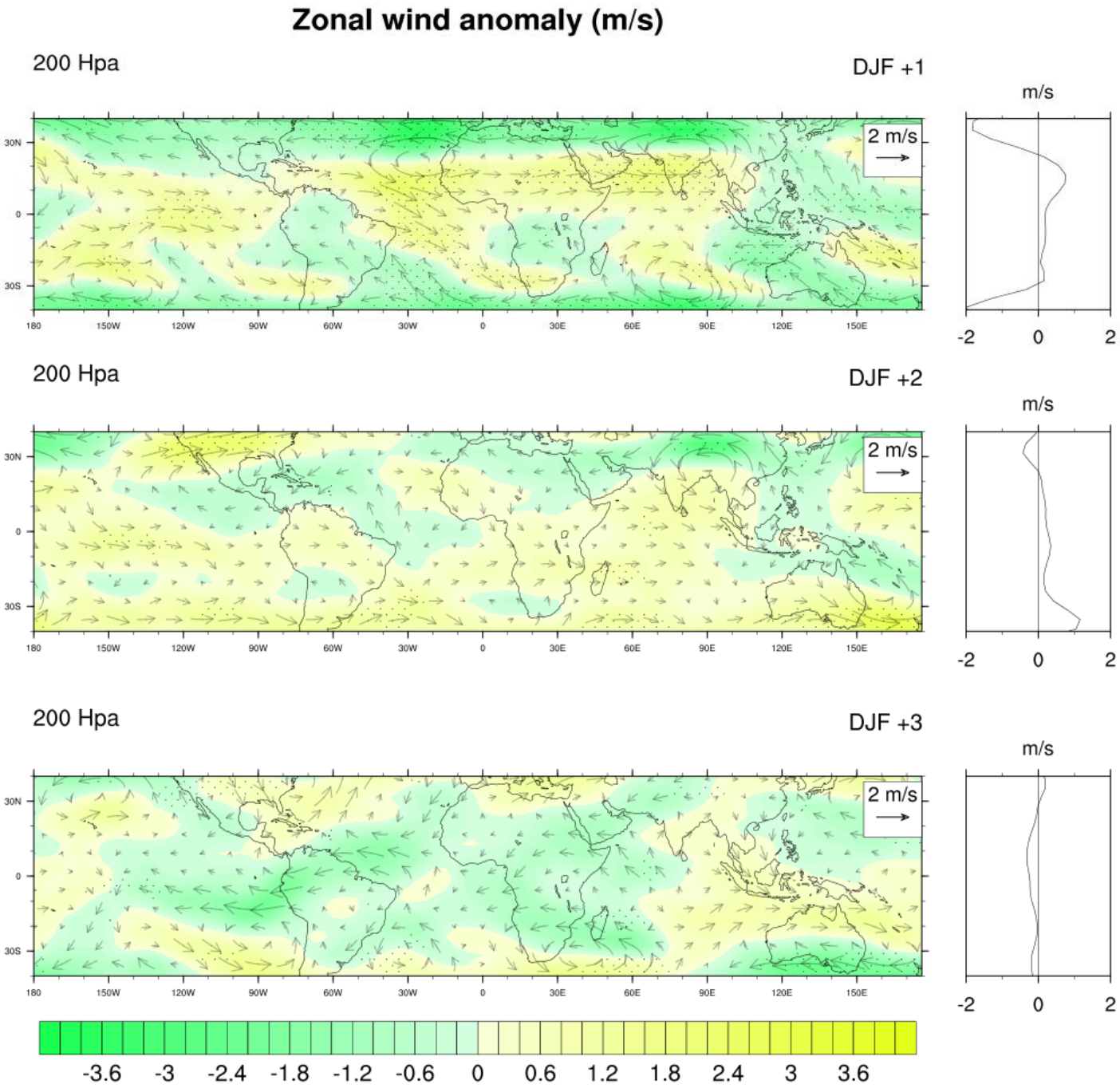

A9: Averaged zonal wind anomaly at 200 hPa (m/s) for the first, second and third boreal winter (DJF) following the 13 major tropical volcanic eruptions (EnsembleL1L2 simulation). Negative anomalies indicate a stronger east to west component than normal. Dotted areas represent 95% inter-eruption confidence level.

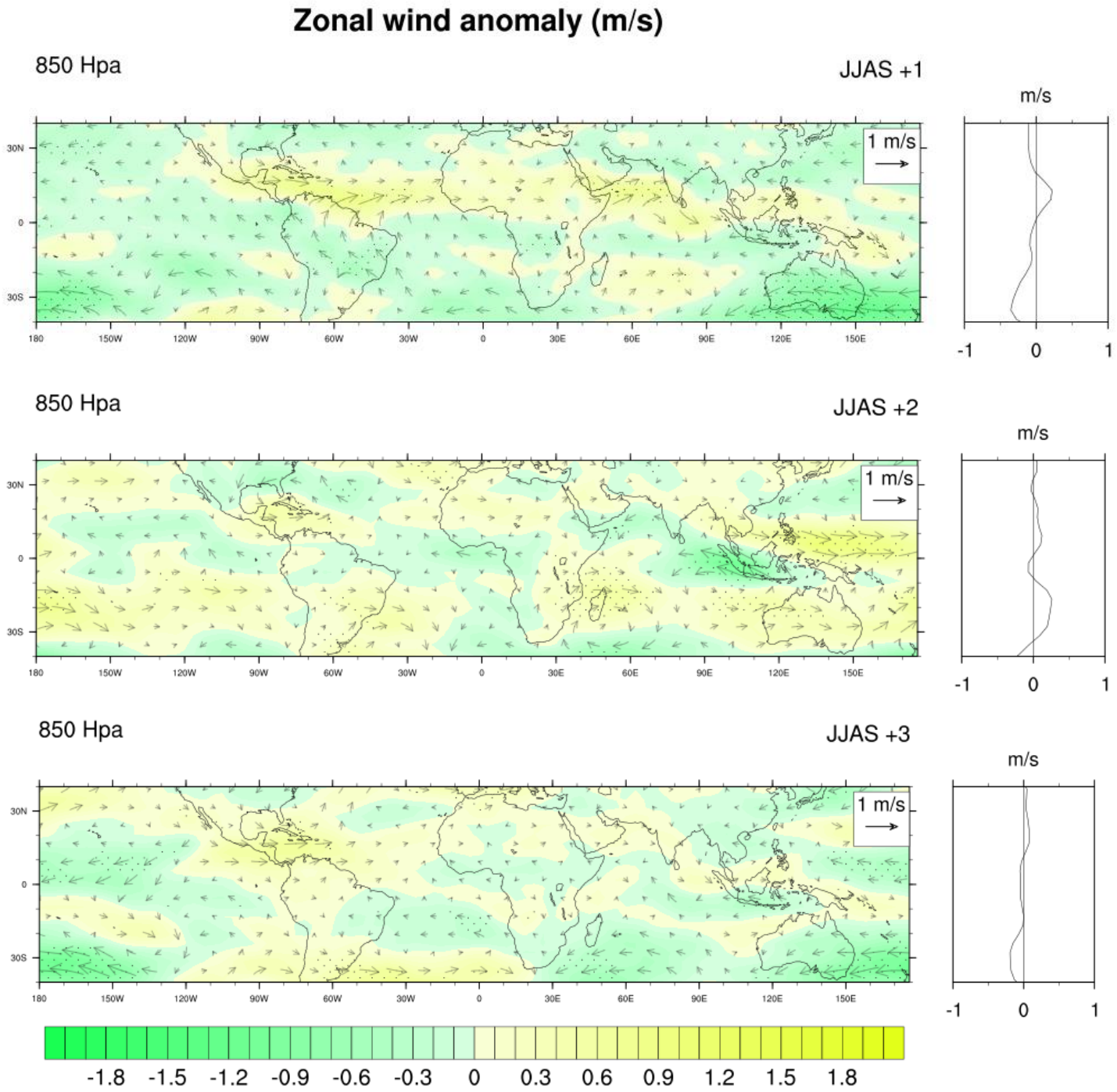

A10: Averaged zonal wind anomaly at 850 hPa (m/s) for the first, second and third boreal summer (JJAS) following the 13 major tropical volcanic eruptions (EnsembleL1L2 simulation). Negative anomalies indicate a stronger east to west component than normal. Dotted areas represent 95% inter-eruption confidence level.

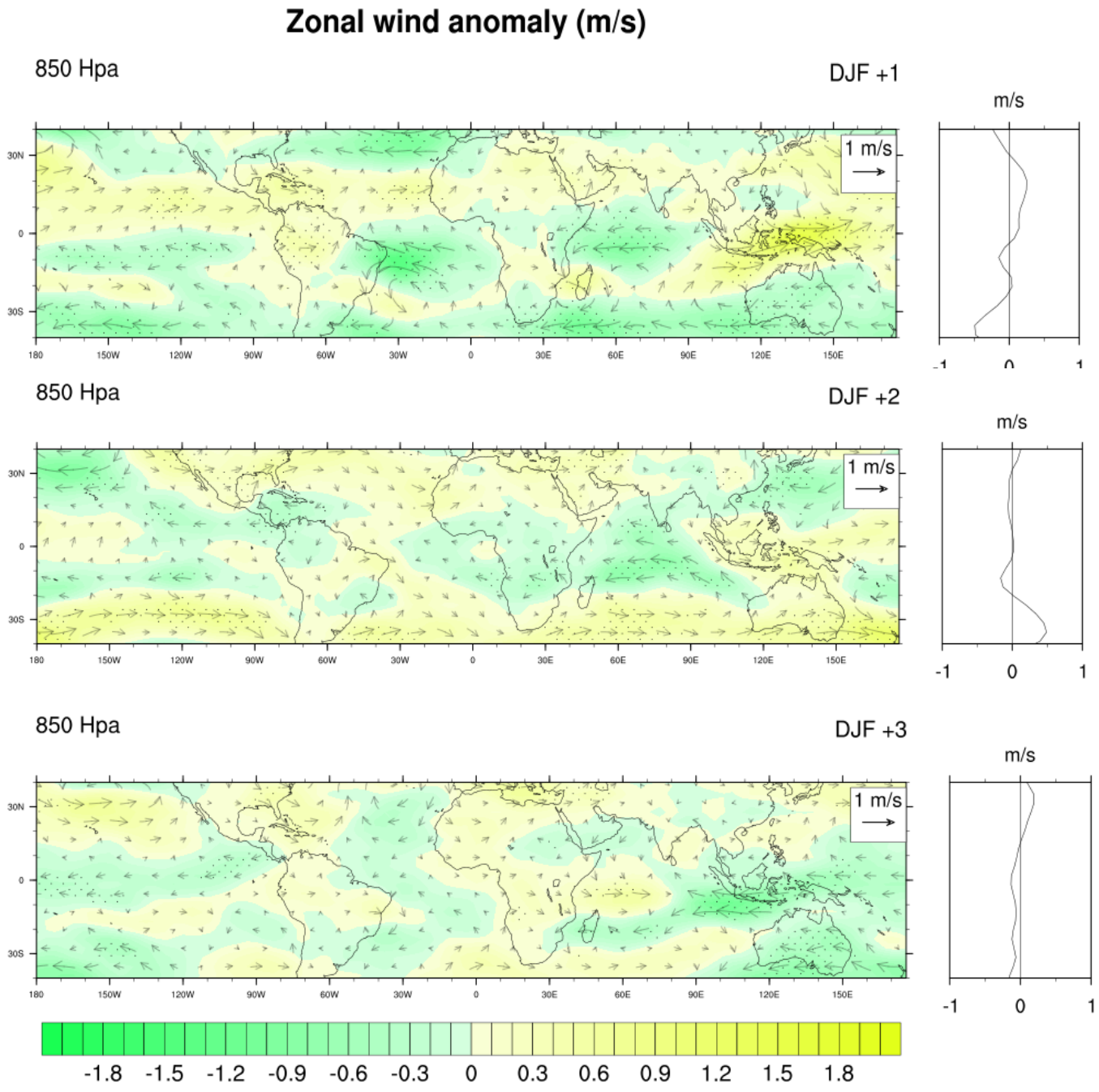

A11: Averaged zonal wind anomaly at 850 hPa (m/s) for the first, second and third boreal winter (DJF) following the 13 major tropical volcanic eruptions (EnsembleL1L2 simulation). Negative anomalies indicate a stronger east to west component than normal. Dotted areas represent 95% inter-eruption confidence level.

Bibliography :

- Agnihotri, R., K. Dutta, and W. Soon, 2011: Temporal derivative of Total Solar Irradiance and anomalous Indian summer monsoon: An empirical evidence for a Sun-climate connection. Journal of Atmospheric and Solar-Terrestrial Physics, 73, 1980-1987.

- Allen, M. R., and W. J. Ingram, 2002: Constraints on future changes in climate and the hydrologic cycle, Nature, 419 (6903), 224.

- Anchukaitis, K. J., B. M. Buckley, E. R. Cook, B. I. Cook, R. D. D'Arrigo, and C. M. Ammann, 2010: Influence of volcanic eruptions on the climate of the Asian monsoon region. Geophysical Research Letters, 37, L22703

- Anet, J.G., S. Muthers, E. Rozanov, C.C Raible, T. Peter, A. Stenke, A.I. Shapiro, J. Beer, F. Steinhilber, S. Brönnimann, F. Arfeuille, Y. Brugnara, and W. Schmutz, 2013 : Atmospheric Chemistry and Physics, 13, 10951-10967.

- Anet, J. G., E. Rozanov, S. Muthers, T. Peter, S. Brönnimann, F. Arfeuille, J. Beer, A.I. Shapiro, C. C. Raible, F. Steinhilber, and W. K. Schmutz, 2013 : Impact of a potential 21st century "grand solar minimum" on surface temperatures and stratospheric ozone. Geophysical Research Letters, 40, 4420-4425.

- Arfeuille, F., D. Weisenstein, H. Mack, E. Rozanov, T. Peter, and S. Brönnimann, 2014: Volcanic forcing for climate modelling: a new microphysics-based data set covering years 1600-present. Climate of the Past, 10, 359-375.

- Arfeuille, F. B. P. Luo, P. Heckendorn, D. Weisenstein, J. X. Sheng, E. Rozanov, M. Schraner, S. Brönnimann, L. W. Thomason, and T. Peters, 2013: Modeling the stratospheric warming following the Mt. Pinatubo eruption: uncertainties in aerosol extinctions. Atmospheric Chemistry and Physics, 13, 11221-11234.

- Arfeuille, F., 2012: Impact of large volcanic eruptions on the stratosphere and climate. Ph.D. thesis, ETH Zurich.

- Auchmann, R., S. Brönnimann, L. Breda, M. Bühler, R. Spadin, and A. Stickler, 2012: Extreme climate, not extreme weather: the summer of 1816 in Geneva, Switzerland. Climate of the Past Discussions, 7, 3745-3774.

- Budich, R., M. Gioretta, J. Jungclaus, R. Redler, and C. Reick, 2010 : The MPI-M Millennium Earth System Model: An assembling guide for the COSMOS configuration, Tech. rep., Max-Planck Institute for Meteorology, Hamburg, Germany.

- Compo, G.P., J.S. Whitaker, P.D. Sardeshmuckh, N. Matsui, R.J. Allan, X. Yin, B.E. Gleason, R.S. Vose, G. Rutledge, P. Bessemoulin, S. Brönnimann, M. Brunet, R.I. Crouthamel, A.N. Grant, P.Y. Groisman, P.D. Jones, M.C.Kruk, A. C. Kruger, G. J. Marshall, M. Maugeri, H. Y. Mok, O. Nordli, T.

F. Ross, R.M. Trigo, X. L. Wang, S. D. Woodruff, and S. J. Worley, 2011: The Twentieth Century Reanalysis Project. Quarterly Journal of the Royal Meteorological Society, 137, 1-28.

- Cook, E. R., J. Anchukaitis, B. M. Buckley, R. D'Arrigo, G. C. Jacoby, W. E. Wright, 2010: The Monsoon Asia Drought Atlas: A new tool for modeling Asian monsoon variability over the past millennium, 1st Asia 2K Workshop in Nagoya, Japan.

- Crowley, T., 2000: Causes of climate change over the past 1000 years. Science, 289 (5477), 270-277.

- D'Arcy Wood, G., 2014: Tambora: The eruption that changed the world. Princeton University Press, 280 pages.

- D'Arrigo, R., R. Wilson, and A. Tudhope, 2008: The impact of volcanic forcing on tropical temperatures during the past four centuries. *Nature*, **2**, 51-56.

- Dai, A., K.E. Trenberth, and T. Quian, 2004: A Global Dataset of Palmer Drought Severity Index for 1870-2002: Relationship with Soil Moisture and Effects of Surface Warming. Journal of Hydrometeorology, 5, 1117-1130.

- Egorova, T., E. Rozanov, V. Zubov, and I. L. Karol, 2003: Model for investigating ozone trends (MEZON), Izv. Atmos. Ocean. Phys., 39, 277–292.

- Feng, S., Q. Hu, Q. Wu, and M. E. Mann, 2013: A Gridded Reconstruction of Warm Season Precipitation for Asia Spanning the Past Half Millennium. J. Climate, 26, 2192-2204.

- Fischer, E., J. Luterbacher, E. Zorita, S. Tett, C. Casty, and H. Wanner, 2007: European climate response to tropical volcanic eruptions over the last half millennium. Gephysical Research Letters, 34 (5), 5707.

- Fouquart, Y. and B. Bonnel, 1980: Computations of solar heating of the Earth's atmosphere: A new parameterization, Beitr. Phys. Atmos., 53, 35–62.

- Gao C., L. Oman, A. Robock, and G. L. Stenchikov, 2007: Atmospheric volcanic loading derived from bipolar ice cores: Accounting for the spatial distribution of volcanic deposition. Journal of Geophysical Research, 112, D09109.

- Harington, C.R., 1992: The Year without a summer? World Climate in 1816. Ottawa: Canadian Museum of Nature.

- Haurwitz, M. W., and G. W. Brier, 1981: A critique of the superposed epoch analysis method: Its application to solar-weather relations, Mon. Weather Rev., 109(10), 2074–2079.

- Haywood J. M., A. Jones, N. Bellouin, and D. Stephenson, 2013: Asymmetric forcing from stratospheric aerosols impacts Sahelian rainfall. Nature Climate Change, 3, 660-665.

- Ho. M., A. S. Kiem, and D. C. Verdon-Kidd, 2012: The Southern Annular Mode: A comparison of indices. Hydrol. Earth Syst. Sci., 16, 967-982.

- Iles C. E., and G. C. Hegerl, 2014: The Global precipitation response to volcanic eruptions in the CMIP5 models. Environ. Res. Lett. , 9, 1-10.

- Jacobi J., D. Perrone, L. L. Duncan, and G. Hornberger, 2013: A Tool for Calculating the Palmer Drought Indices (User Manual). 10.1002/wrcr.20342.

- Jones G. S., J. M. Gregory, P. A. Stott, S. F. B. Tett, and R. B. Thorpe, 2005: An AOGCM simulation of the climate response to a volcanic super-eruption. Climate Dynamics, 25, 725-738.

- Joseph R., and N. Zheng, 2009: Seasonally modulated tropical drought induced by volcanic aerosol. American Meteorological Society, 24, 2045-2060.

- Jungclaus, J. H., N. Keenlyside, M. Botzet, H. Haak, J. J. Luo, M. Latif, J. Marotzke, U. Mikolajewicz, and E. Roeckner, 2006 : Ocean circulation and tropical variability in the coupled model ECHAM5/MPI-OM, J. Climate, 19, 3952–3972.

- Jungclaus J. H., S. J. Lorrenz, C. Timmreck, C. H. Reick, V. Brovkin, K. Six, J. Segschneider, M. A. Giorgetta, T. J. Crowley, J. Pongratz, N. A. Krivova, L. E. Vieria, S. K. Solanki, D. Klocke, M. Botzet, M. Esch, V. Gayler, H. Haak, T. J. Raddatz, E. Roeckner, R. Schnur, H. Widmann, M. Claussen, B. Stevens, and J. Marotzke, 2010: Climate and carbon-cycle variability over the last millennium. Climate of the Past Discussions, 6, 1009-1044.

- Kajikawa Y., B. Wang, and J. Yang, 2010: A multi-time scale Australian monsoon index. Royal Meteorological Society, 30, 1114-1120.

- Kalnay E., M. Kanamitsu, R. Kitsler, W. Collins, D. Deaven, L. Gandin, M. Iredell, S. Saha, G. White, J. Woollen, Y. Zhu, M. Chelliah, W. Ebisuzaki, W. Higgins, J. Janowiak, K. C. Mo, C. Ropelewski, J. Wang, A. Leetma, R. Reynolds, R. Jenne, and D. Jospeh, 1996: The NCEP/NCAR 40-Year Reanalysis Project. Bulletin of the American Meteorological Society, 77, 437-471.

- Krüger K., M. Toohey, and D. Metzner, 2014: Do large volcanic eruptions influence the Southern Annular Mode? SPARG GA, Queenstown, NZ.

- Lau K.M., K. M. Kim and S. Yang, 2000: Dynamical and Boundary Forcing Characteristics of Regional Components of the Asian Summer Monsoon. Journal of Climate, 17, 2461-2482.

- Mlawer, E. J., S. J. Taubman, P. D. Brown, M. J. Iaocono, and S. A. Clough, S. A. : Radiative transfer for inhomogeneous atmospheres: RRTM, validated correlated-k model for the longwave, J. Geophys. Res. , 102, 663–682, 1997

- Mitchell, J. M., 1961: Recent secular changes of the global temperature, Ann. N. Y. Acad. Sci., 95, 235–250.

- Muthers, S., J.G. Anet, A. Stenke, C.C. Raible, E. Rozanov, S. Brönnimann, T. Peter, F.X. Arfeuille, A.I. Shapiro, J. Beer, F. Steinhilber, Y. Brugnara, and W. Schmutz, 2014 : The coupled atmosphere-chemistry-ocean model SOCOL-MPIOM. Geoscientific Model Development,

- Muthers, S., 2014: Chemistry-Climate Interactions in the Coupled Atmosphere-Chemistry-Ocean Model SOCOL-MPIOM. Ph.D. Thesis, University of Bern.

- Newhall, C. G., and S. Self, 1982: The Volcanic Explosivity Index (VEI): An estimate of explosive magnitude for historical volcanism. Journal of Geophysical Research, 87, 1231-1238.

- Oman, L., A. Robock, G.L. Stenchikov, and T. Thordarson, 2006: High-latitude eruptions cast shadow over the African monsoon and the flow of the Nile. Geophysical Research Letters, 33, L18711.

- Ridley H. E., Y. Asmerom, J. U. L. Baldini, S. F. M. Breitenbach, V. V. Aquino, K. M. Prufer, B. J. Culleton, V. Polyak, F. A. Lechleitner, D. J. Kennett, M. Zhang, N. Marwan, C. G. Macpherson, L. M. Baldini, T. Xiao, J. L. Peterkin, J. Awe, and G. H. Haug, 2015: Aerosol forcing of the position of the intertropical convergence zone since AD 1550. Nature Geoscience, 8, 195-200.

- Robock, A., 2000: Volcanic eruption and climate. Reviews of Geophysics, 38 (2), 191-220.

- Roeckner, E., G. Bäuml, L. Bonaventura, R. Brokopf, M. Esch, M. Giorgetta, S. Hagemann, I. Kirchner, L. Kornblueh, E. Manzini, A. Rhodin, U. Schlese, U. Schulzweida, and A. Tompkins, 2003: Report No. 349 the atmospheric general circulation model ECHAM5 – Model description, Tech. Rep. 349, Max-Planck Institute for Meteorology, Hamburg, Germany.

- Rotstayn, L. D., and U. Lohmann,2002: Tropical Rainfall Trends and the Indirect Aerosol Effect. Journal of Climate, 15, 2103-2116.

- Schneider, D. P., C. M. Ammann, B. L. Otto-Bliesner, and D. S. Kaufman, 2009: Climate response to large, high-latitude and low-latitude volcanic eruptions in the Community Climate System Model. Journal of Geophysical Research, 114, D15101

- Schneider, T., T. Bischoff, and G. H. Haug, 2014: Migrations and dynamics of the intertropical convergence zone, Nature, 513, 45-53.

- Shapiro, A. I., W. Schmutz, E. Rozanov, M. Schoell, M. Haberreiter, A. V. Shapiro, and S. Nyeki, 2011 : A new approach to the long-term reconstruction of the solar irradiance leads to large historical solar forcing, Astron. Astrophys., 529, A67.

- Shindell T. D., G. A. Schmidt, M. E. Mann, G. Faluvegi, 2004: Dynamic winter climate response to large volcanic eruptions since 1600. Journal of Geophysical Research, 109, D05104.

- Sigl, M., J. R. McConnell, L. Layman, O. Maselli, K. McGwire, D. Pasteris, D. Dahl-Jensen, J. P. Steffensen, B. Vinther, R. Edwards, R. Mulvaney, and S. Kipfstuhl , 2013: A new bipolar ice core record of volcanism from WAIS Divide and NEEM and implications for climate forcing of the last 2000 years. *Journal of Geophysical Research*, **118**, 1151–1169.

- Solomon S., 1999: Stratospheric ozone depletion: a review of concepts and history. Reviews of Geophysics, 37 (3), 275-316.

- Spencer, R. W., J. R. Christy, and N. C. Grody, 1990: Global atmospheric temperature monitoring with satellite microwave measurements: Method and results 1979-1984, J. Climate, 3, 1111-1128.

- Stenke A., C. R. Hoyle, B. Luo, E. Rozanov, J. Gröbner, L. Maag, S. Brönnimann, and T. Peter, 2013: Climate and chemistry effects of a regional scale nuclear conflict. Atmospheric Chemistry and Physics, 13, 9713-9729.

- Trenberth K. E., and A. Dai, 2007: Effects of Mount Pinatubo volcanic eruption on the hydrological cycle as an analog of geoengineering. Geophysical Research Letters, 34, L15702.

- Valcke, S., 2013: The OASIS3 coupler: a European climate modelling community software, Geosci. Model Dev., 6, 373–388.

- Wang, B., R. Wu and K. M. Lau, 2001: Interannual Variability of the Asian Summer Monsoon: Contrast between the Indian and the Western North Pacific-East Asian Monsoons. American Meteorological Society, 14, 4073-4090.

- Wang, B., Z. Wu, J. Li, J. Liu, C. Chang, Y. Ding, and G. Wu, 2008: How to Measure the Strength of the East Asian Summer Monsoon. Journal of Climate, 21, 4449-4463.

- Webster, P. J., and S. Yang, 1992: Monsoon and ENSO: Selectivity interactive systems. Q. J. R. Meteorol. Soc, 118, 877-926.

- Wegmann, M., S. Brönnimann, J. Bhend, J. Franke, D. Folini, M. Wild, J. Lüterbacher, 2014: Volcanic Influence on European Summer Precipitation through Monsoons: Possible Cause for “Years without Summer”. Journal of Climate, 27, 3683-3691.

- Wegmann, M., 2012: Impacts of explosive volcanic eruptions on large-scale climate variability in model ensemble data for the last 400 years. Msc. Thesis, University of Bern.